CELLULAR 5G AND V2X ANTENNAS DESIGN FOR AUTOMOTIVE APPLICATIONS

by

MOHAMED OSMAN HUSSEIN KHALIFA

A dissertation submitted in partial fulfillment of the
requirements for the degree of

DOCTOR OF PHILOSOPHY IN ELECTRICAL AND COMPUTER ENGINEERING

2022

Oakland University
Rochester, Michigan

Doctoral Advisory Committee:

Daniel N. Aloi, Ph.D., Chair
Amanpreet Kaur, Ph.D.
Eddie Cheng, Ph.D.
Reza Azadegan, Ph.D.

All the thanks are due to
ALLAH (God),

to my lovely and great wife
ANAN,

my adorable daughter
MARIAM,

My newborn son
OSMAN

and my parents
Dr. Osman H. Khalifa
and Mahasin A. Arman

ACKNOWLEDGMENTS

I would like to express my deepest gratitude to my advisor, Professor Daniel N. Aloi for offering me encouragement, guidance, and support to pursue research in my field of interest.

I would also like to thank my doctoral advisor committee, Assistant Professor Amanpreet Kaur, Professor Eddie Cheng, and Dr. Reza Azadegan for their guidance, mentorship, and efforts in reviewing my work and providing valuable insights that helped to be where I am today.

My ultimate gratefulness to my wife who has been the perfect companion throughout this journey. Without her help and confidence, this work will inevitably fail. Thanks again for supporting me through the tough times and standing by my side.

Special thanks to my parents, brother, and sisters for their continuous support and steadfast confidence in me. They have my everlasting love and respect.

Mohamed Osman Hussein Khalifa

PREFACE

The basis of this research stemmed from my passion of preserving humans' lives and improving humanity quality of life. As the number of vehicles increases in the roads, accidents and delay times reach all times high. How will we make the roads safer environment for travelling and reduce traffic congestions? It is my passion not only to find out but also to develop solutions for future generations. Fortunately, 5G and V2X technologies represents real life solutions for traffic problems and with the help of the antennas developed in this work, it will be possible for the automakers to build cheap, compact, and high-performance antennas to further extend the reach of 5G and V2X communication systems.

Many Challenges imposed by the available physical volume for 5G and V2X antennas or due to other wireless services antennas coexisted within the same package require innovative design ideas to lessen these problems effects and ensure successful operation of the desired antennas.

Honestly, there was no way to achieve the current level of success without a very strong support group. First, my parents, who supported me with love, care, and understanding. Second, my wife and daughter, who immersed me with love and tenderness. Finally, my advisor and committee members, who provided me with guidance and mentorship throughout this research journey. Thank you all for your unwavering support.

ABSTRACT

CELLULAR 5G AND V2X ANTENNAS DESIGN FOR AUTOMOTIVE APLICATIONS

by

MOHAMED OSMAN HUSSEIN KHALIFA

Adviser: Daniel N. Aloi, Ph.D.

The work presented in this dissertation involves investigation and development of antennas and antenna systems that can contribute to autonomous vehicles realization. The antennas targeted in this work are namely Fifth Generation (5G) cellular antennas and Vehicle to Everything (V2X) antenna. The studies conceived in this work followed a scientific approach which starts by accurately simulating the antennas using three-dimensional Electromagnetics (EM) solver High Frequency Simulator System (HFSS) software on one meter rolled edges GND. Then antenna and antenna systems were measured on one-meter GND inside anechoic chamber and also measured either on the top of vehicle roof or at the vehicle's windshield.

Phase one of this work starts by presenting a multi-wideband branched monopole antenna that covers 5G cellular bands between 617MHz- 5000MHz. This antenna utilizes two arms and L-Shape slot structure to provide coverage for low, mid, and high 5G cellular bands and also to reject Global Navigation Satellite System (GNSS) frequency bands. The antenna has compact size, light weight, low cost, and excellent gain

characteristics at the solid angle facing cellular base station communication towers. The design, simulated, and measured results were presented and discussed in detail.

Phase two of this work uses the element developed in phase one to construct high order Multiple-Input-Multiple-Output (MIMO) structure in order to boost overall system throughput, capacity, and data rate. Three MIMO systems configurations were studied, the first two are 2x2 5G cellular MIMO systems with similar individual antenna elements and opposite antennas orientations whereas the third configuration is a 4x4 5G cellular MIMO system. The individual antennas performance, diversity radiation pattern, and correlation between antennas were reported and discussed for all three MIMO configurations.

Phase three of this work presents a V2X cavity-backed slot antenna that can be mounted in the vehicle's windshield or rear-view mirror. The antenna is GND independent, and it provides excellent below horizon performance allowing the vehicles to communicate with other objects of less height. The antenna can be used as a building block to implement a full V2X system that provides null-free omnidirectional coverage at V2X solid angle of interest while providing aesthetic look for the vehicle which makes it very attractive in the automotive industry. The antenna was simulated and measured, and its radiation pattern, gain, and efficiency were presented and discussed in detail.

TABLE OF CONTENTS

TABLE OF CONTENTS—Continued

TABLE OF CONTENTS—Continued

LIST OF TABLES

LIST OF FIGURES

LIST OF ABBREVIATIONS

1G	First Generation
2G	Second Generation
3G	Third Generation
4G	Fourth Generation
5G	Fifth Generation
ADS	Advanced Design System
AWS	Advanced Wireless Services
BRS	Broadband Radio Services
DAB	Digital Audio Broadcast
DCS	Digital Communication System
DG	Diversity Gain
DSRC	Dedicated Short-Range Communication
ECC	Envelope Correlation Coefficient
EM	Electromagnetic
FAKRA	Fachkreis Automobile
fc	Center Frequency
FM	Frequency Modulation
FR4	Flame Retardant 4
GHz	Giga Hertz
GNSS	Global Navigation Satellite System
GND	Ground Plane

GSM	Global System for Mobile Communication
HFSS	High Frequency Structure Simulator
IMT	International Mobile Telecommunications
IoT	Internet of Things
LAG	Linear Average Gain
LTE	Long Term Evolution
MHz	Mega Hertz
MIMO	Multiple-Input Multiple-Output
OEM	Original Equipment Manufacturer
PCB	Printed Circuit Board
PCS	Personal Communications Services
PIFA	Planar Inverted-F Antenna
RF	Radio Frequency
SADRS	Satellite Digital Audio Receiver System
SMS	Short text Messages Service
SNR	Signal to Noise Ratio
SUV	Sport Utility Vehicle
V2I	Vehicle-to-Infrastructure
V2P	Vehicle-to-Pedestrian
V2V	Vehicle-to-Vehicle
V2X	Vehicle-to-Everything

VLP	Vertical Linear Polarization
VOIP	Voice Over Internet Protocol
VSWR	Voltage Standing Wave Ratio
WLAN	Wireless Local Area Network
XPR	Cross Polarization Ratio

CHAPTER ONE

INTRODUCTION AND WORK CONTRIBUTIONS

1.1 Introduction

Recently, there has been an increasing demand in the automotive industry for wireless systems and antennas. Wireless communication technologies such as Wireless Local Area Network (WLAN), Second Generation (2G), Third Generation (3G) and Long Term Evolution (LTE) have been developed to increase the data rate and efficiency of wireless systems but still cannot be deployed in certain applications on the vehicle such as V2X communication which analyzes the vehicle's communication with everything such as Vehicle-to-Vehicle (V2V), Vehicle-to-Infrastructure (V2I), and Vehicle-to-Pedestrian (V2P) communications. 5G technology should be able to address these applications with its enhanced data rate, low latency, increased reliability, and high user capacity. In fact, 5G is going to play a very important role in the automotive industry for self-driving cars and Internet of Things (IoT) since it helps to establish a connection to assist drivers on the road (i.e. traffic, accident prevention, or simply for entertainment systems). Compared to the LTE network, 5G is expected to have 100 times the data rate up to 10 Gbps at peak, 1000 times the capacity of connected nodes, 10-100 times power consumption efficiency by allocating Radio Frequency (RF) resources based on user usage, and very low latency with a maximum of 1msec [1]-[2].

The upcoming 5G system has larger frequency bandwidth requirements in both the low and high frequency bands including millimeter waves. It would also require a MIMO system on the vehicle with multiple antennas in order to gain better diversity and

throughput to meet the requirement of this advanced system. The shark-fin modules on the vehicle contain many antennas for various applications such as: GNSS, satellite radio, WLAN, FM, Digital Audio Broadcast (DAB), and MIMO cell antennas. Hence, considering space limitation with coupling and shadowing effects between antennas, it is challenging to design elements that meet the required performance within desired dimensions [3]. The motivation and challenges for this work, Literature review, work contributions, and dissertation organization are discussed next in this chapter.

1.1.1 The Evolution of Cellular Communications

In 1979, the mobile network first generation was introduced in Japan. The 1G permitted a speed of 2.4Kb/s with limited coverage and it was not supporting roaming services. The 2G introduced in 1991 used digital signaling to push speed limit to 64Kb/s and it also improved reliability and information security by using the Global System for Mobile Communications (GSM) standard. It is noteworthy to mention that Short text Messages Service (SMS) was first introduced within the 2G era. 2001 witnessed the introduction of the 3G that supported much higher speeds (256Kb/s) and it also allowed for global standards harmony. The 3G made it possible for some additional services to be real such as Video streaming, teleconferencing and Voice over Internet Protocol (VoIP). Finally, the fourth generation (4G) LTE, pushed the speed further to 1Gb/s and it also made applications like online gaming and high-definition video streaming also possible. We are now on the edge of the 5G, which is developed to support the escalating demands of a universe of IoT, telemedicine, explosion of consumer video, and future autonomous transportation. In addition to dramatically decrease the latency, the speed will be increased to up to as much as 100 times as of now. The ability to support many more

connected devices with greater network efficiency and reduced latency is driving the transition to 5G.

The introduction of 5G in the automotive industry will unlock potentials for autonomous vehicles and connected cars and bus-stops. Such services will be mapped into safety, augmented reality and navigation, ecosystem scalability, fleet monitoring, and sustainability. In Summary, to realize these high speed and low latency requirements, the current 5G frequency coverage required in automotive industry requires inclusion of high frequencies that goes up to 5GHz as well as band B71 (617MHz – 698MHz) which has recently been freed up by TV broadcast to be used in 5G applications and it puts some challenges in the way of designing a multi-wideband antenna that covers such a big frequency range from 617MHz to 5GHz.

1.1.2 General Requirements for Vehicular Antennas

To have good vehicle reception in general, some requirements are to be satisfied by the antenna. First of all, for most antennas the antenna must be omnidirectional i.e. the antenna should have the ability to receive from any direction around the car. If one antenna is not enough to satisfy the requirement, then two or multiple antenna elements forming an antenna array must be considered. Second, in general an antenna should be placed on vehicle and as high as possible over ground. Placing antenna higher over ground results in better reception and transmission characteristics.

Moreover, the distance between antenna and receiver must be kept at minimum to prevent attenuation caused by increased cable length. In addition to that, the antenna surroundings can also degrade the performance of the antenna and therefore, materials and clearances surrounding the antenna must carefully be considered. In general, a

clearance of three times antenna size box around the antenna should not be obstructed which makes it very challenging to design cellular antenna with frequencies less than 1GHz. However, this requirement can easily be satisfied with GNSS-antennas or Cellular above 1 GHz. The spurious noise generated by vehicle engine can also negatively impact receiving the signal, so the antenna must be kept away from the engine with all other placement requirements taken into account. Finally, the polarization of the antenna is very important, as some signals are transmitted specially polarized, for example Cellular antenna are usually vertically polarized to receive RF signals from cell towers while GNSS patches are right hand circular polarized to allow satellite signals reception.

In Summary, for antennas on vehicles, several factors come to play including over-ground elevation, omnidirectional reception, engine spurious noise, antenna-to-receiver cable attenuation, and antenna polarization. All these factors should be considered for successful automotive antenna design.

1.1.3 Vehicular Antennas Placement Overview

Watching different cars on the road in terms on antenna placements, it seems that there are several placements to be found. Figure 1.1 displays the best practices to place antennas on vehicles and those locations are discussed in detail on this section.

1.1.3.1 Roof

Most automakers place antennas on top of vehicle's roof. The reasoning behind this is that the vehicle's roof is high above ground, and it is unobstructed which allow for excellent reception from all directions. Since omnidirectional reception is a must in all wireless applications, antenna placement on vehicle's roof represents the best option for most vehicles, except convertibles.

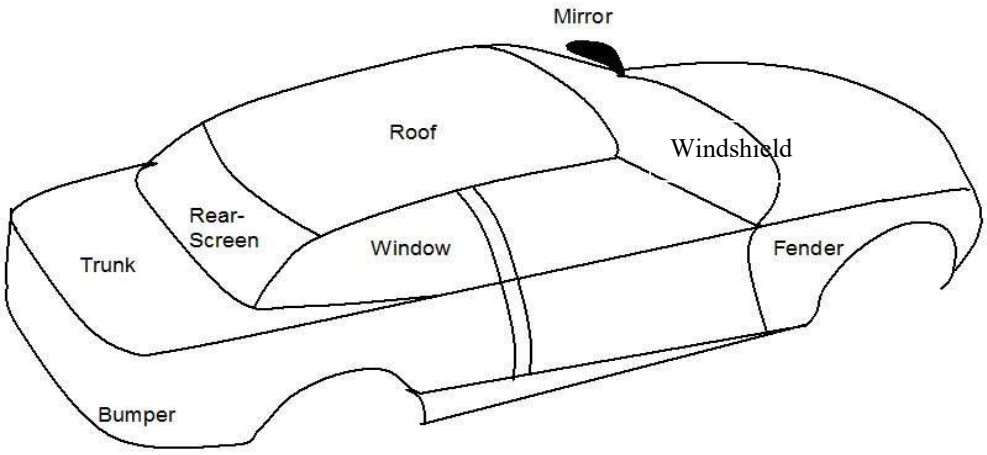

Figure 1.1. Antenna Placement Location on Car

1.1.3.2 Spoiler

To further increase the downward force for racing cars at higher speeds, spoiler is used. Sometimes, the spoiler is made of plastic which makes it suitable for antennas to place. Spoiler represents the second preferred location to place antennas whenever it is present.

1.1.3.3 Windshield, Rear-Screen, and Windows

Since 1980 embedding antennas in windshields and other car's screen has been very popular. As windows and screens are available in most if not all cars, applying antennas on such fairly big space is usually a straightforward process. This process sometimes requires huge engineering efforts. However, once the design is developed, producing such antennas is often of low cost, good performance, and resilient. On-glass antennas is very attractive solution for automakers specially when aesthetic look for the vehicle is a must.

1.1.3.4 Fender and Bumper

When a vehicle's fender and bumper are made of plastic, multiple antennas can be placed inside. The disadvantages of such designs are possible loss of communication because fenders and bumpers are often more exposed to accidents than the rest of car parts. Moreover, degraded antenna performance may result due to engine noise and low antenna height above the ground.

1.1.3.5 Trunk Cover

Trunk cover represents the optimum place to fit antennas in convertible vehicles and that is because roof, windows, and screens can be hidden. However, to ensure successful antenna operation inside the convertible vehicle trunk, the trunk cover must be made of plastic or a double-layer structure with metal frame and plastic cover on top.

1.1.3.6 Mirrors

Side mirrors in big vehicles such as Sport Utility Vehicles (SUV) and trucks represents a good place to fit several antennas inside. Placing multiple high frequency antennas such as V2X inside mirrors of regular vehicles can be made possible by building side mirrors outer shell from plastic materials. In fact, side mirrors of some trucks offer huge room in which not only high frequency antennas could be placed but also relatively large size low frequency antennas such as FM and GSM cell antennas plus other technologies like GNSS and SDARs antennas. However, such antennas may require huge engineering effort to ensure comparable performance to on-roof placed antennas since modern vehicles side mirrors are often packed by defrosters, cameras, and other electronics for blinkers and blind spot detection systems.

In Summary, Cellular antennas can generally be placed on the roof, spoiler, car screens, fender, bumper, or in convertible's trunk. The commonly used antenna design topologies are monopoles [4] and [5], helical antennas [6]– [8] and on Printed Circuit Board (PCB) antennas [9]– [12]. In fact, by hiding antennas in places like in the glove compartment, under the dashboard, or side-view mirrors, additional benefits such as aesthetic appeal of the vehicle and less exposure external factors (accidental damage, vandalism, and theft) can be obtained. However, in such locations it becomes inevitable to deal with complex scenarios stems from the interactions with the vehicle structure. In particular, the proximity of antenna to other electronic components in these locations, affect the antenna performance in a way that is extremely difficult to predict let alone to compensate for and consequently, these locations will not be considered in this study. Protruding modules cannot get bigger in size as they influence the vehicle aerodynamics and disturb their aesthetic appearance, which is a major selling point for passenger vehicles. However, Shark-fin antenna casing style on the roof of the car which originally developed to lessen drag and remove another source of noise from the cabin, has now proven to further improve aerodynamic efficiency, potentially making cars more efficient [13].

Based on the above discussion, to achieve the best performance and improve the aerodynamic of the vehicle, a Shark-fin casing mounted on the car roof will be the best candidate to contain the proposed 5G cellular antenna. The Shark-fin package may also contain one or more antenna for other wireless applications such V2X antenna. However, due to shadowing problems and other requirements outlined in section 1.2, V2X antenna will be placed in the windshield.

1.2 Motivation and Challenges

Some of the challenges that usually face the RF designers in the development and integration of single or Multiple 5G and V2X antenna elements and trying to fit them in the vehicle without compromising their performance are outlined below:

- 5G cellular antennas covers a very wide range of frequencies including low-band (617MHz- 960MHz), two mid-bands (1710MHz- 2170MHz) plus (2490MHz- 2690MHz), and high-band (3400MHz- 5000MHz). This vast range of frequencies makes the task of coming up with a Multi-Wide Band antenna design with good performance characteristics very challenging. In fact, covering low 5G cellular frequencies represents a design bottleneck since the available space within the Shark-fin for each antenna is much smaller than the wavelengths at the which the antenna expected to operate, issues such as performance degradation due to limited antenna size and bandwidth limitations will happen. In addition to the need of getting good 5G cellular performance, antenna element cost is also of great importance for successful commercialization of the antenna product.
- With more wireless applications antenna elements being integrated within the same antenna module in modern vehicles, shadowing and coupling between antennas inside an automotive Shark-fin start to occur. Shadowing happens because of misarrangement of antenna elements with respect to each other which can cause blockage of electromagnetic waves (EM) that is translated to radiation pattern nulls in the direction of that blockage. Shadowing can also appear in a shape of tilted radiation pattern due to EM reflections. Antenna elements that share some frequency bands can strongly couple to each other if filters are not to

be used. The inter-antenna distance is frequency dependent. Coupling between antennas usually happens when a transmitted/received signal gets absorbed by unintended neighbor antenna and hereby reduce the targeted antenna efficiency. These issues cause 5G cellular system performance degradation that express itself in terms of dropped phone calls and radio mutes. Thus, reduce coupling by designing 5G antenna element with built-in rejection for other applications antennas such as high precision GNSS (which usually coexist with 5G cellular antenna in the same module with frequencies from 1160MHz- 1610MHz that lie in the mid of 5G cellular frequencies from 617MHz-5GHz) is of great importance.

- To allow for high-speed internet access, 5G communication system is usually equipped with MIMO antennas to allow for 2 or more layers of orthogonal data streams to be received or transmitted via the antenna system. However, with the use of MIMO antennas, issues like correlation between antennas starts to happen. Correlation between similar antennas depends on radiation pattern orientation of individual antennas relative to each other as well as the distance between them which is in turn frequency dependent. The limited size of the Shark-fin module puts a huge burden on the design process of decorrelated MIMO antenna system. In addition to that, the MIMO antennas must be carefully placed to yield good diversity performance with low correlation figures.
- In order to establish reliable V2X communication system. V2X antennas must demonstrate high performance, omnidirectional pattern, and below horizon coverage. Trials to integrate such antennas inside a Shark-fin module with other

applications' antennas often comes at a performance cost. V2X antenna usually has a small footprint since it operates at relatively high frequencies (5.85GHz-5.925GHz). With such a small size antenna, there is a high possibility of EM waves blockage from bigger antennas inside the same antenna module and consequently nulls in antenna radiation pattern that can sabotage overall V2X system operation and safety. Below horizon reception for V2X antenna is a necessity to ensure sound operation of V2X system. However, V2X antenna integrated inside a Shark-fin module on top of a vehicle roof will likely lose this feature because of the big ground plane (GND) underneath the antenna. Moreover, modern vehicle styling purposes encourages the elimination of protruding mechanical parts such as Shark-fin for aesthetic look of the vehicle. For the above reasoning, it is quite important to mount the V2X antenna in a location such that all mentioned problems are mitigated.

1.3 Literature Survey

Below is a through literature review of the work that has been made in vehicular antenna system with regards to 5G cellular antenna design, cellular MIMO antenna system, and V2X antennas.

1.3.1 5G Cellular antenna

The antennas in [14], [16], [21], [22] are multi-band antennas that cover a wide range of 5G systems. However, a fully wide-band antenna that covers the B71 band is desired and is presented in this work and tested on a vehicle roof to provide practical performance. The dimensions of the antenna in [15] are too large for an automotive Shark-fin radome and the antenna does not fully cover the desired band from 617MHz up to

5GHz. The low-profile antenna in [17] covers the band from 790MHz-2690MHz and provides acceptable performance at 30 degrees above the horizon whereas in 5G system the requirements are stricter and require higher performance from 3-15 degrees above the horizon. In [18], [19], [20] the designed antennas fit in a shark-fin radome for vehicles, however the measured bands do not cover the required bands for 5G.

1.3.2 5G MIMO Antenna Systems

In [25] [26], 2X2 MIMO systems based on Monopole and Planar Inverted-F Antenna (PIFA) elements respectively have been introduced, however the bandwidth of operation is very small (700-925MHz). The 2X2 MIMO systems bandwidth have been increased to cover from 790MHz to 3GHz with reasonable antenna dimensions and an Envelope Correlation Coefficient (ECC) of less than 0.3 and 0.05 in [27] and [28] respectively but the bandwidth of operation doesn't cover 5G frequencies (617MHz-5GHz). In [29]-[33], the authors have developed 2X2 MIMO structures that are constructed from either Monopoles or PIFA elements with a less than 0.5 ECC however, these MIMO systems are only covering LTE (698MHz-3GHz) frequency bands and not 5G frequencies. A much broader bandwidth (700MHz-6GHz) with less than 0.16 of ECC (using first method in [34]) is achieved by authors in [35] but it doesn't include the B71 band (617MHz-698MHz) as well as it comes at an increased volume (70x70x29mm^3) which makes it impossible to fit in production Shark-fins. Finally, a 4X4 MIMO system is presented in [36], However, B71 frequency band is not covered, there is no information about system volume, and the work has not been supported by either GND or vehicle measurements data.

1.3.3 V2X Antenna

In [42], two V2X antennas are designed to fit in an automotive shark-fin however, low average gain of -2.3dBi was reported at 5.9GHz. A tri-polarized antenna was designed to cover 5G and V2X frequencies in [43] with an H-plane gain of 2.05 to 2.88dBi in the V2X band however, it comes with an increased antenna volume with dimensions of 76X76X17mm^3. Similar drawbacks of large volumes can also be seen in [44], [24], and [45]-[47] with less than zero gain in [45] and [46] whereas a gain of 0.97dBi was reported in [47]. A mean realized gain of 0.043dBi was achieved in [48] with a multiband antenna that covers LTE and V2X with a big volume of 120X70X0.1mm^3. In addition to those similar large volumes multiband designs that covers both LTE and V2X with maximum realized gain values of -0.5dBi and 2dBi are reported in [49] and [50] respectively. In [51], a quarter-wave balun fed Vivaldi antenna with dimensions of 190X187.5X187.3mm^3 was designed and an average gain of -5dBi was reported around 5.9GHz. The work in [52] shows a peak gain of 8dBi at 5.9GHz however, it does not show average gain values and it does not tell at which elevation angles this peak gain is achieved.

1.4 Work Contributions and Dissertation Organization

An overview of the main contributions of this work is provided in this section and it is summarized in the following points:

- Chapter 2 describes the development process and results of a novel branched monopole structure that can tackle the challenge of covering the multi-wideband of 5G cellular frequencies. In particular, the antenna makes it possible to cover the 5G low-band (617MHz- 960MHz) frequencies with a compact size that can easily fit in an automotive shark-fin. The developed

antenna has an inherited GNSS frequency bands rejection which in addition to improve the overall antenna module performance by reducing coupling effects, it also eliminates the need for further filtering at the PCB board level and thereby reduce the overall cost of the antenna system RF front end. The antenna element is designed to be compact in size with no need to be printed on dielectric which cut the element cost further. The antenna is constructed from sheet metal and equipped with two arms that enable coverage of whole 5G cellular band with less than 3.2:1 Voltage Standing Wave Ratio (VSWR). The antenna structure also reduces the typical antenna height of 121 mm ($\lambda/4$ at freq.= 617MHz) to only 60 mm that makes around 50% height reduction and makes it feasible to pack the antenna in the shark-fin module.

- Chapter 3 demonstrates that the antenna in Chapter 2 can be used as a building block element to construct high orders MIMO structures. In fact, 3 possible MIMO system configurations will be discussed. The first two configurations are 2X2 MIMO systems however in the second configuration (Configuration II), individual antennas are oriented in the opposite direction to the antennas in the first configuration (Configuration I). The third configuration is a 4X4 MIMO antenna system which is made of the same building block element with individual antennas location and orientation optimized to enhance the MIMO antenna system performance. Important MIMO system performance metrics such as correlation and Diversity Gain (DG) will be discussed with regards to the mentioned configurations.

- Chapter 4 presents the implementation of a cavity-backed slot antenna that is used for V2X communication. The antenna is designed to work around 5.9GHz with excellent matching characteristics (VSWR< 2) and directive radiation pattern that covers 120 degrees azimuth span towards the front of the vehicle with up to 6.5dB realized vertical gain. The developed antenna is GND independent (by design) and can be integrated to the vehicle's windshield or rear-view mirror to enhance V2X antenna system transmission and reception for below horizon originating EM signals. The mounting location of the antenna also guarantee null-free radiation pattern with no other bigger antenna elements around as well as modernized look for the vehicle.
- Chapter 5 provides a conclusion of work that made in this research as well as suggestions for possible future works.
- The Appendix presents tabulated summary of literature review studied throughout the research effort.

CHAPTER TWO

MULTI-WIDEBAND BRANCHED MONOPOLE ANTENNA

2.1 Introduction

With the rapid development in the cellular telecommunications industry, increased number of frequency bands have been added by communication services such as 2G, 3G, 4G, LTE, GSM, Digital Communication System (DCS), International Mobile Telecommunications (IMT), Personal Communications Services (PCS), Broadband Radio Services (BRS), and C Band listed in Table 2.1 require multi-wideband antennas. For these antennas to be of great use, they need to have a compact size, omnidirectional pattern, vertical polarization, high efficiency, low cost, and easy to manufacture. Thus, a monopole antenna can be among best candidates given such requirements. Unfortunately, typical monopole is a single band antenna with 10%- 20% bandwidth. Table 2.2 presents cellular frequency bands together with the corresponding typical monopole heights needed to cover them. As it can be seen from Table 2.2, it is impossible to cover all targeted 5G cellular bands with an individual monopole and thus a more sophisticated design for a monopole antenna needs to be implemented. Successful implementation of 5G cellular antenna must have omnidirectional pattern, low cost, good matching characteristics, good vertical gain performance, shark-fin compatible size, high efficiency, and ease of manufacturability. Important design goals and performance specifications against which the proposed antenna was designed are summarized and reported in Table 2.3. The designed branched monopole structure will be discussed next in this chapter.

Table 2.1. 5G Cellular Frequency Bands

Cellular Band	Frequency Range (MHz)
Digital Dividend (US)	617-698
Lower and Upper SMH/ Lower 800 (Japan)	699-875
Extended GSM	880-960
DCS	1710-1880
PCS	1850-1990
IMT	1920-2170
WCS	2350-2360
C Band	3300-5000

Table 2.2. Monopole heights and bandwidths corresponding to the 5G frequency bands

Service	Digital Dividend	Lower/ upper SMH	GSM	DCS	PCS	IMT	WCS	C Band
Band (MHz):	617-698	699-875	880-960	1710-1880	1850-1990	1920-2170	2350-2360	3300-5000
Center Frequency (MHz):	657	787	920	1795	1920	2045	2355	4150
% BW:	12.3	22.3	8.7	9.5	7.3	12.2	0.42	41
Height (λ/4 mm):	114.08	95.23	81.47	41.75	39.04	36.65	31.83	18.06

Table 2.3. 5G Cellular Design Goals and Guidelines

Parameter	Value
Polarization	Vertical Linear Polarization (VLP)
Return Loss	5.4 dB (3.3 VSWR) across all 5G Bands
Efficiency	60%
LAG	-3 dBi across θ = 70-90 degree
Dimensions	Maximum Height: 60 mm Maximum Length: 45 mm Maximum Width: 17 mm

2.2 Branched Monopole Antenna Design

2.2.1 Work Overview

The goal of this design is to develop a 5G cellular antenna that covers frequencies from 617MHz to 5GHz with a VSWR less than 3.3 and an omnidirectional gain with good characteristics at Theta angles mentioned in Table 2.3. The antenna was first simulated using HFSS software on a 1-meter GND. Then the antenna was placed inside an anechoic chamber and measured on a 1-meter rolled edge GND. Finally, the antenna was mounted on top of a vehicle roof and vehicle-level measurements in anechoic chamber was performed. Next antenna parameters, design methodology, and antenna placement are discussed.

2.2.2 Design Methodology and Parameters

The antenna is made of sheet metal with dimensions of 60mm (height) x 39.8mm (length) x 15mm (width) and it is mounted on Flame Retardant 4 (FR4) circuit board material. A coaxial cable with Fachkreis Automobile (FAKRA) connector is used to feed the antenna as shown in Figure 2.1a. Different current paths have been created by equipping the antenna with two arms covering different frequency bands. The low band (617 MHz – 960 MHz) is attributed to arm 1 whereas mid and high bands (1.71 GHz - 2.69 GHz) and (3.3 GHz – 5 GHz) are covered using arm 2 in Figure 2.1b. As a general design guideline, Arm1 and Arm2 of the branched monopole structure must be loaded at $\lambda_{LB}/4$ and $\lambda_{HB}/4$ distance from GND respectively (where λ_{LB} and λ_{HB} is the wavelength at the center frequency of the low band and high band respectively) to obtain good radiation and impedance matching characteristics. Top loading arm1 branch of the monopole further increases the length of arm1 enabling the antenna to cover much lower frequencies**.** In order to separate the low and the higher bands an L-Shape Slots structure has been cut from the antenna as depicted in Figure 1b. This structure acts as a series LC to ground (band stop filter) and it allows GNSS band rejection. It is possible to control the inductor and capacitor values of this band stop filter by changing L-Shape slots structure parameters (Ls and Lg1) and Ha1 length as it will be seen in parametric study section. The height Ha2 = 29.3mm represents the average current path for arm2 to radiate at 2.5GHz whereas arm 1 current experiences a longer path of H+L= 98.5mm allowing arm1 to radiate around 765MHz. Arm1 is also lengthened by adding Ha1 improve the matching of the low band, however this extra length contributes in forming the L-Shape slots structure and its effect on the antenna matching will be studied in section 2.4.

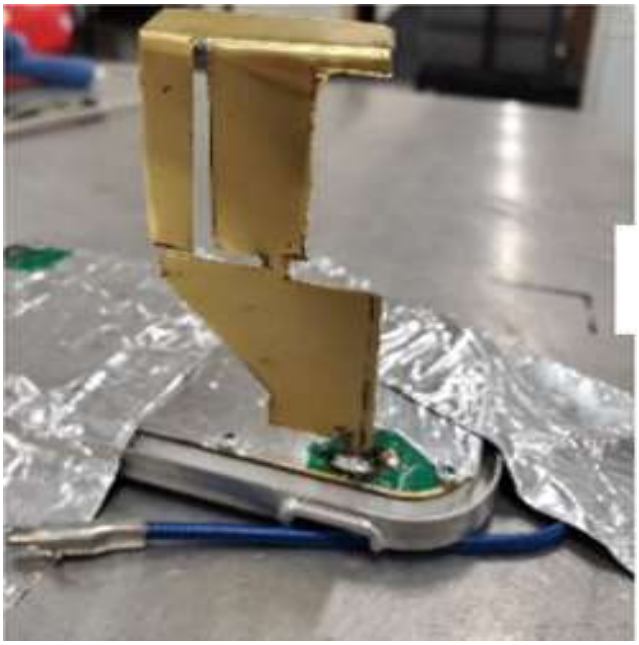

(a)

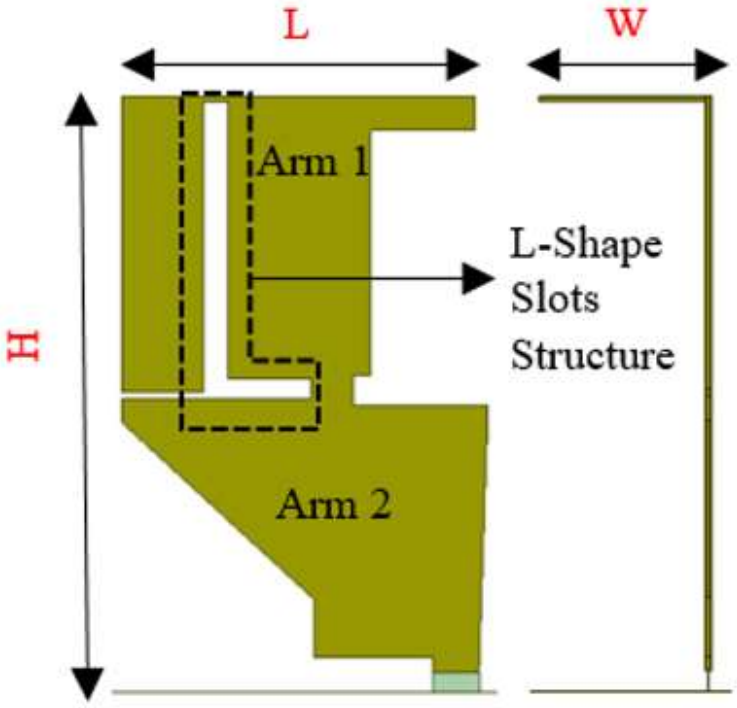

(b)

Figure 2.1. Cellular 5G antenna in (a) isometric view of realized antenna; and (b) front and side view of the antenna with L-Shape slots structure.

The antenna geometrical dimensions are presented in Figure 2.2 with their corresponding optimal values listed in Table 2.4. Individual values selections are going to be discussed more in future sections. Figure 2.3 shows that the antenna has been placed symmetrically towards the rear of the roof of the vehicle ready for chamber measurements, simulation results, on 1-meter GND measurements, and vehicle-level measurements are collectively discussed in the following section.

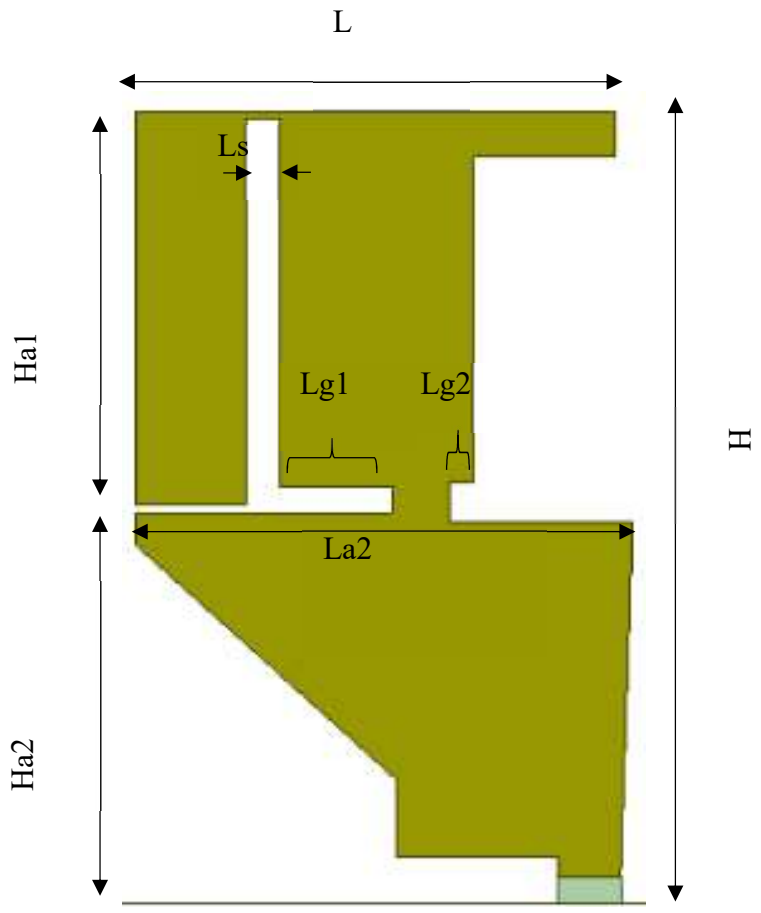

Figure 2.2. Cellular 5G antenna geometrical dimensions.

Table 2.4. Values of Geometrical Parameters of the Designed Antenna

Parameter	Value (mm)
H	60
L	38.5
W	14.9
Ha1	30
Ha2	29.3
Lg1	9
Lg2	2
Ls	2.6
La2	39.8

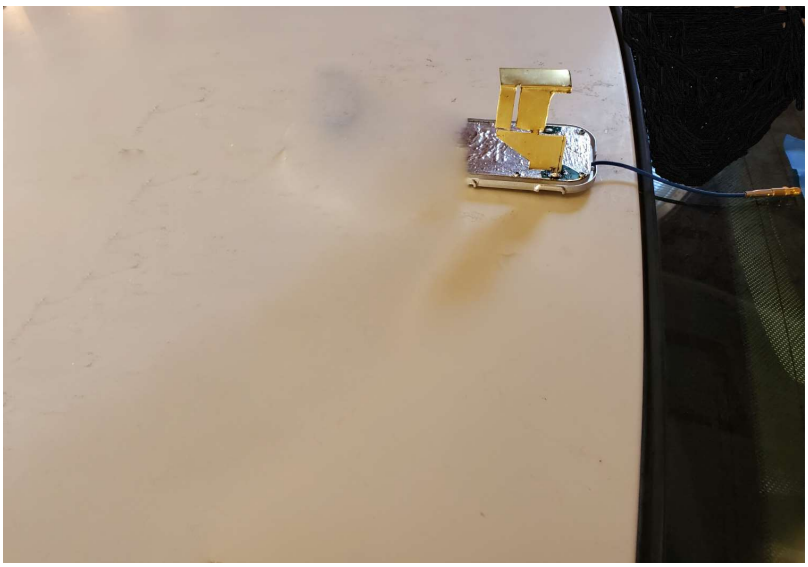

Figure 2.3. Cellular 5G antenna placement on vehicle's roof.

2.3 Branched Monopole Antenna Results

2.3.1 Matching and Surface Current Density

The antenna's simulated and measured reflection coefficient is shown in Figure 2.4. Across the frequency range 617MHz- 960MHz, the return loss is better than 5.6 dB whereas a return loss of better than 10 dB is noticed across higher frequency ranges from 1710MHz- 2490MHz and 3300MHz- 5000MHz. Figure 2.4 also demonstrates good agreement between the simulated and measured reflection coefficient with both of them showing reasonable rejection at the L1/L2/L5 GNSS frequency bands.

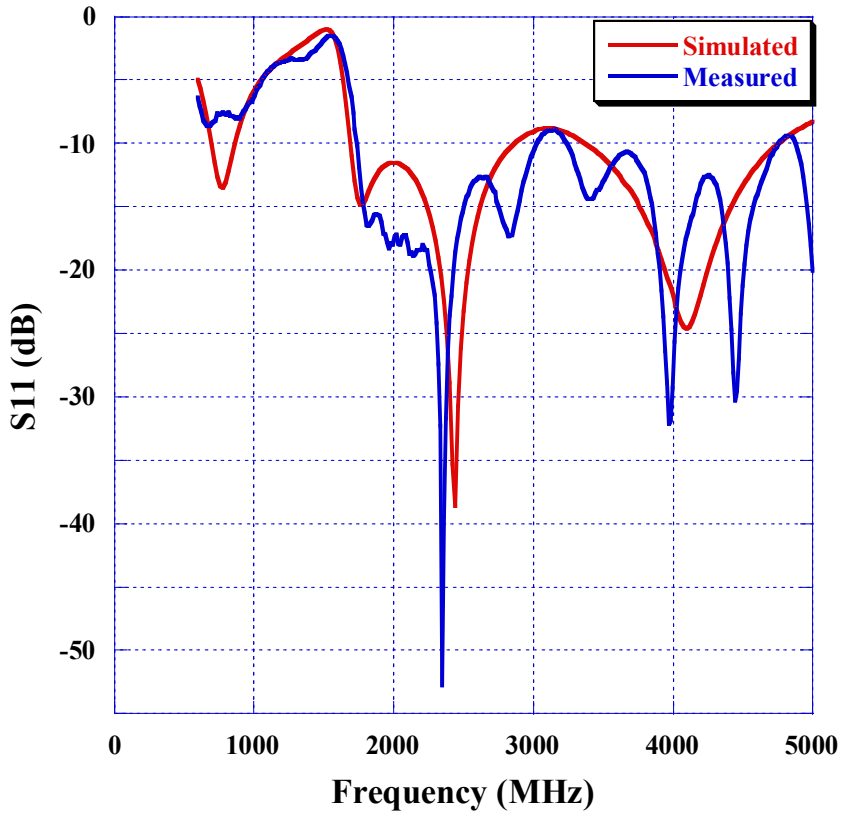

Figure 2.4. On 1-meter GND 5G cellular antenna simulated and measured reflection coefficient in dB.

The simulated surface current distribution on the antenna in (A/m) is shown in Figure 2.5 where a sample that represents low, mid, and high bands was taken to illustrate the operation principle of the antenna. The low frequency band presents the most intense current in the antenna, especially in the arm 1 structure. The surface current starts shifting slightly and transitions into the arm 2 structure at higher frequencies while being prevented from going to arm 1 due to the L-Shape slots structure which acts like a GNSS band stop filter.

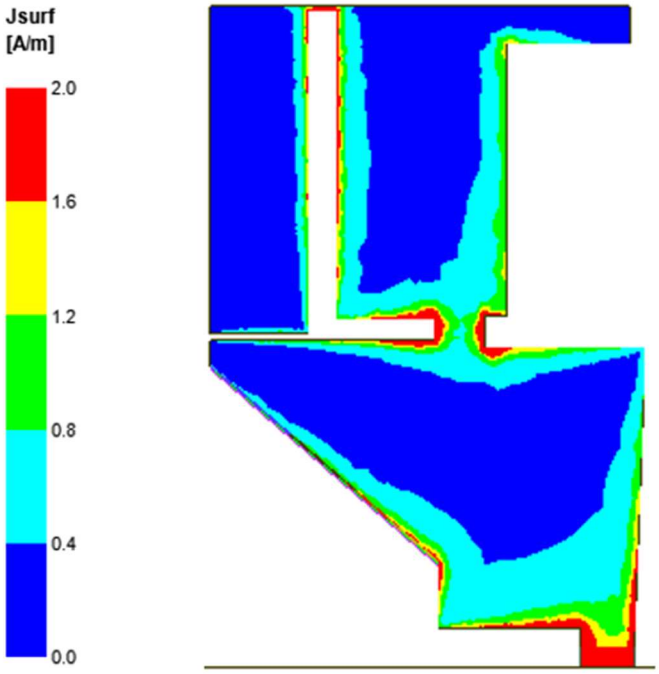

(a)

Figure 2.5. Simulated service current density measured in (A/m) at sample frequencies: (a) 617MHz, (b) 1900MHz, (c) 3900MHz, and (d) 5000MHz.

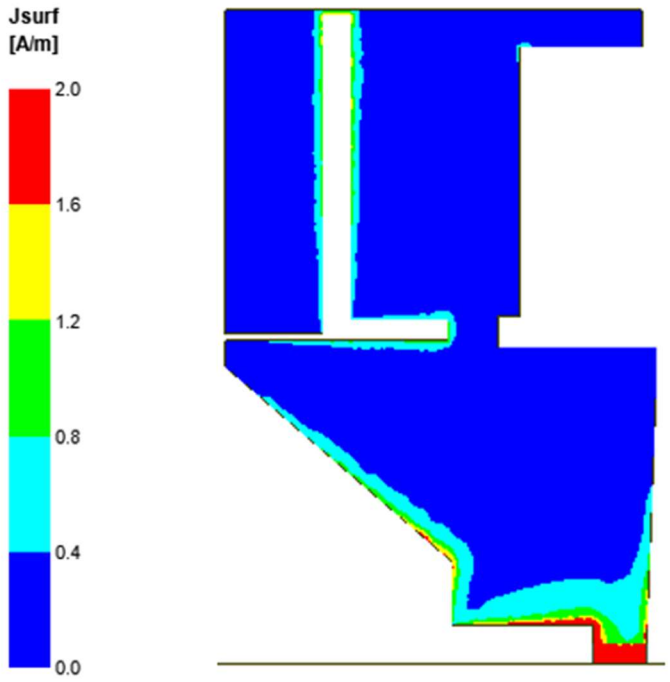

(b)

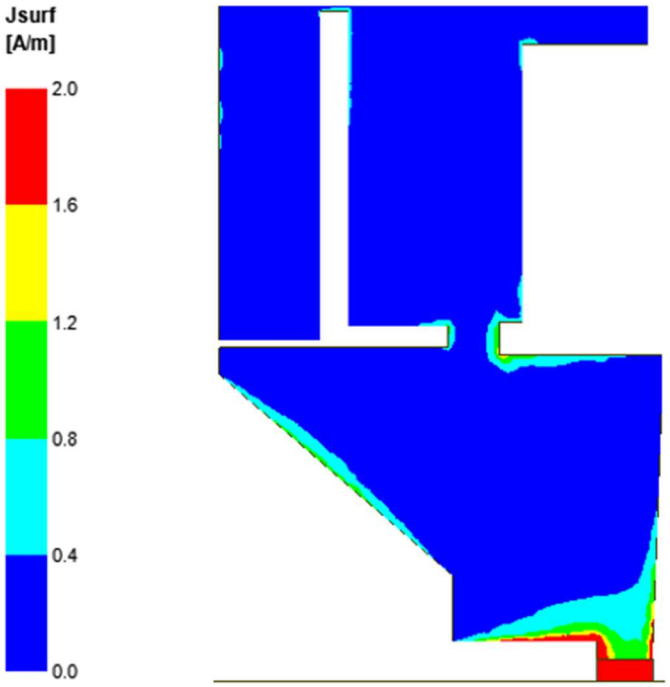

(c)

Figure 2.5. Continued.

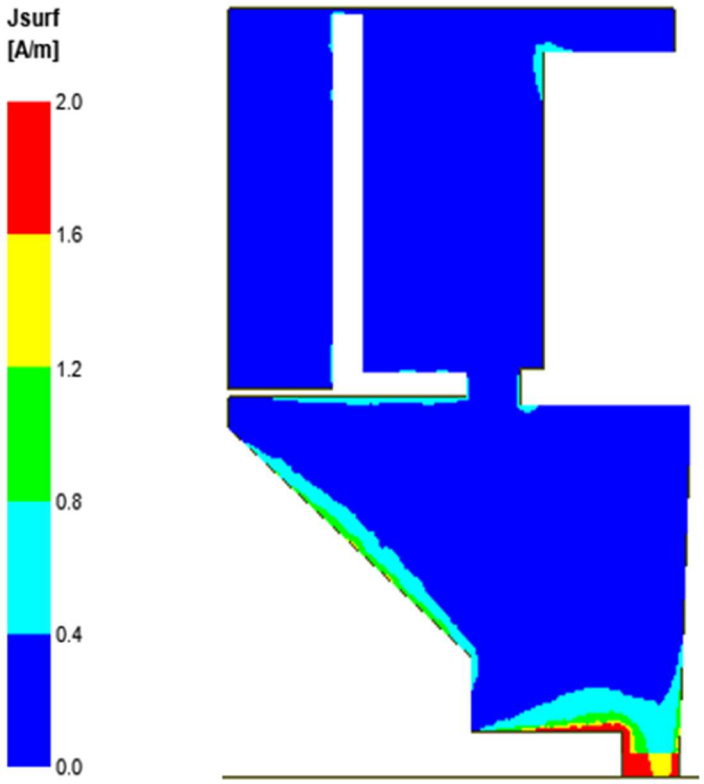

(d)

Figure 2.5. Continued.

2.3.2 Antenna Radiation Pattern, Gain, and Efficiency

An omni-directional pattern is important for cellular coverage around the vehicle across theta angles 70-90 degrees. In Figure 2.6, the vertically polarized gain vs. azimuth angles at a theta angle of 80 degrees are shown at different frequencies (namely 617MHz, 1.9GHz, 3.9GHz, and 5GHz). The three data traces on each sub-plot correspond to the simulated antenna performance, measurements on a one-meter diameter GND, and measurements on the vehicle roof. The antenna gain measurements follow the same omni-directional behavior; however, the results for the measurements on the vehicle appears to be more directive towards the front-end of the vehicle at 3.9 GHz and 5 GHz because electromagnetic waves reflections due to roof curvature, which explains the more directive behavior of the radiation pattern at high frequencies. Moreover, the LAG observed from vehicle radiation patterns is found to be –0.2dBi, 2dBi, -0.1dBi, and 2.8dBi at frequencies 617MHz, 1.9GHz, 3.9GHz, and 5GHz, respectively. Figure 2.7 shows simulated vertical (Gain Theta) and horizontal (Gain phi) performance of the proposed antenna at 80 deg of Theta at the aforementioned frequencies. The huge difference between the two polarizations indicates that the antenna is adequately vertically polarized and consequently capable of reducing mismatch loss from base stations.

Figure 2.8 shows the simulated and measured total antenna efficiency. The GND measurement has an average of 87% efficiency across all frequency bands whereas the vehicle measurement has a reduced average efficiency of 83%. This discrepancy is attributed to reflections of electromagnetic waves from the roof curvature and paint which worsens the grounding of the antenna especially at the lower frequencies.

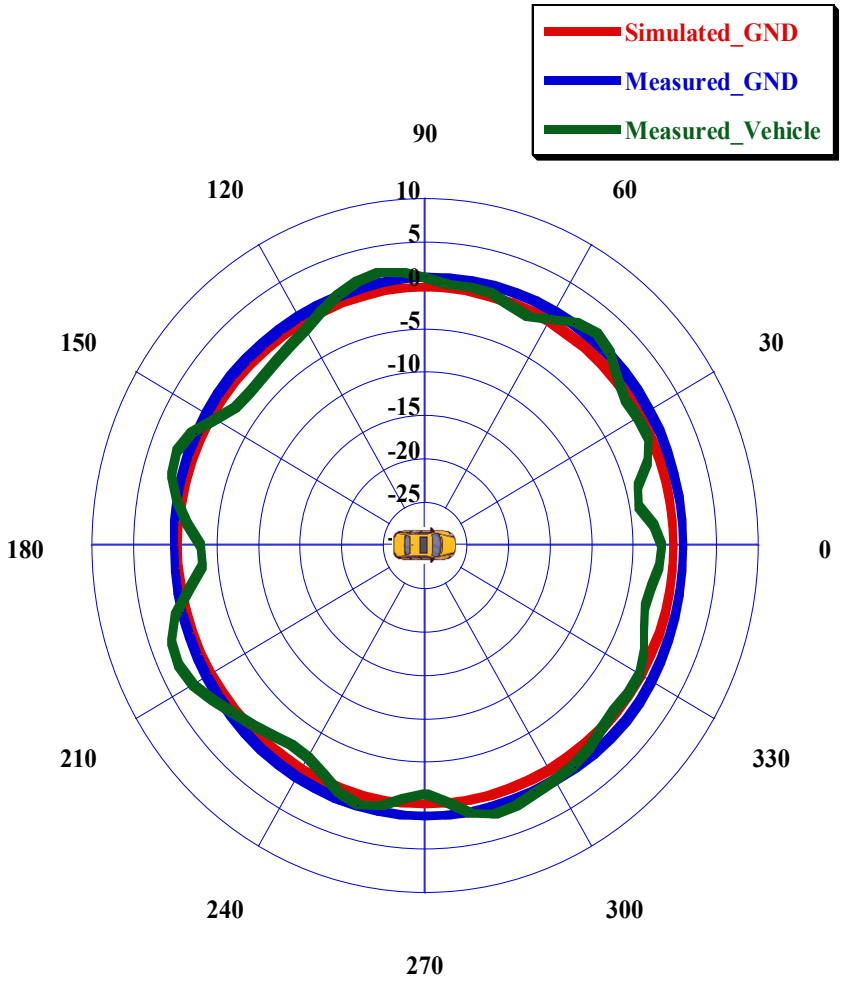

(a)

Figure 2.6. Comparison of 5G cellular antenna simulated, measured on GND, measured on vehicle realized vertical gain at θ = 80 degree and frequencies: (a) 617MHz, (b) 1900MHz, (c) 3900MHz, and (d) 5000MHz.

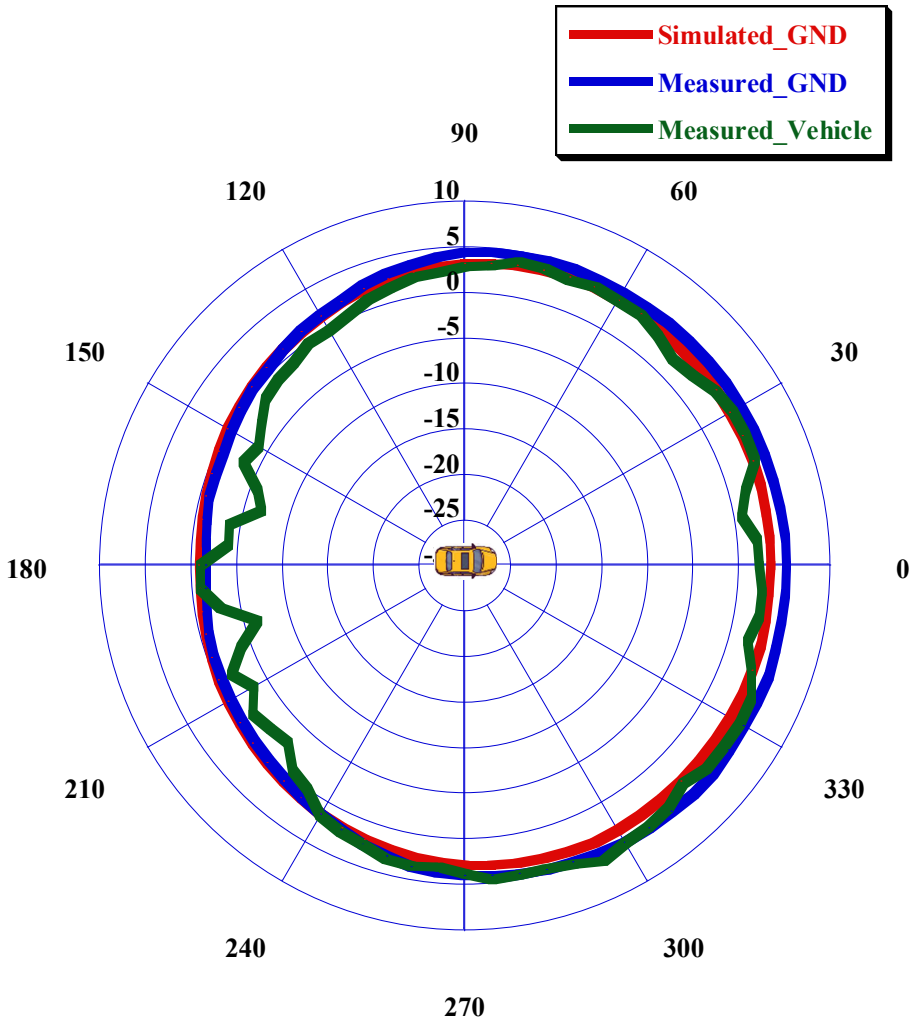

(b)

Figure 2.6. Continued.

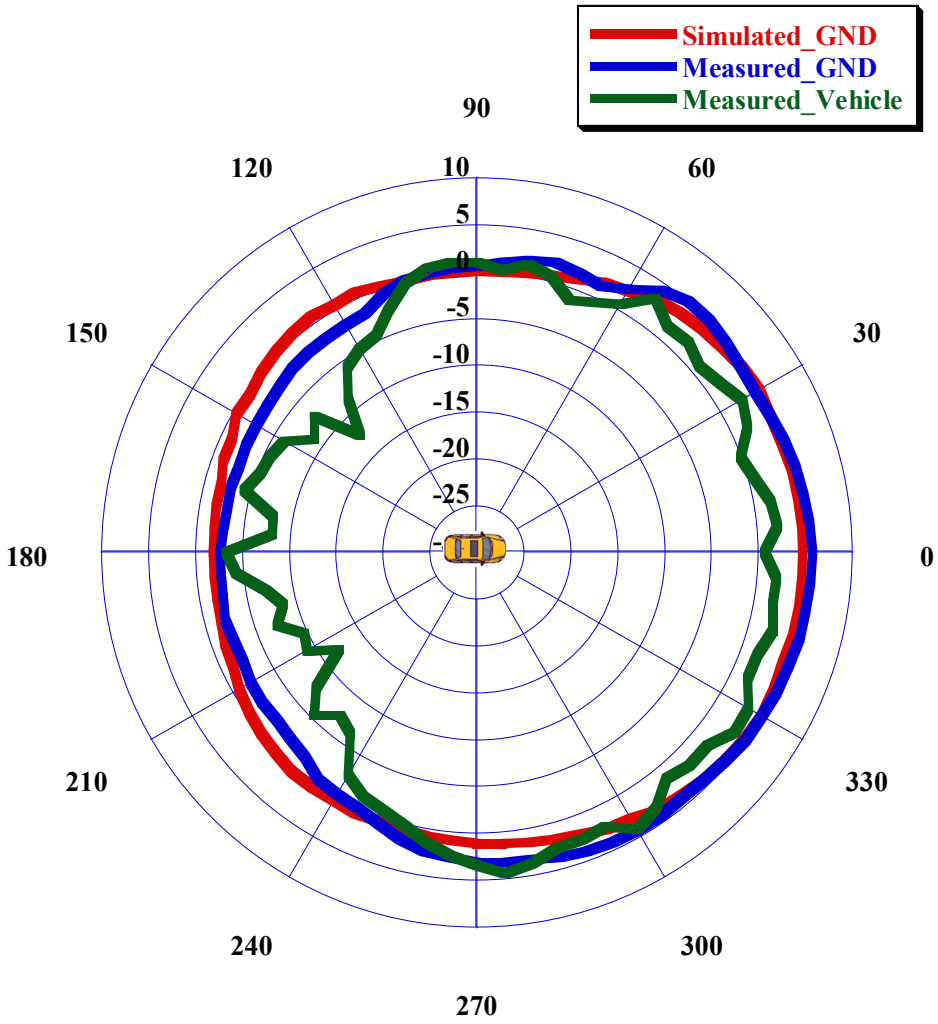

(c)

Figure 2.6. Continued.

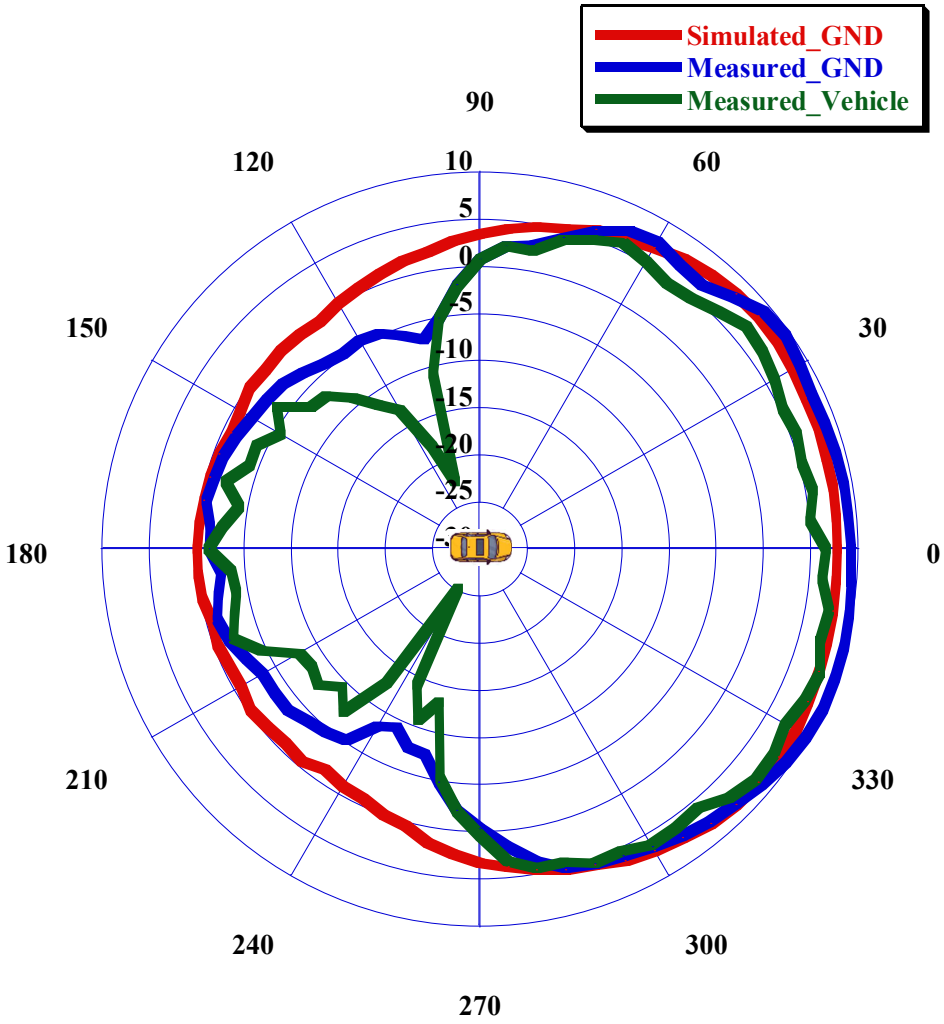

(d)

Figure 2.6. Continued.

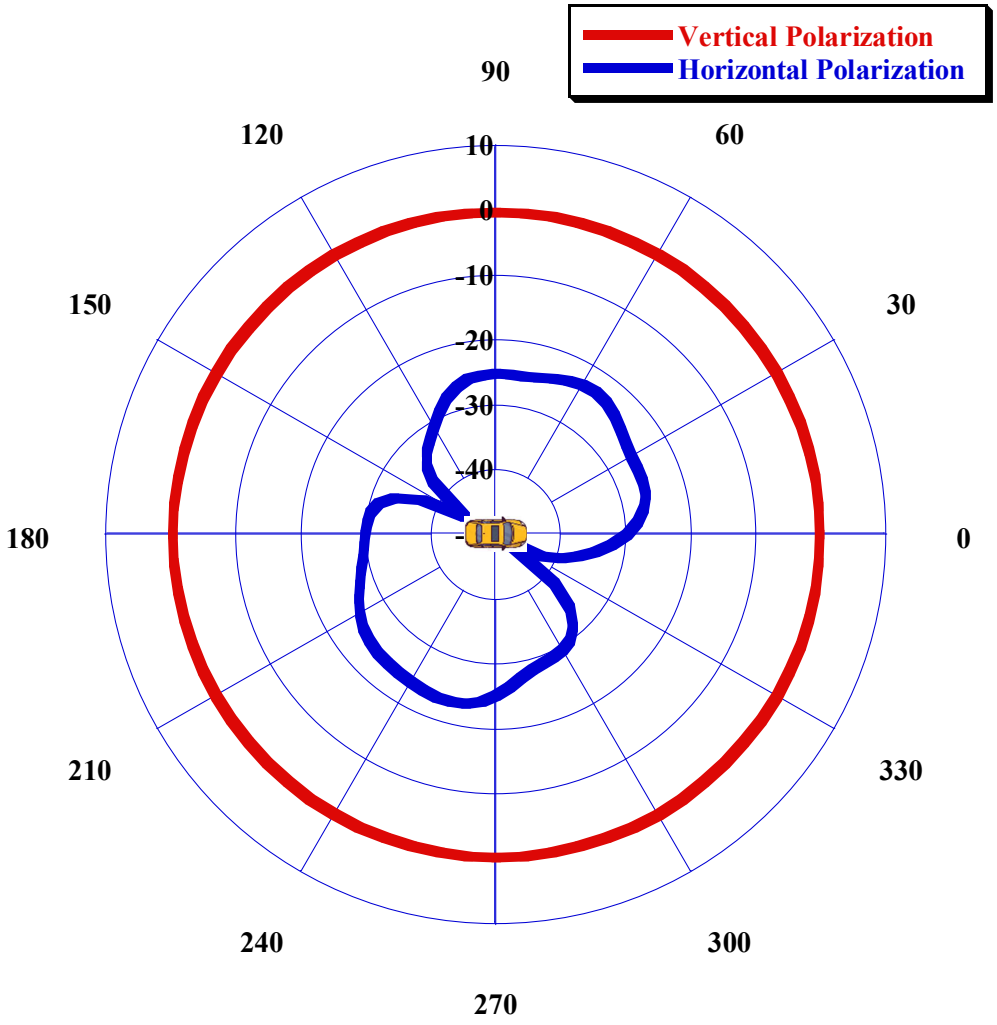

(a)

Figure 2.7. Comparison of 5G cellular antenna simulated vertical gain (gain Theta) and horizontal gain (gain Phi) polarizations at θ = 80 degree and frequencies: (a) 617MHz, (b) 1900MHz, (c) 3900MHz, and (d) 5000MHz.

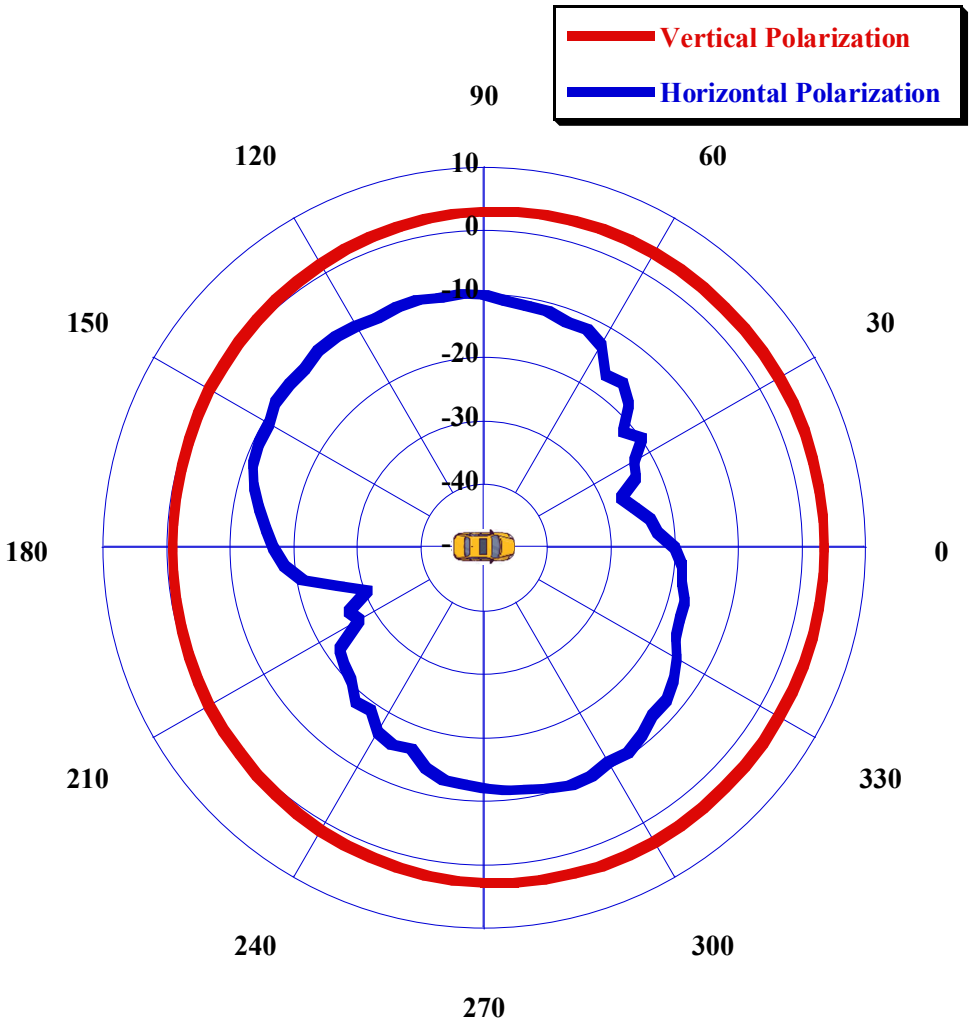

(b)

Figure 2.7. Continued.

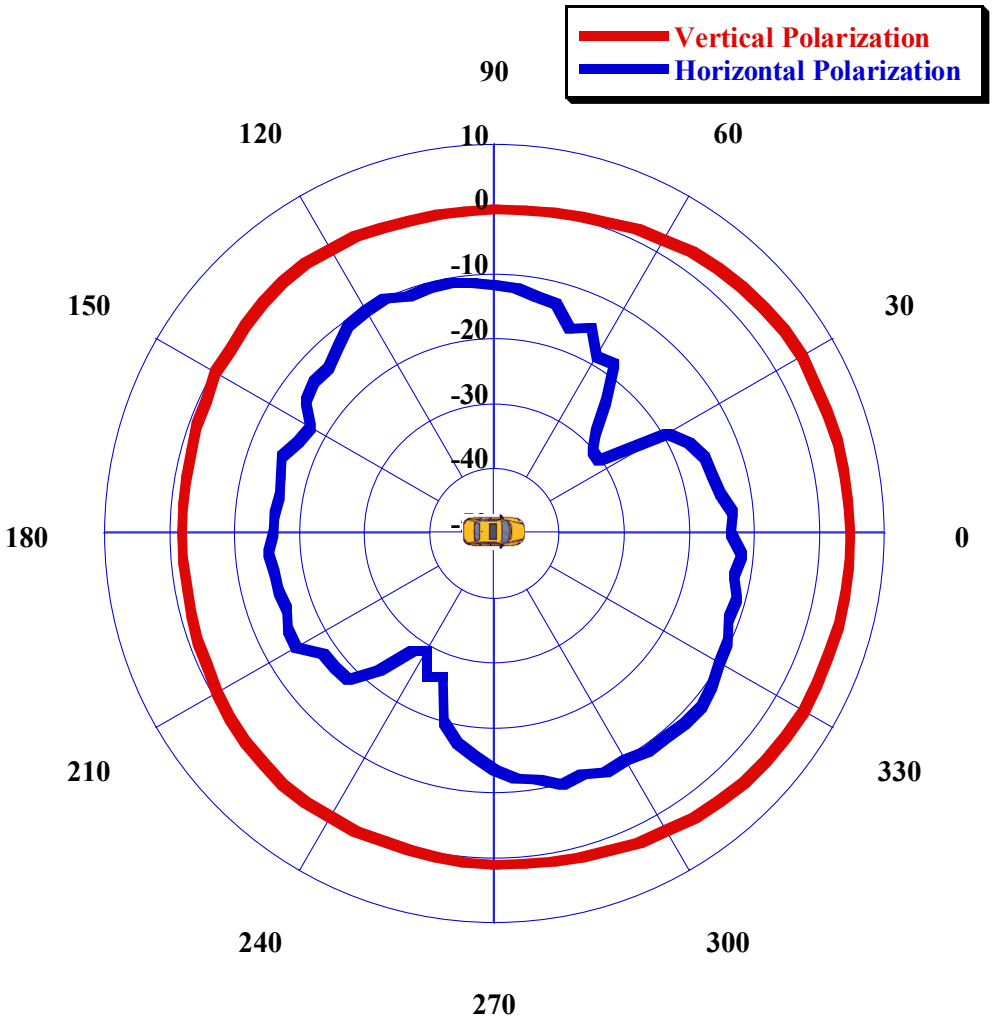

(c)

Figure 2.7. Continued.

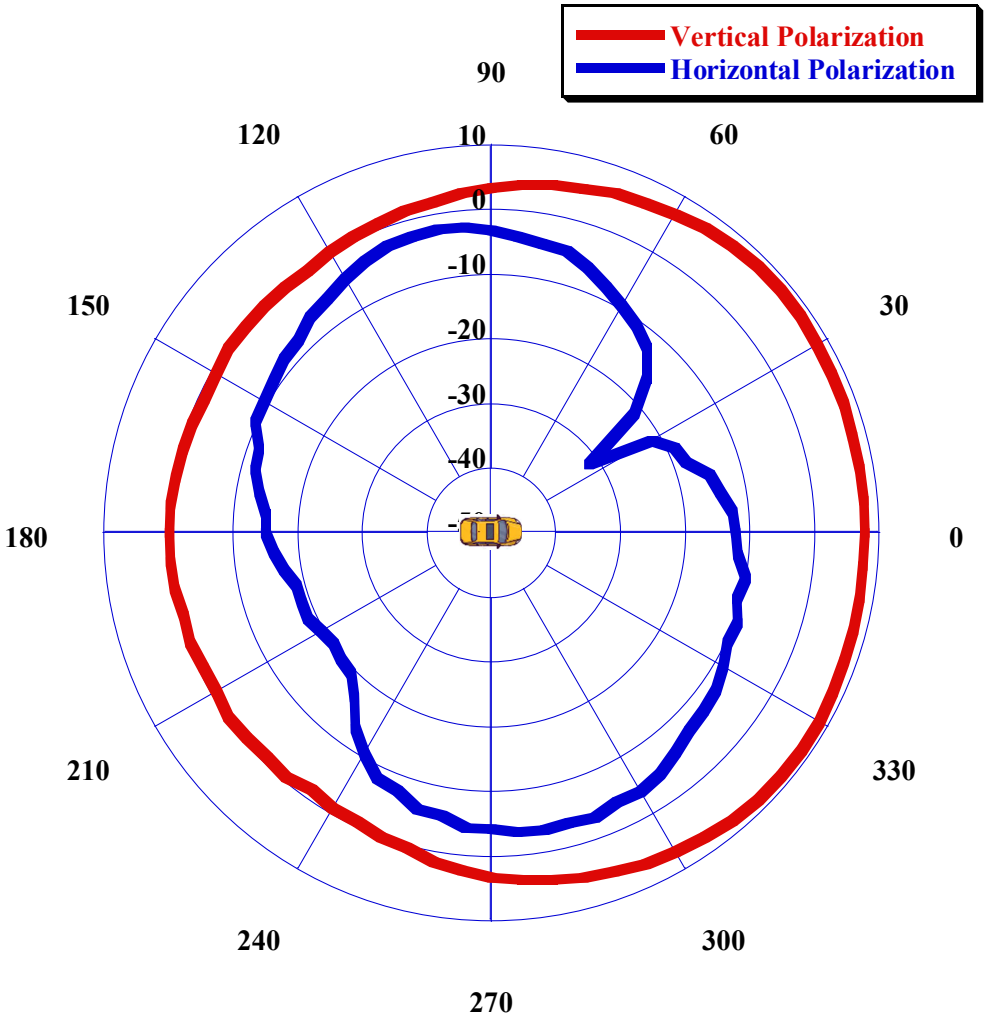

(d)

Figure 2.7. Continued.

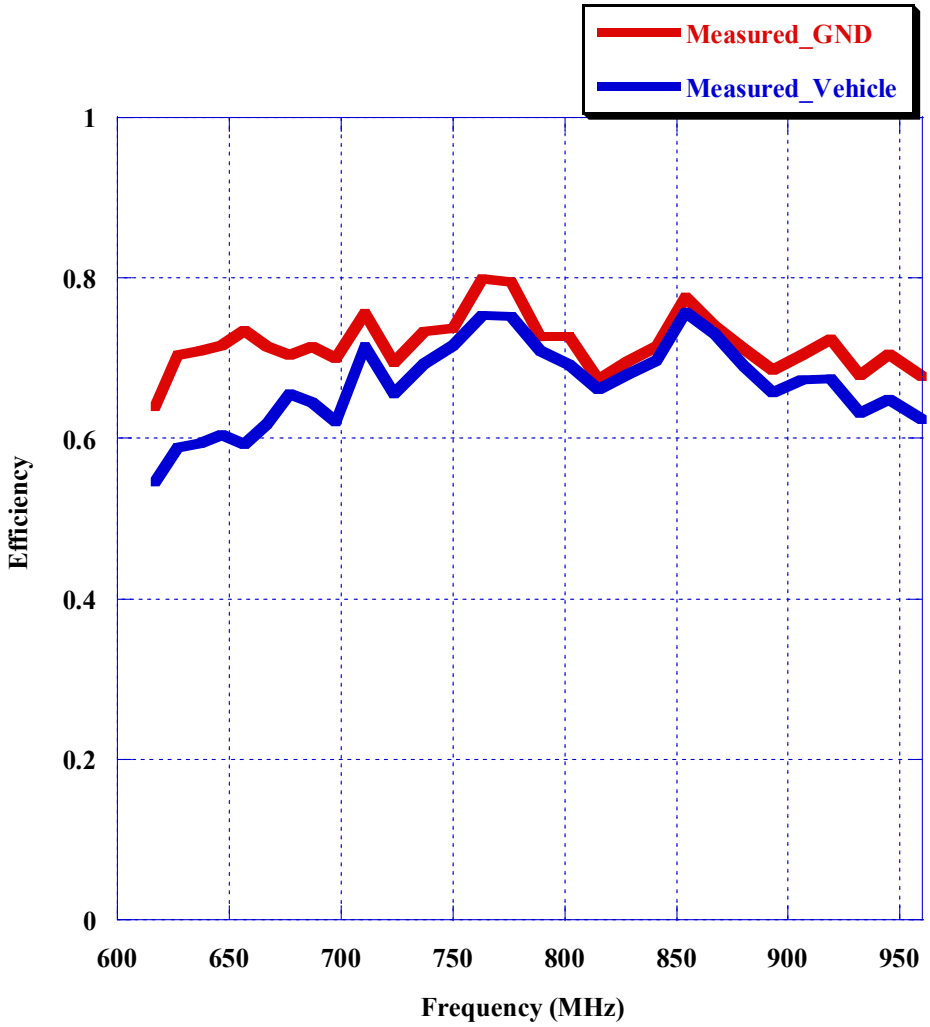

(a)

Figure 2.8. Comparison of total cellular 5G antenna efficiency measured on GND and on vehicle roof for frequency ranges (a) 617MHz- 960MHz, (b) 1710MHz- 2690MHz, and (c) 3400MHz- 5000MHz.

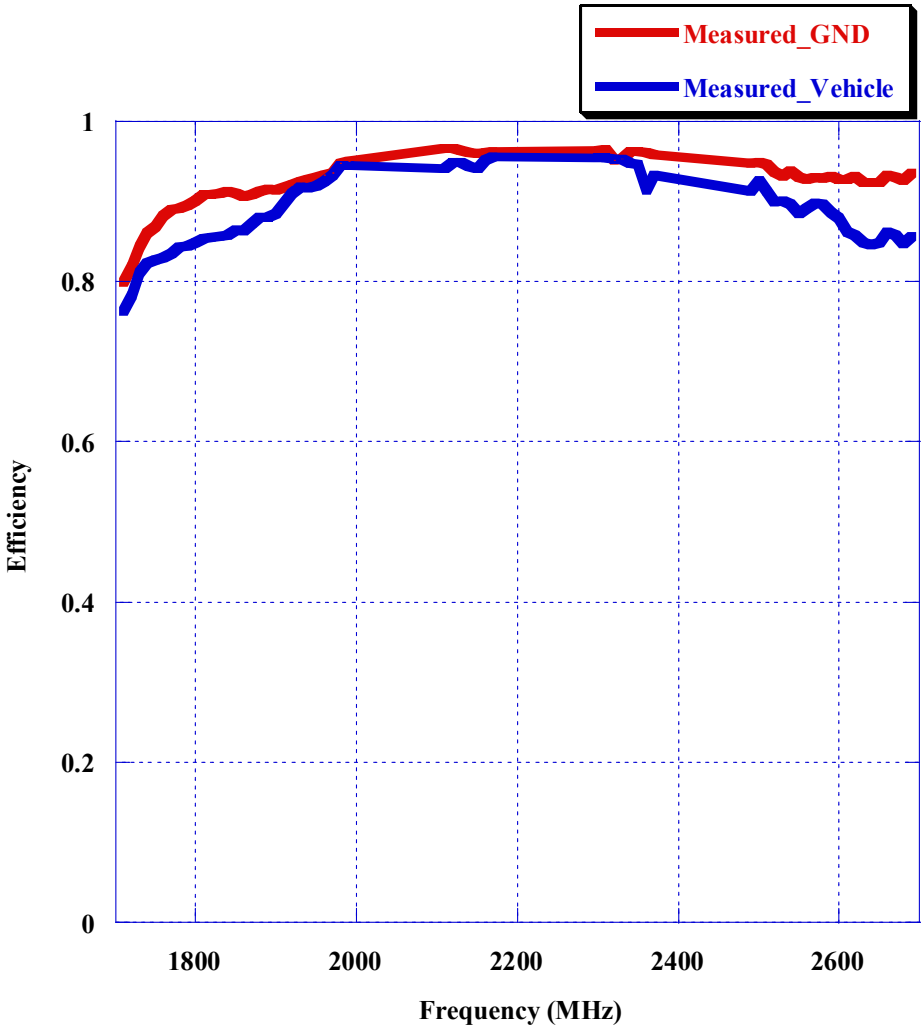

(b)

Figure 2.8. Continued.

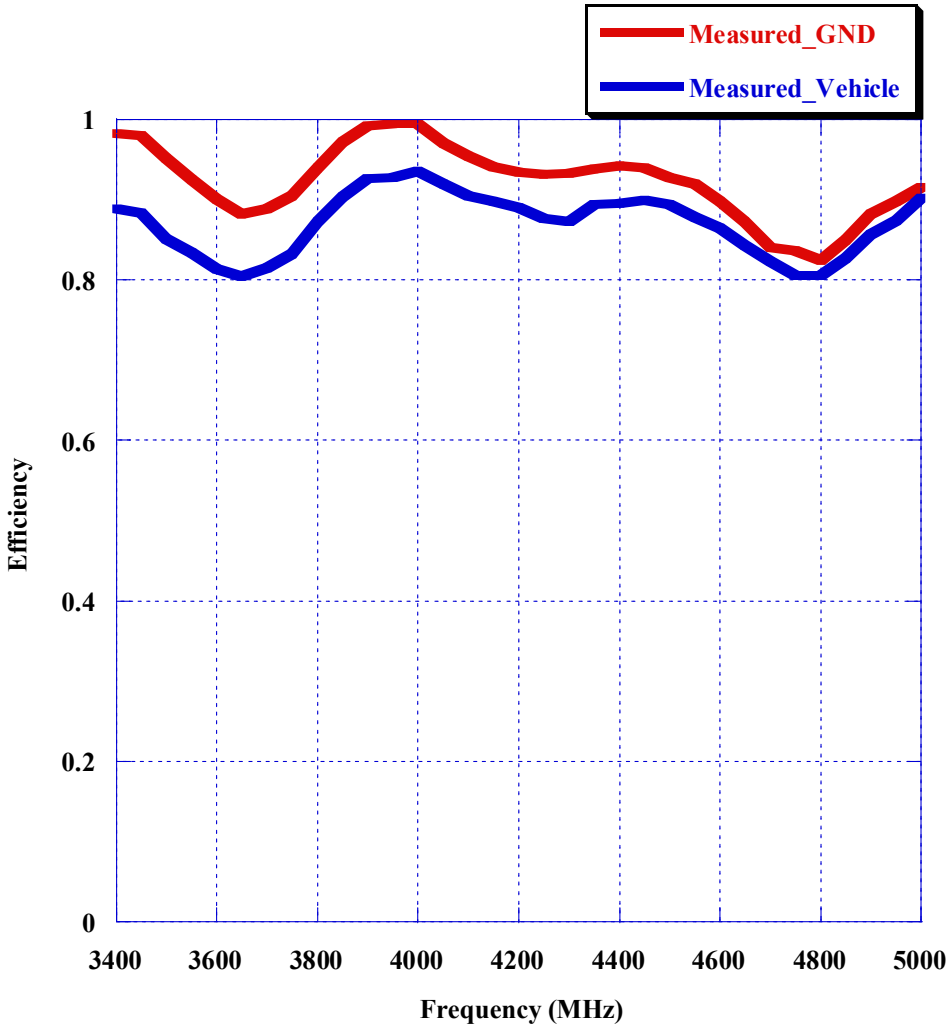

(c)

Figure 2.8. Continued.

An effective method to measure the 5G antenna performance in automotive industry is by calculating the LAG across the theta angles from 70 to 90 degrees above the horizon as in Table 2.3. These angles mimic the incoming RF signals incident from cellular towers. LAG in decibels is for a given frequency (f) and polarization (γ) given by:

$$LAG_{dB}(f,\gamma) = 10log_{10}\left[\frac{\sum_{i=1}^{M}\sum_{j=1}^{N} sin(\theta_i)G_{linear}(f,\theta_i,\varphi_j,\gamma)}{MN}\right] \quad (2.1)$$

where, θ_i is a discrete theta angle in degrees referenced via the index i; M is the number of theta angles (which is 21 angles for theta from 70 to 90 deg); φ_j is the phi angle in degrees referenced by the index j; N is the number of phi angles (which 360 angles for phi from 0 to 359 deg); and $G_{linear}(\theta_i, \varphi_j)$ in the gain in linear units for a discrete point on the spherical surface for a given frequency (f) and polarization (γ).

Figure 2.9 shows the LAG in dBi measured across frequency. In general, vehicle LAG is slightly lower than the GND LAG. However, both measurement scenarios have LAG values that are greater than -1 dBi across the entire band which indicates good antenna performance as well as passing the design goals listed in Table 2.3.

The results in this section demonstrate that the designed antenna has generally good performance in terms of matching characteristics, vertical gain, and efficiency and all these performance metrics are conforming with design goals listed in Table 2.3. it is also evident that there is a small difference between antenna simulation and measurements indicating a sound antenna element design. Next parametric study is presented.

2.4 Parametric Study

In this section parametric study of several significant geometrical parameters and features in the antenna element is presented. In reference to Figure 2.2, the parameters that are investigated include:

- separation length between the sheets in arm 1 (Ls)
- length of the slots in arm 1 (Lg1, Lg2)
- length of the vertical sheet in arm 1 (Ha1)
- length of arm 2 that controls the high bands (La2).

Figure 2.9 shows the effect of L-Shape slot structure on the antenna performance. Figure 2.9(a) shows the variation of reflection coefficient for four different values of Ls including 0.6mm, 2.6mm, 4.6mm, and 0mm whereas Figure 2.9(b) shows the variations for three values of Lg1 namely 6mm, 9mm, and 13mm. It is noticed that the two parameters Ls and Lg1 have an effect particularly on the GNSS rejection peak. In fact, increasing Ls/Lg1 slot will lower the GNSS rejection filter center frequency. On the other hand, reducing Ls/Lg1 length will shift GNSS rejection peak towards higher frequencies and this is clearly shown in a particular case when there is no Ls gap (Ls=0mm). Choosing Ls and Lg1 to be 2.6mm and 9mm respectively as proposed in the design is optimal to balance the reflection coefficient around GNSS rejection peak and consequently improving the antenna matching at low band frequencies specially around 960MHz.

Furthermore, changing the value of parameter Ha1 has an important role in the low frequency band, and it also alters the L-Shape slots structure and thus shift the GNSS

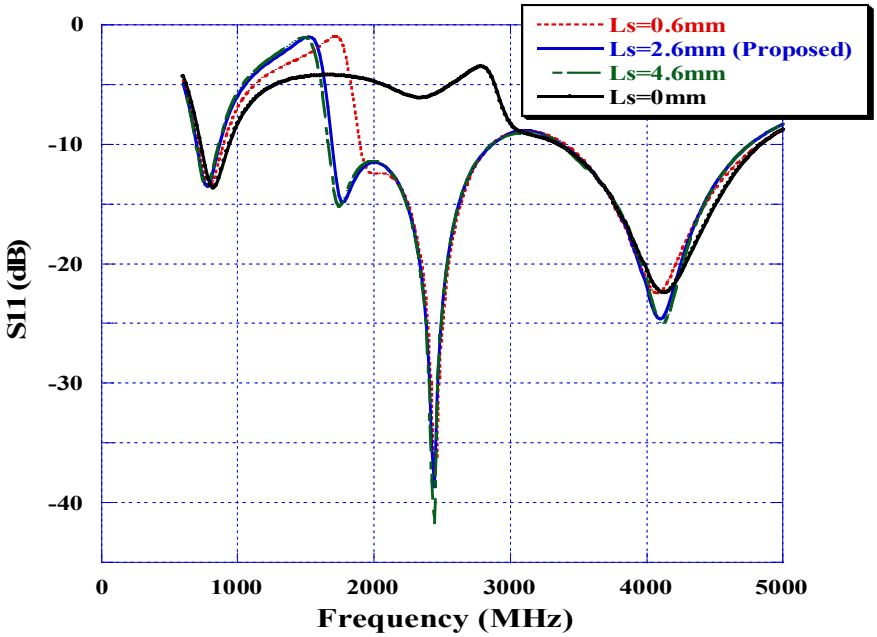

(a)

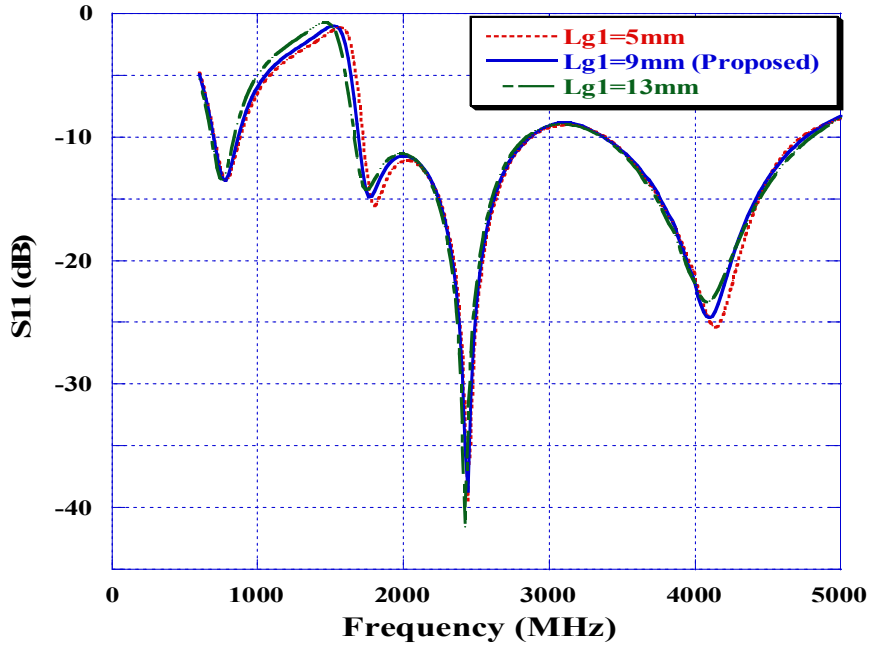

(b)

Figure 2.9. Simulated reflection coefficient of varying L-Shape slots structure parameters: (a) Ls and (b) Lg1.

rejection in frequency. As shown in Figure 2.10, increasing the value of Ha1 supports a larger wavelength current in the low frequency band which shifts antenna resonance at 617-960MHz band towards lower frequencies. In addition, reducing or increasing Ha1 length change the location of GNSS band rejection peak. A special case when Ha1 is tall enough to bridge arm1 and arm2 together is shown in Figure 2.10 with Ha1=30.7mm, in this case the GNSS band reject filter can no longer operate and hence keeping Ha1 less than 30.7mm is crucial for GNSS band stop filter operation. A value of Ha1=30mm was selected since it grants optimal reflection coefficient performance across low band as well as it allows balanced GNSS band rejection.

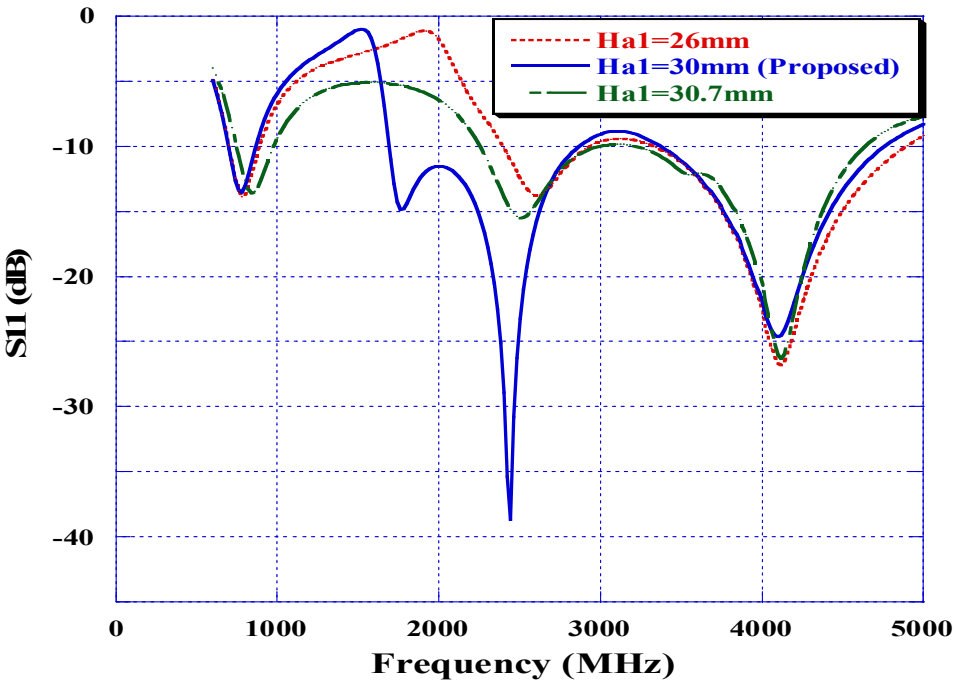

Figure 2.10. Simulated reflection coefficient of varying vertical sheet length Ha1.

In Figure 2.11, the length of arm 2 was analyzed for three different values: 35.8mm, 39.8mm, and 43.8mm. The parameter La2 has a significant effect on the high frequency bands. It was concluded that increasing the length of arm 2 worsening the reflection coefficient at 4-5GHz band since the resonance shifts to lower frequencies while reducing its length will have a better reflection coefficient at 4-5GHz band while having a slightly worse reflection coefficient at 3– 4GHz band.

Lg2 Slot variation shown in Figure 2.12 also has an insignificant effect on the high band resonance around 4.2GHz. Finally, as it can be seen in Figure 2.13, increasing the width of the antenna (W) does not only lower the low band resonance but it also has similar effect on the rest of antenna bands.

In summary, antenna distinctive geometrical features were deeply studied and improved the understanding of antenna working principle. Table A.1 in the APPENDIX compares the developed antenna in this chapter to related literature antennas in the automotive industry.

2.5 Conclusions

A multi-wideband branched monopole antenna was presented in this Chapter that functions across the 5G frequency band from 617 MHz to 5 GHz. It consists of two arms with different dimensions to provide resonances at low and high bands. The antenna was simulated and then measured on a one-meter GND and on a vehicle's roof inside an anechoic chamber. The measurements show exhibited VSWR performance less than 3.2:1 (5.6dB return loss) and an average efficiency of 87% on a GND and 83% on the vehicle. The LAG performance was better than -1dBi across the entire frequency band for the elevation range from 0 degrees to 20 degrees above the horizon.

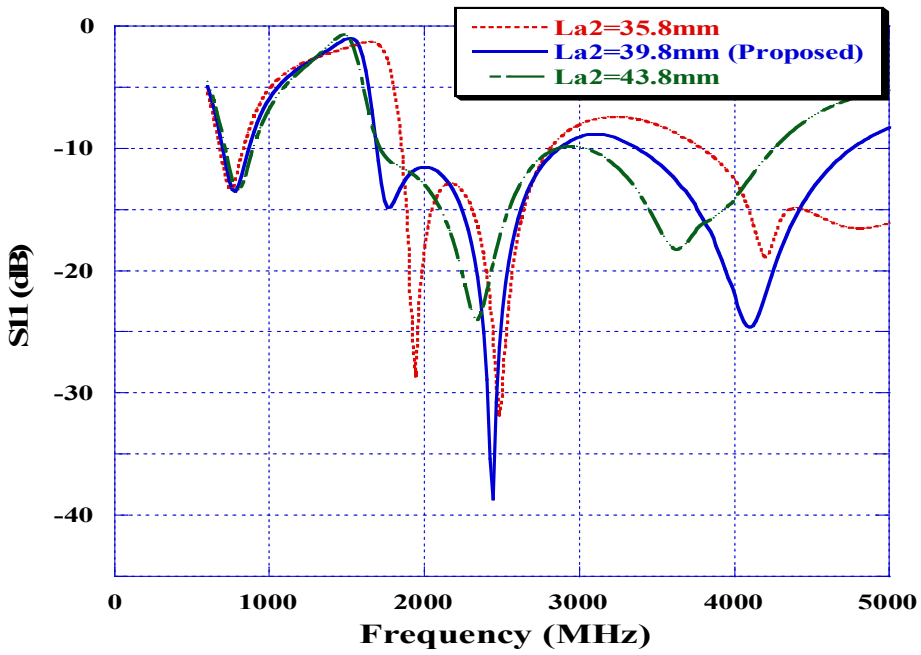

Figure 2.11. Simulated reflection coefficient of varying arm2 length La2.

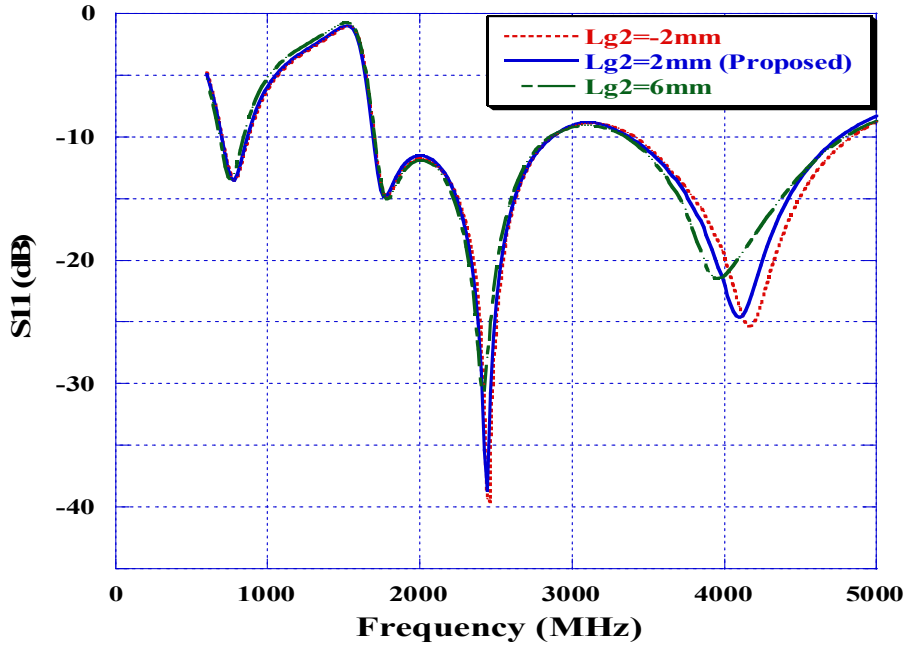

Figure 2.12. Simulated reflection coefficient of varying length of Lg2 slot.

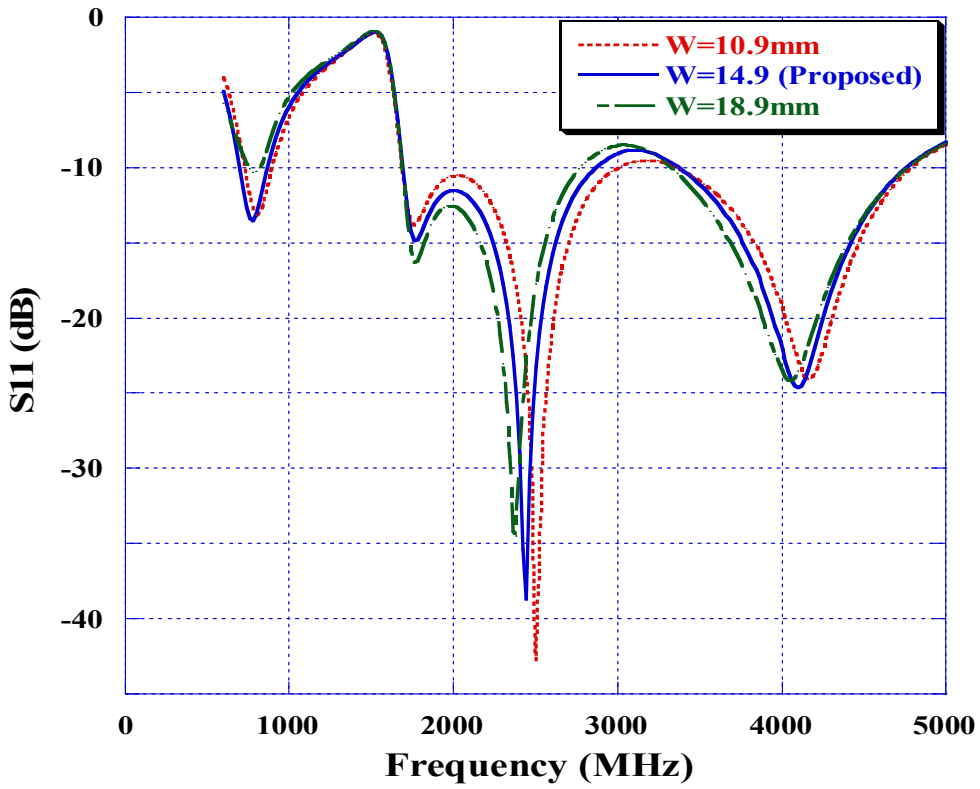

Figure 2.13. Simulated reflection coefficient of varying antenna width (W).

The parametric study of different geometrical variables was analyzed and revealed that the antenna has a resilient design which makes it suitable for manufacturing with an acceptable tolerance of each parameter's dimension. In general, the proposed antenna design is a good candidate for on-vehicle roof shark-fin antennas. The antenna is very attractive for automotive applications since it is easy to manufacture and has compact size, light weight, and low cost.

CHAPTER THREE

5G CELLULAR MIMO SYSTEM STRUCTURES

3.1 Introduction

With the expansion of the cellular systems being integrated in cars to support the connected vehicle effort, a need for multiple antennas support wireless service has emerged. The MIMO system consists of two or more antennas that receive or transmit multiple layers of orthogonal data streams from cellular base stations which allow for increased channel capacity, data rate and the total throughput of the system without increasing the operating frequency band or the transmit power [37]. To this date, 2x2 MIMO configuration with de-correlated antennas that receive two data streams is being used to realize downlink reception in modern vehicles [38]. The performance of the MIMO system is highly dependable on the efficient design of the MIMO antennas that should lower correlation between them and a high total antenna efficiency [39].

MIMO antenna systems performance metrics and implemented high order MIMO structures are presented next in this Chapter.

3.2 MIMO Antenna Systems Performance Metrics

3.2.1 Envelope Correlation Coefficient

An important characteristic of the communication systems is the ECC between MIMO system antennas. Small ECC values are crucial to increase transmission capacity as well as to improve the multipath fading. ECC tells how independent MIMO antennas radiation patterns are, for example, for a 2x2 MIMO system with vertically and horizontally polarized antennas ECC value will be 0. There are 2 ways to calculate the

ECC in a MIMO system [34], the first method used S parameters to find ECC and it assumes lossless/60% or more efficient antennas which is sometimes unrealistic. Whereas the second method (which is more accurate) used throughout this work utilizes radiation patterns of individual antennas to calculate the ECC of MIMO system.

The ECC can be related to the electric field radiation pattern through the equation in [34] as below:

$$\rho_{e,ij} = \left| \frac{\int_0^{2\pi}\int_0^{\pi}(XPR\,.\,E_{\theta i}\,.\,E_{\theta j}^{*}\,.\,P_{\theta} + XPR\,.\,E_{\phi i}\,.\,E_{\phi j}^{*}\,.\,P_{\phi})\sin(\theta)\,d\theta d\phi}{\sqrt{\prod_{k=i,j}\int_0^{2\pi}\int_0^{\pi}\left(XPR\,.\,E_{\theta k}\,.\,E_{\theta k}^{*}\,.\,P_{\theta} + XPR\,.\,E_{\varphi k}\,.\,E_{\varphi k}^{*}\,.\,P_{\phi}\right)\sin(\theta)d\theta d\phi}} \right|^2 \quad (3.1)$$

Where $E_{\theta i}$ and $E_{\theta j}$ are the values of electric field in the theta axis while $E_{\emptyset i}$ and $E_{\emptyset j}$ are the values of electric field in phi axis. Cross-polarization Ratio (XPR) tells the difference between incident electromagnetic wave vertical and horizontal polarization. P_{θ} and $P_{\emptyset}$ are the theta and phi power densities. Equation (3.1) can be simplified by setting XPR = 1 assuming uniform power densities.

3.2.2 Diversity Gain

Another MIMO system performance metric is the DG which is defined as the quantified improvement in signal-to-noise ratio (SNR) by the receiving signals from the MIMO antennas and usually calculated in dB. The DG can be calculated as in [40]:

$$DG = DG_0.DF.K \quad (3.2)$$

Where DG_0 is the ideal case diversity gain which is 10dB. DF is the degradation factor which shows how much the ECC impacts DG and is calculated as: $\sqrt{(1-\rho)}$. K represents the ratio of the mean effective gain (MEG) between the MIMO antenna

elements ($K = MEG_i/MEG_j$). MEG is the effective gain ratio at the antenna element, in other words MEG is the received to incident power ratio at the element. (K∼=1) condition should be satisfied for received signals by MIMO systems assuming good channel characteristics.

3.3 Comparative Study of 5G Cellular MIMO Systems

In this section, three different MIMO antennas configurations are being studied. The building block for each configuration is the branched Monopole element in Figure 2.1. The MIMO configurations are then simulated and measured on a 1-meter GND and on a vehicle's roof inside an anechoic chamber. The obtained data from simulations and chamber measurements are directly reported whereas ECC and DG results are generated using Octave software for each MIMO configuration in this section. The general design guidelines that are targeted are listed in Table 3.1.

3.3.1 Configuration I of a 2x2 5G MIMO system

The two Monopole elements were cut from a metal sheet, fed with coaxial cables, and placed in such a way that will result in an omnidirectional combined radiation pattern as well as a minimal ECC value. The system is simulated using HFSS then measured on 1-meter GND and on a car's roof with a port-to-port distance of 135mm. Typically, port-to-port distance is set to be greater than have of the wavelength at the lowest frequency to ensure low coupling between antennas. In this case it was set to 114 mm which is higher than $\frac{\lambda_{\text{Lowest\_freq}}}{2*\sqrt{\varepsilon_r}}$ on FR4 PCB with relative permittivity ($\varepsilon_r = 4.4$)) between Monopole elements. Figure 3.1 shows Configuration I of a 2x2 5G MIMO system simulation setup on GND while Figure 3.2 depicts the on a car roof placement.

Table 3.1. 5G Cellular MIMO system Design Goals and Guidelines

Parameter	Value
Polarization	VLP
Return Loss	5.4 dB (3.3 VSWR)
Average Total Efficiency	60%
Isolation	10dB
ECC	Less than 0.5

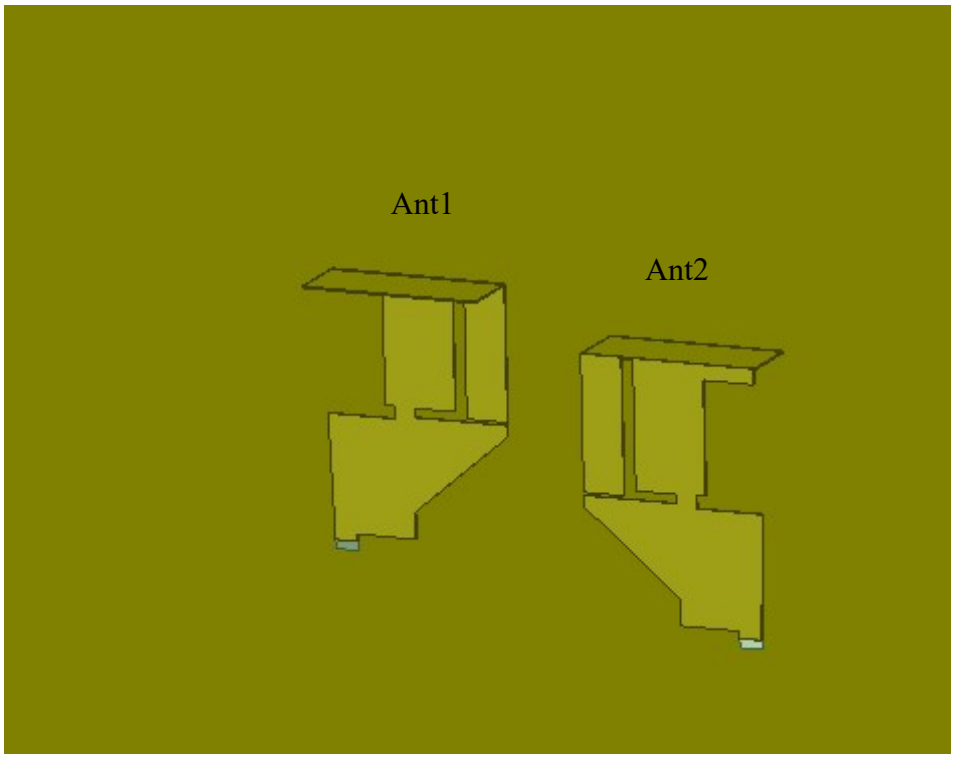

Figure 3.1. Configuration I of a 2x2 5G MIMO system simulation setup.

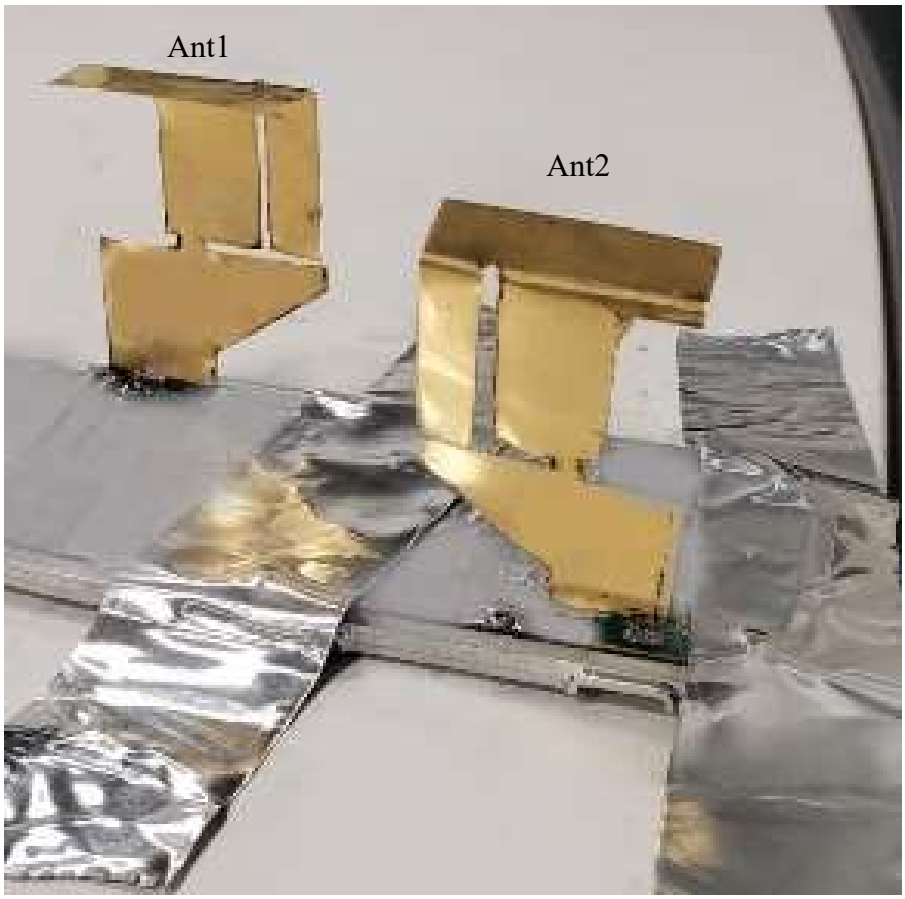

Figure 3.2. Configuration I of a 2x2 5G MIMO system placement on vehicle roof.

The performance of Antenna1 (Ant1) and Antenna2 (Ant2) of this MIMO system has been reported in terms of reflection coefficient and isolation as in Figure 3.3 Both antennas show an agreement between simulation and GND measurement. Good reflection coefficient values have been observed of a worse of -5.6dB and -6.4dB at 617MHz of Ant1 and Ant2 respectively with reasonable GNSS bands (1160MHz-1610MHz) rejection. Figure 3.3(c) shows a good isolation between Ant1 and Ant2 in this configuration of a worse case 12dB (expressed as -12 dB in S21 format).

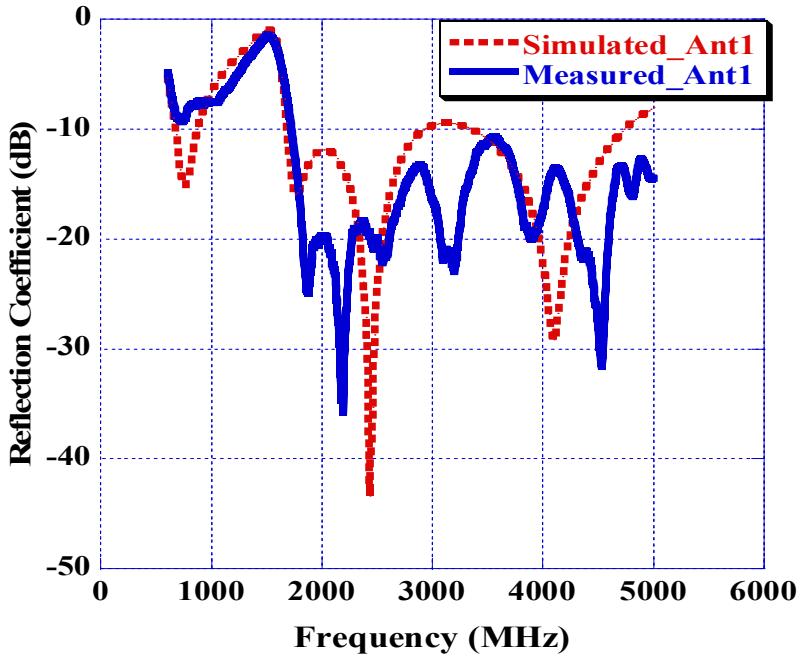

(a)

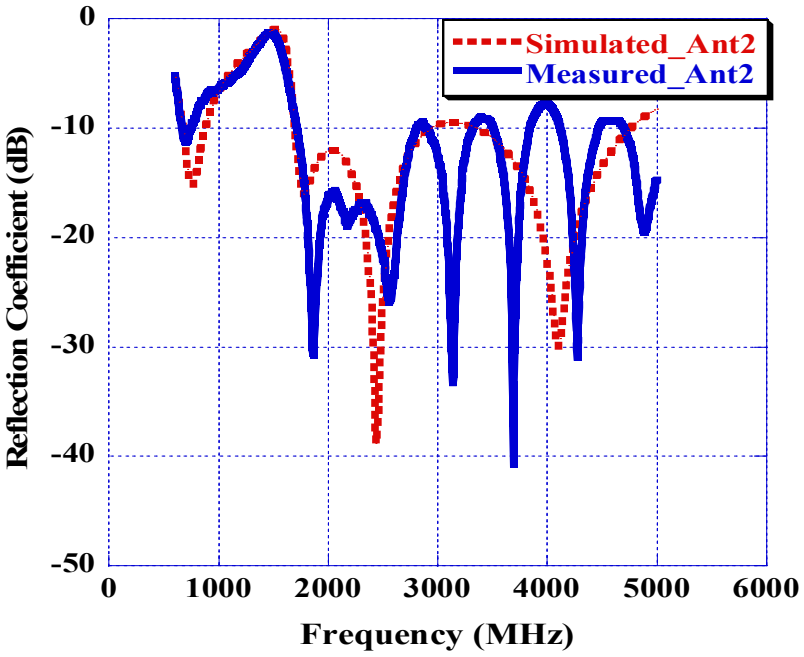

(b)

Figure 3.3. Configuration I of a 2x2 5G MIMO system simulated and measured (a) Ant1 reflection coefficient in dB, (b) Ant2 reflection coefficient in dB, and (c) Isolation between Ant1 and Ant2 in dB.

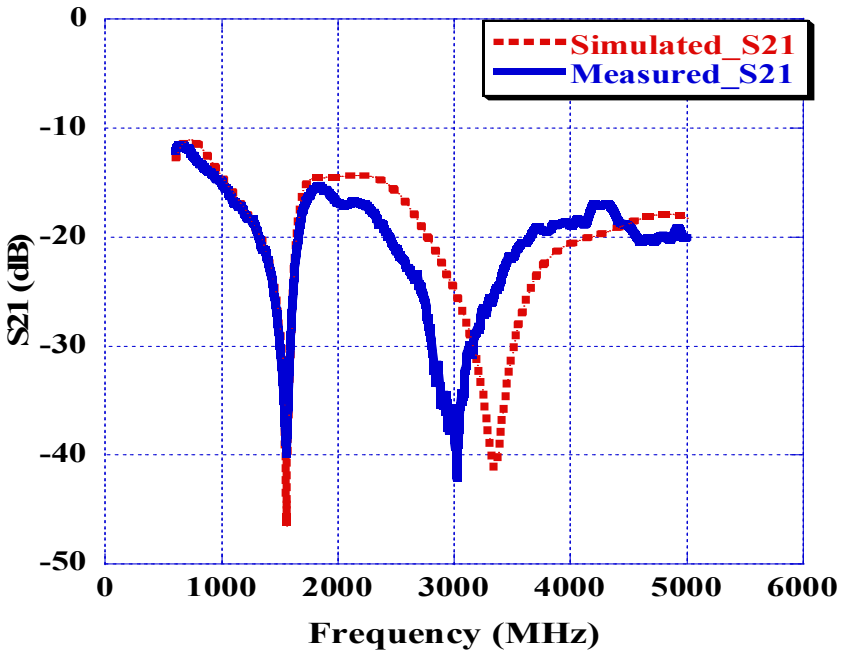

(c)

Figure 3.3. Continued.

Next, the total efficiencies of Ant1 and Ant2 have been captured after a successful placement of the MIMO system on 1-meter GND and then on a car roof and the results are shown in Figure 3.4. Both antennas exhibit higher efficiencies when placed on GND compared to placement on a car roof. It can be noticed that both antennas measured on GND have an average total efficiency of 79.8% across all 5G frequency bands while the average total efficiencies decrease to 74% and 71% when measured on a car roof for Ant1 and Ant2 respectively. Even with small coupling between the two antennas, individual antenna efficiencies got reduced compared to the standalone antenna discussed in Chapter 2

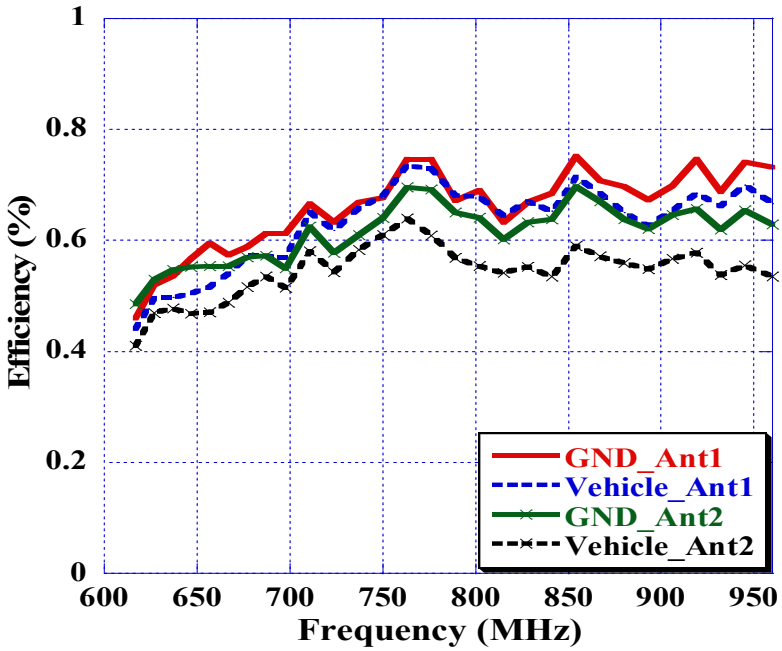

(a)

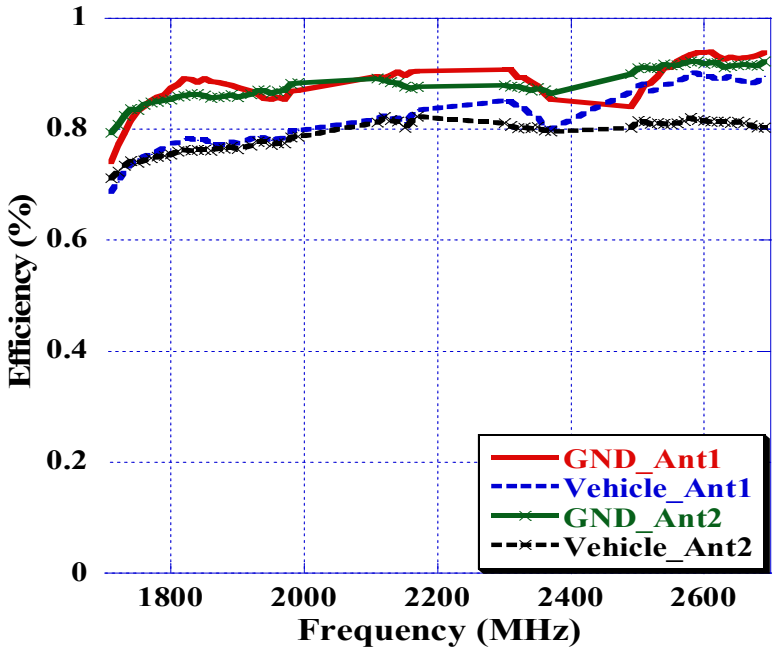

(b)

Figure 3.4. Antenna efficiency for Configuration I 5G MIMO system measured on GND and on vehicle roof for frequency ranges (a) 617MHz- 960MHz, (b) 1710MHz-2690MHz, and (c) 3400MHz- 5000MHz.

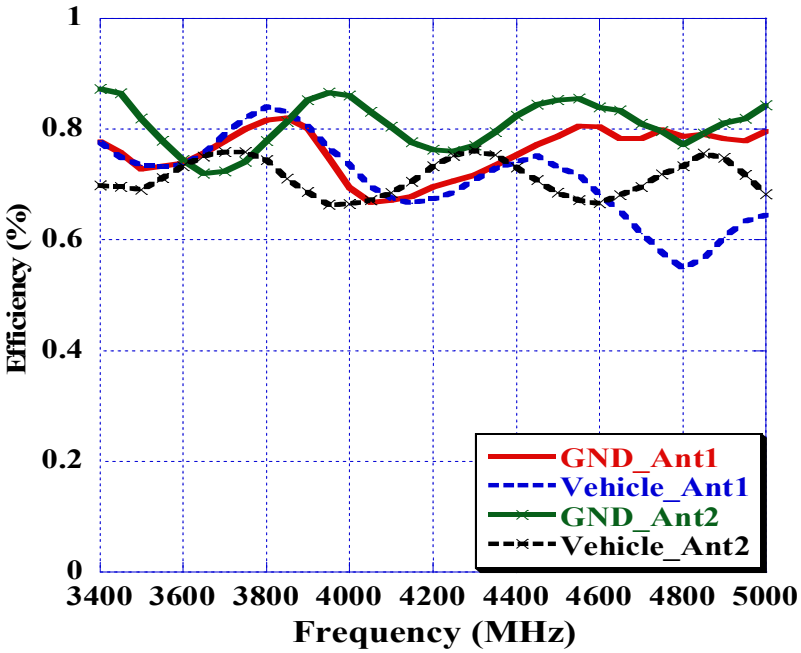

(c)

Figure 3.4. Continued.

Simulation, GND measurement, and vehicle measurement of a combined MIMO system radiation pattern sample is presented In Figure 3.5. The sample represents a Theta horizontal gain cut at θ = 80 degrees and four frequencies namely 617MHz, 1900MHz, 3900MHz, and 5000MHz to provide a good idea about the system performance. The combined MIMO system pattern is obtained by measuring each antenna when the other antenna is loaded by a 50Ohm terminator and then combine the resultant individual antenna patterns selecting the maximum values of Gain-Theta between Ant1 and Ant2 measurements for a specific phi-frequency pair at 80 degrees of theta. Finally, the average gain of the MIMO system combined radiation patterns measured on car roof is

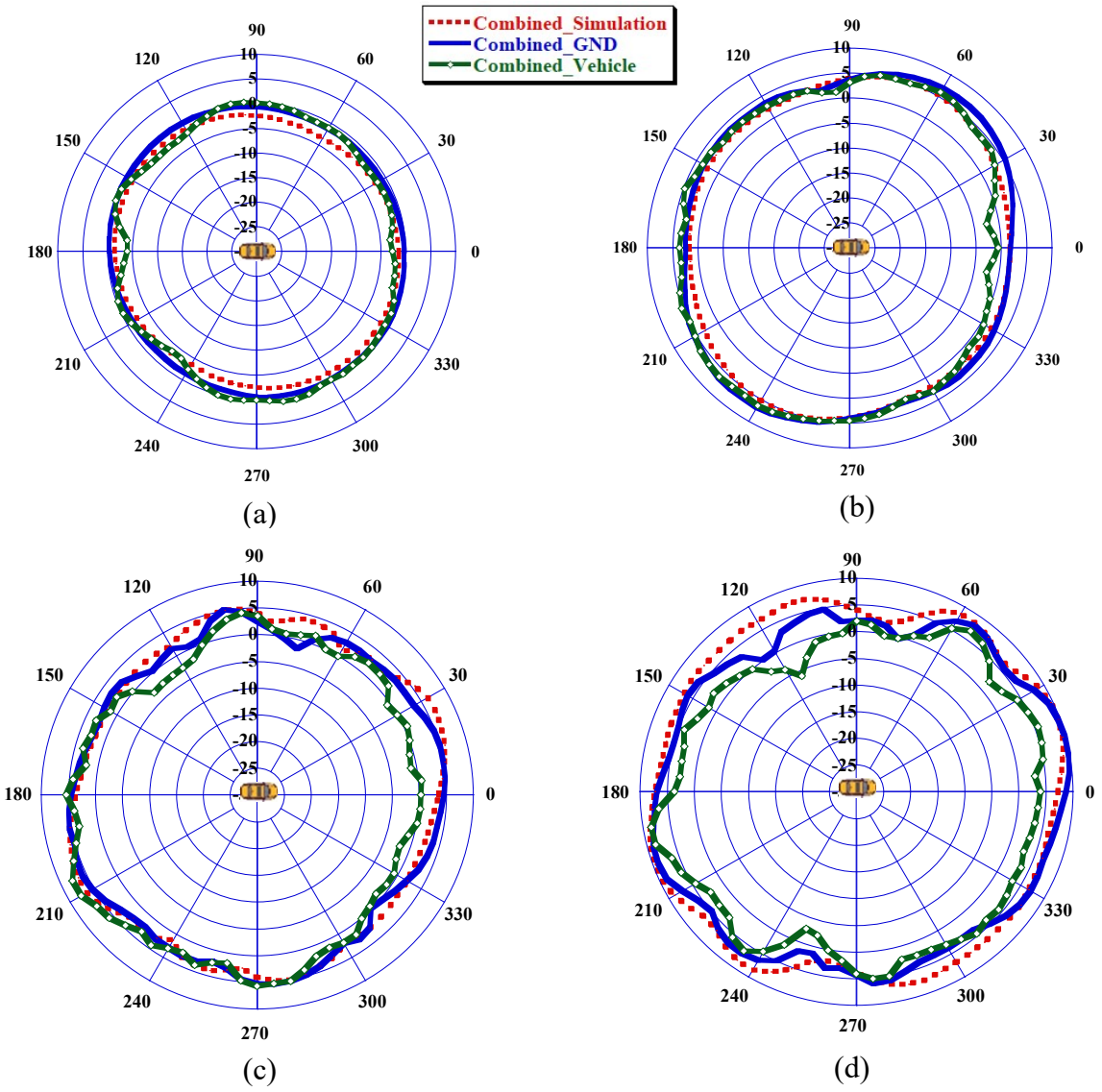

Figure 3.5. Configuration I combined radiation pattern of simulation, GND measurement, and vehicle measurement in (dBi) at θ = 80 deg. for frequencies: (a) 617 MHz, (b) 1900 MHz, (c) 3900 MHz, (d) 5000 MHz.

found to be -1.14dBi, 3.15dBi, 1.81dBi, and 2.84dBi at frequencies 617MHz, 1900MHz, 3900MHz, and 5000MHz, respectively.

ECC and DG on GND and on car roof for Configuration I of a 2x2 5G MIMO systems are depicted in Figure 3.6. The two figures suggests that higher values of ECC and consequently lower values of DG occurs at low frequencies (i.e., 617MHz) because the wavelength is big which leads to more correlation between the antennas. In this MIMO configuration an ECC of better than 0.13 and a DG of better than 9.92dB have been realized.

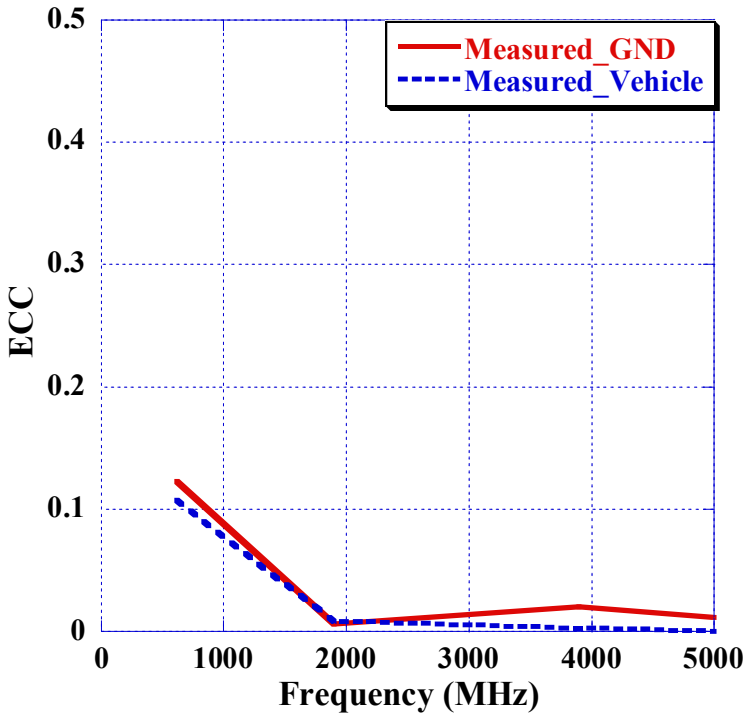

(a)

Figure 3.6. Configuration I of a 2x2 5G MIMO system measured on GND and on vehicle roof (a) ECC, (b) DG.

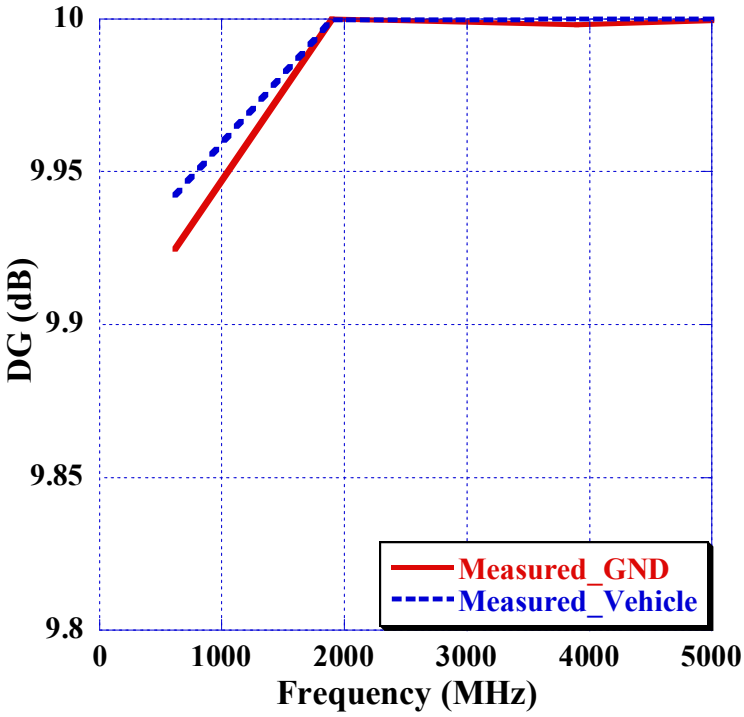

(b)

Figure 3.6. Continued.

3.3.2 Configuration II of a 2x2 5G MIMO system

Similar to Configuration I in subsection 3.3.1, two Monopole elements have been placed on a PCB with a distance of 125mm (from port to port) between them. The monopoles are place on the back of the roof of a car as in Figure 3.7 to allow for an omnidirectional combined radiation pattern.

The performance of Ant1 and Ant2 of this MIMO system has been reported in terms of reflection coefficient and isolation as in Figure 3.8. Both antennas show an agreement between simulation and GND measurement.

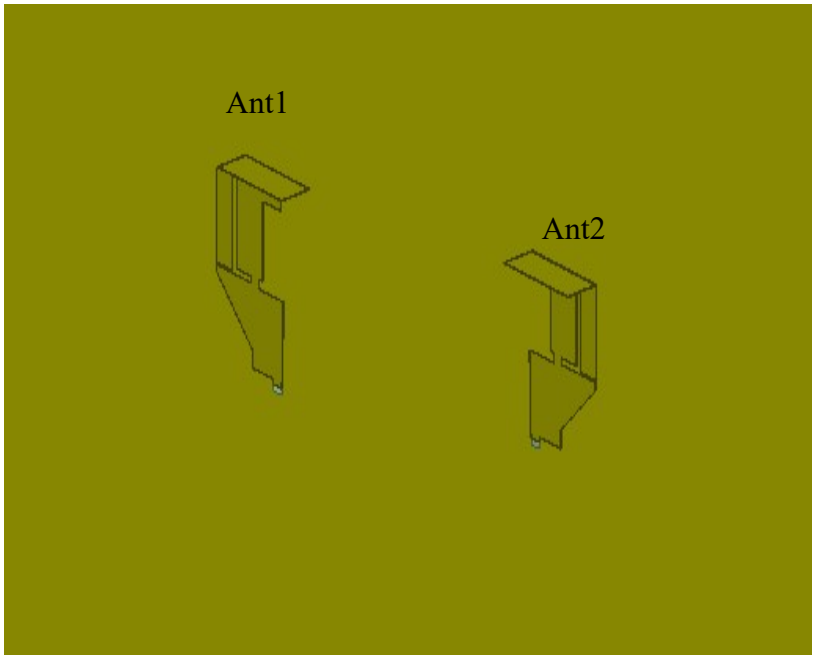

(a)

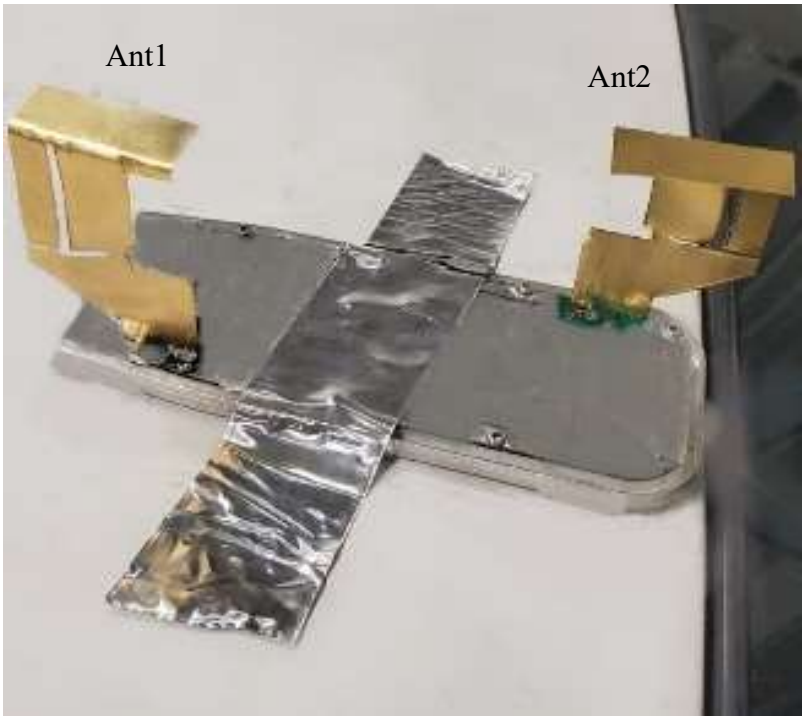

(b)

Figure 3.1. Configuration II of a 2x2 5G MIMO system: (a) simulation setup and (b) placement on vehicle's roof.

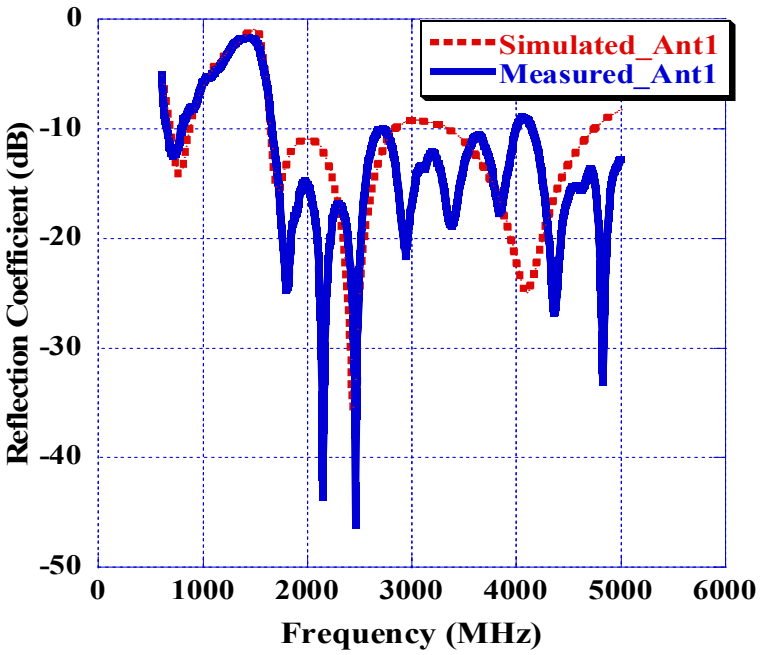

(a)

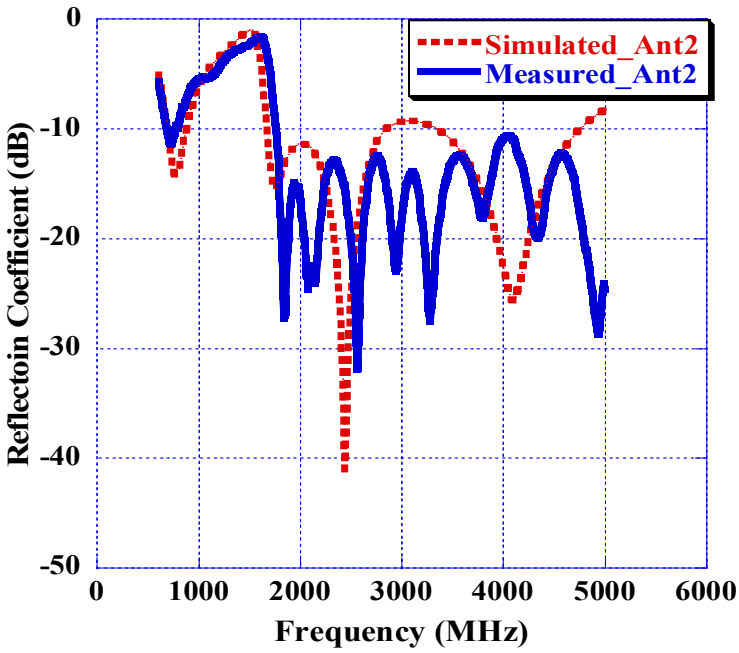

(b)

Figure 3.8. Configuration II of a 2x2 5G MIMO system simulated and measured: (a) Ant1 reflection coefficient in dB, (b) Ant2 reflection coefficient in dB, and (c) Isolation between Ant1 and Ant2 in dB.

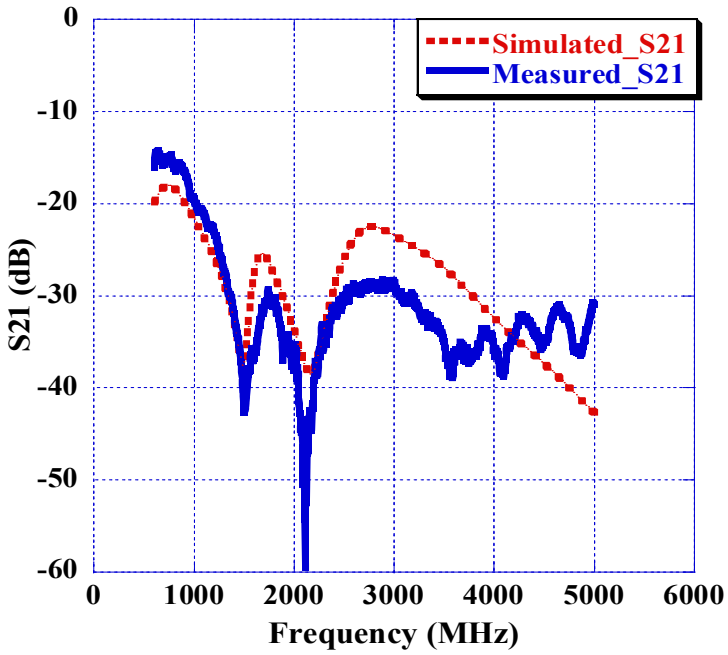

(c)

Figure 3.8. Continued.

Good reflection coefficient values have been observed from GND measurements of a worse of -7.4dB and -6.4dB at 617MHz of Ant1 and Ant2 respectively with reasonable GNSS bands rejection. Figure 3.8 also shows a good isolation between Ant1 and Ant2 in this configuration of a worse case 15dB (expressed as -15 dB in S21 format).

A comparison of on GND and on vehicle measurements of Ant1 and Ant2 total antenna efficiencies in this configuration is illustrated in Figure 3.9. The GND measurement has an average efficiency higher than 76% for both elements across all 5G bands whereas the vehicle measurement is 5% less particularly an average total efficiency of 71.7% was achieved.

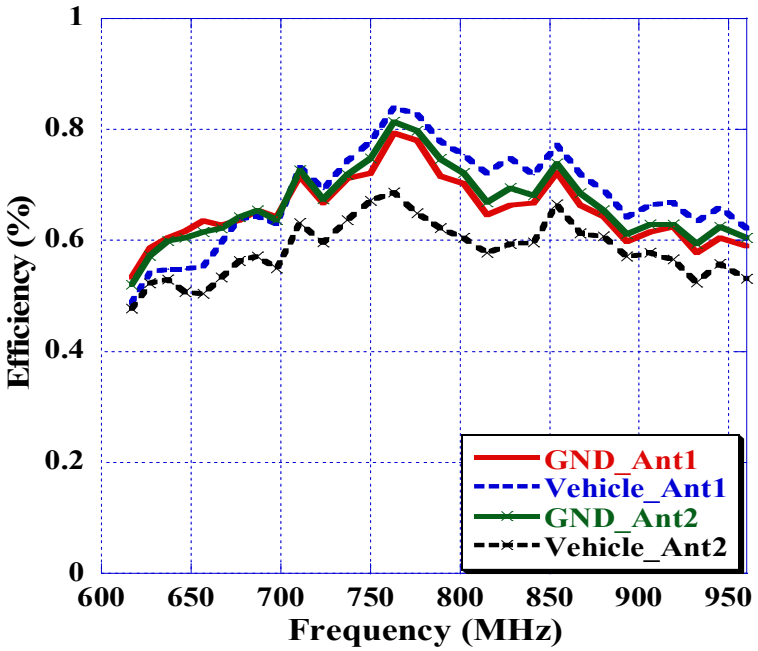

(a)

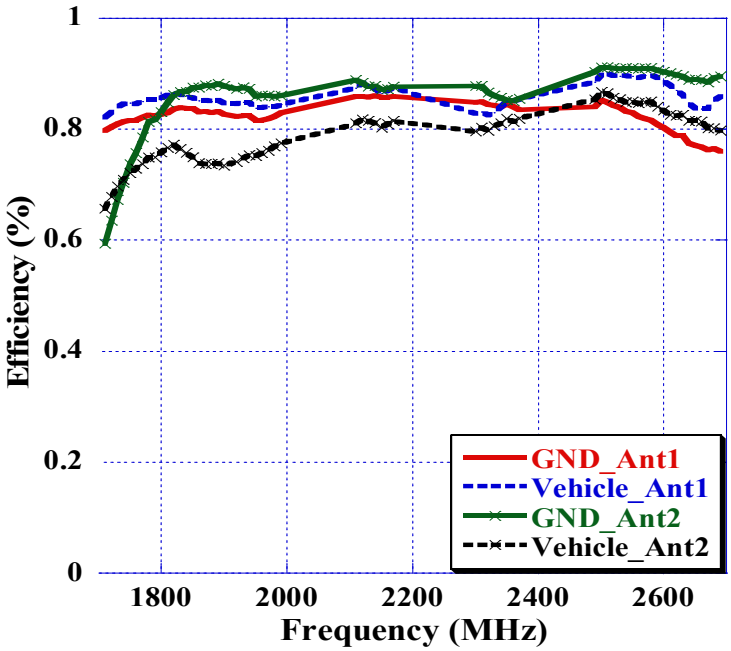

(b)

Figure 3.9. Antenna efficiency for Configuration II 5G MIMO system measured on GND and on vehicle roof for frequency ranges (a) 617MHz- 960MHz, (b) 1710MHz-2690MHz, and (c) 3400MHz- 5000MHz.

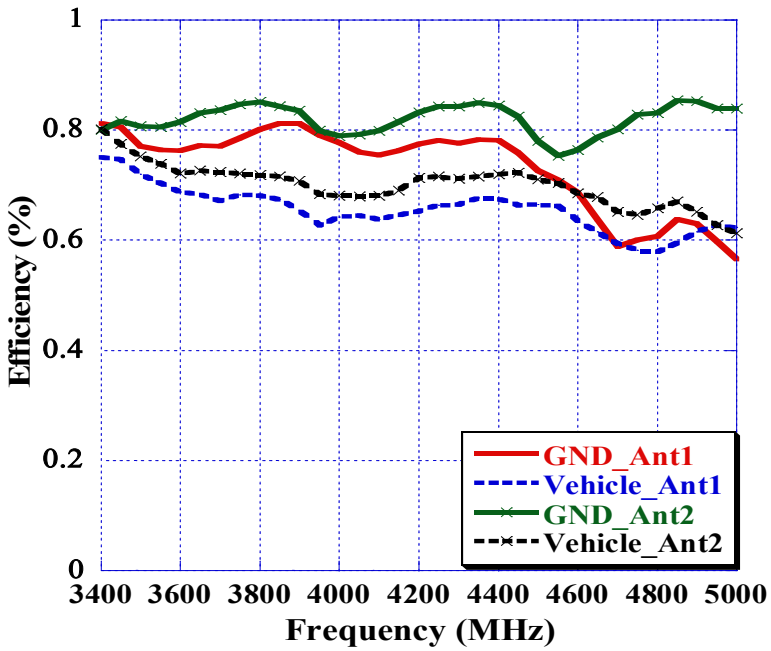

(c)

Figure 3.9. Continued.

ECC and DG on GND and on car roof for configuration II of a 2x2 MIMO systems is depicted in Figure 3.10 where an ECC of better than 0.02 and an approximately 10dB of DG has been achieved using this configuration.

Figure 3.11(a)-(d) presents combined realized vertical gain (Theta gain) radiation patterns of a horizontal cut at θ = 80 degrees for frequencies 617MHz, 1900MHz, 3900MHz and 5000MHz utilizing the same technique described in subsection 3.3.1. The average gain values recorded from the combined vehicle radiation patterns are -0.71dBi, 3.16dBi, 0.57dBi, and 1.51dBi at frequencies 617MHz, 1900MHz, 3900MHz, and 5000MHz, respectively.

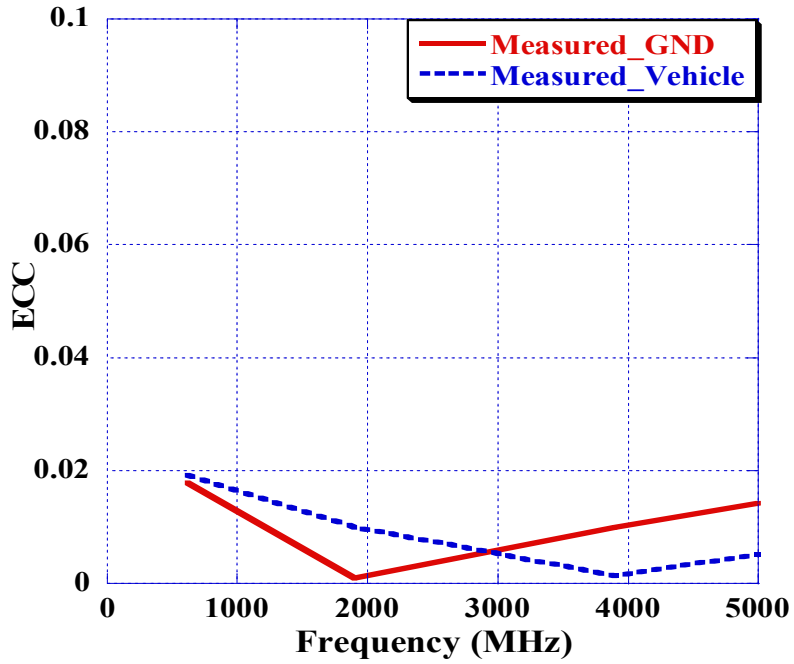

(a)

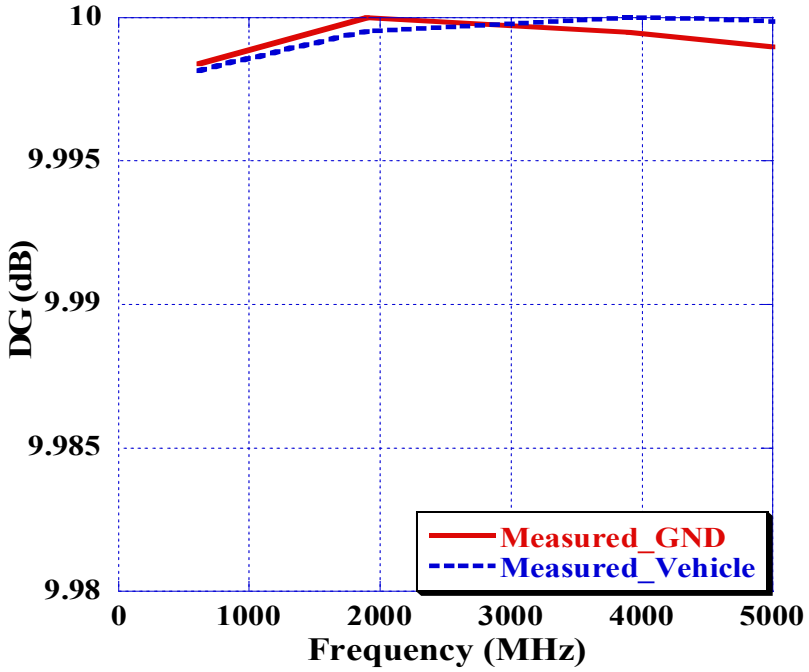

(b)

Figure 3.10. Configuration II of a 2x2 5G MIMO system measured on GND and on vehicle roof (a) ECC, (b) DG.

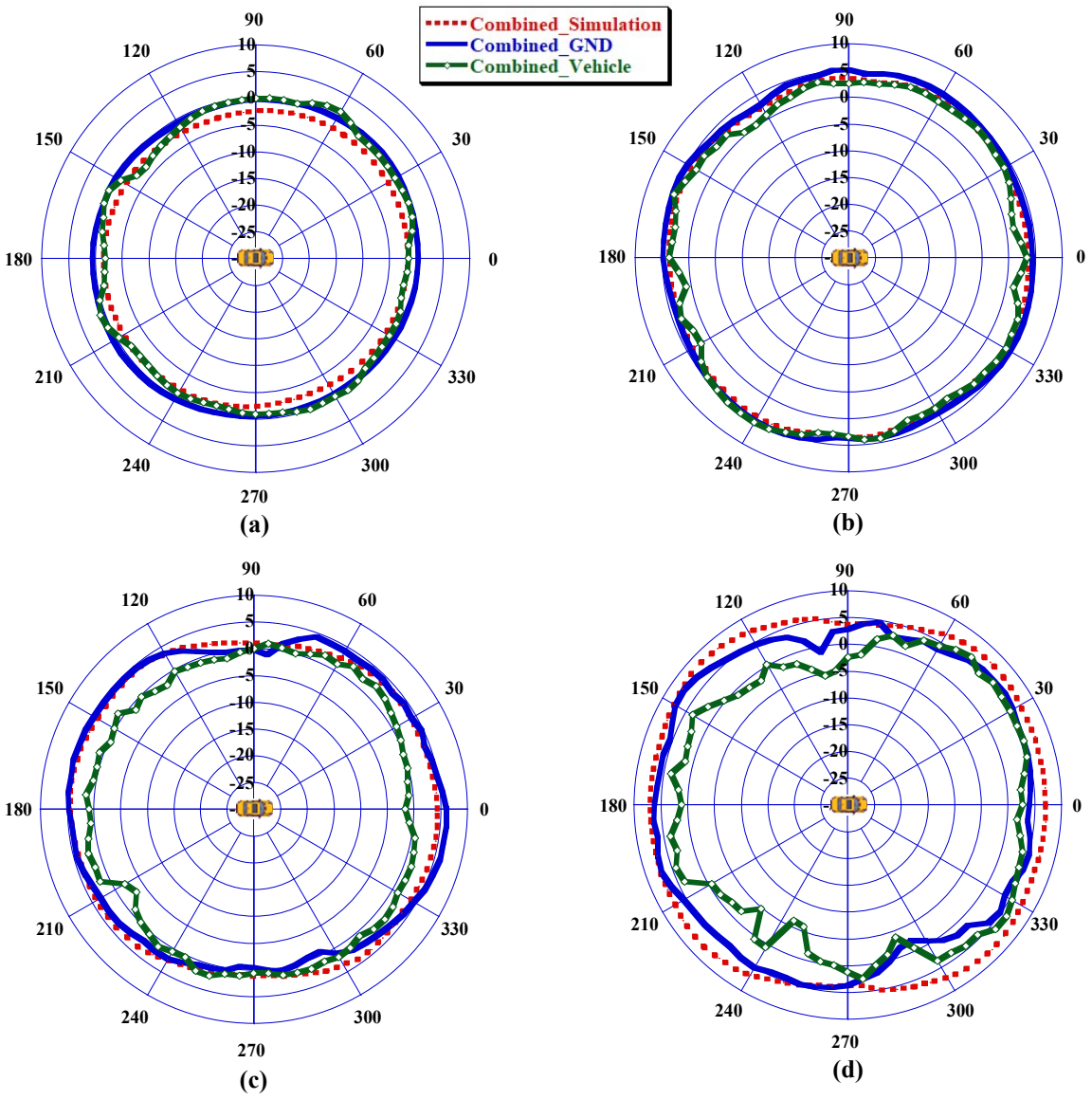

Figure 3.11. Configuration II combined radiation pattern of simulation, GND measurement, and vehicle measurement in (dBi) at θ = 80 deg. for frequencies: (a) 617 MHz, (b) 1900 MHz, (c) 3900 MHz, (d) 5000 MHz.

3.3.3 4x4 monopole-based 5G MIMO system

In this subsection, four Monopole elements are integrated in the same shark-fin package to operate as a 4x4 MIMO system. The building block antenna element for this configuration is the same antenna used in subsections 3.3.1 and 3.3.2. The four elements are placed in such a way that, the combined radiation pattern is omnidirectional with good isolation and correlation figures between individual antennas. The system placement on the car roof and simulation setup are shown in Figure 3.12. The distances between monopole elements in this MIMO systems are listed in Table 3.2.

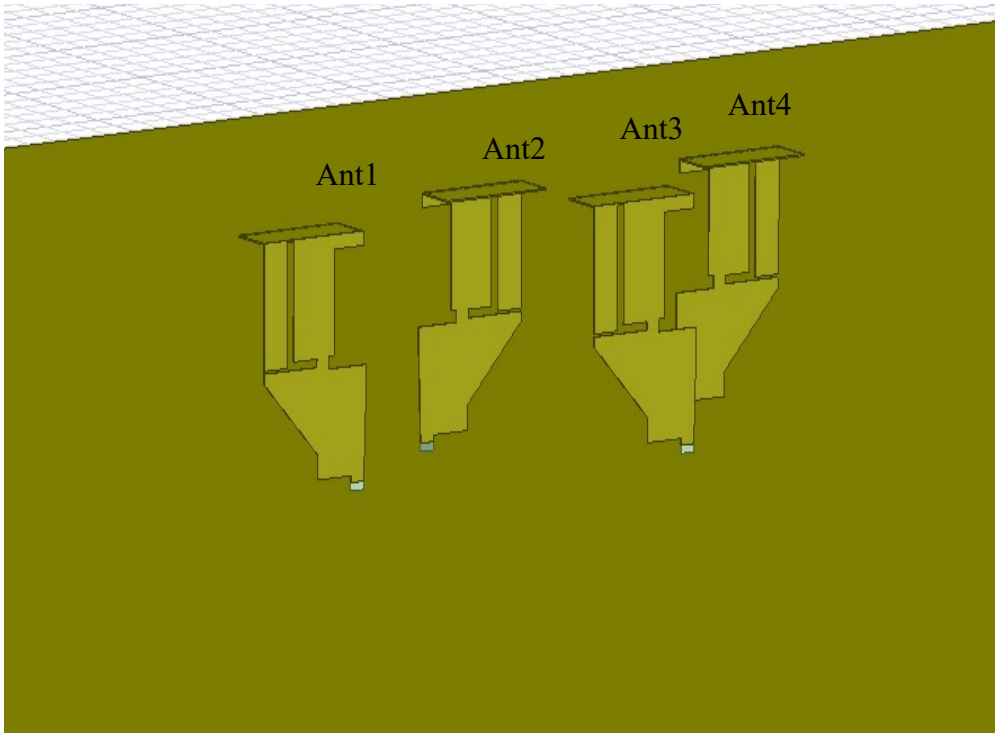

(a)

Figure 3.12. 4x4 5G MIMO system: (a) simulation setup and (b) placement on vehicle's roof.

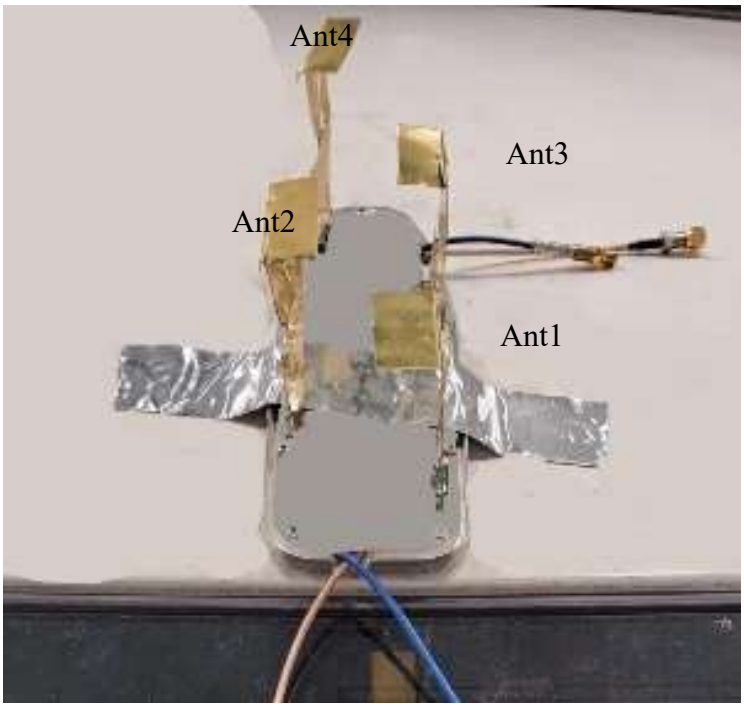

(b)

Figure 3.12. Continued.

Table 3.2. Distances Between Antennas in a 4x4 5G MIMO System Structure

Parameter	Value
Ant1-Ant2	77
Ant1-Ant3	141
Ant1-Ant4	180
Ant2-Ant3	100
Ant2-Ant4	118
Ant3-Ant4	70

The simulated reflection coefficient in dB for each element in this configuration is shown in Figure 3.13. The four elements from Ant1 to Ant4 show good matching characteristics across the whole 5G bands with a reflection coefficient of less than -5.2dB and a reasonable GNSS band rejection. There is also a good agreement between the 1-meter GND simulated and measured reflection coefficient response in each of the four cases.

The isolation in dB between each pair of antennas within this 4x4 MIMO system is shown in Figure 3.14. In general, the shorter the distance between the antennas, the worse the isolation is. However, the antenna placement and orientation also contribute to the overall isolation performance. For instance, placing antennas' arms that carry high frequency band currents facing each other typically results in better isolation performance than placing arms carrying low frequency band currents facing each other. All the six possible scenarios are reported in Figure 3.14 with worse value of 10dB of isolation between Ant1-Ant2 and Ant2-Ant4 can be observed from the GND measurements on the 617MHz- 960MHz band.

Using similar approach for combining individual antennas radiation patterns as in subsections 3.3.1 and 3.3.2, the combined radiation patterns at 80 degrees of theta for the four elements are shown is Figure 3.15. As expected by increasing number of elements in a MIMO system, higher average gain values are observed from the combined vehicle radiation patterns measurements compared to the other 2x2 configurations. The realized average vertical gain is found to be: -0.88dBi, 4.64dBi, 3.14dBi, and 3.74dBi at frequencies 617MHz, 1900MHz, 3600MHz, and 5000MHz, respectively.

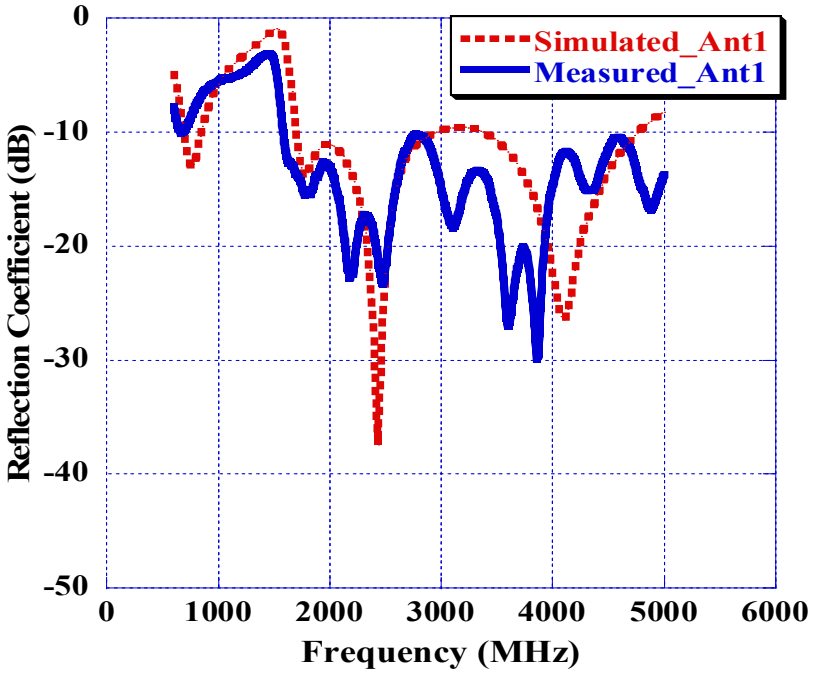

(a)

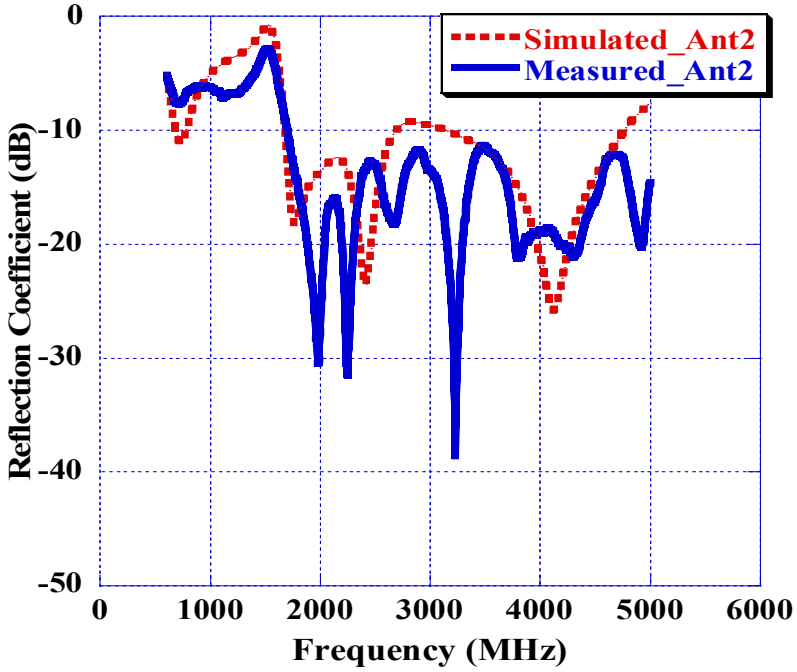

(b)

Figure 3.13. 4x4 5G MIMO system simulated and measured reflection coefficient in dB for: (a) Ant1, (b) Ant2, (c) Ant3, and (d) Ant4.

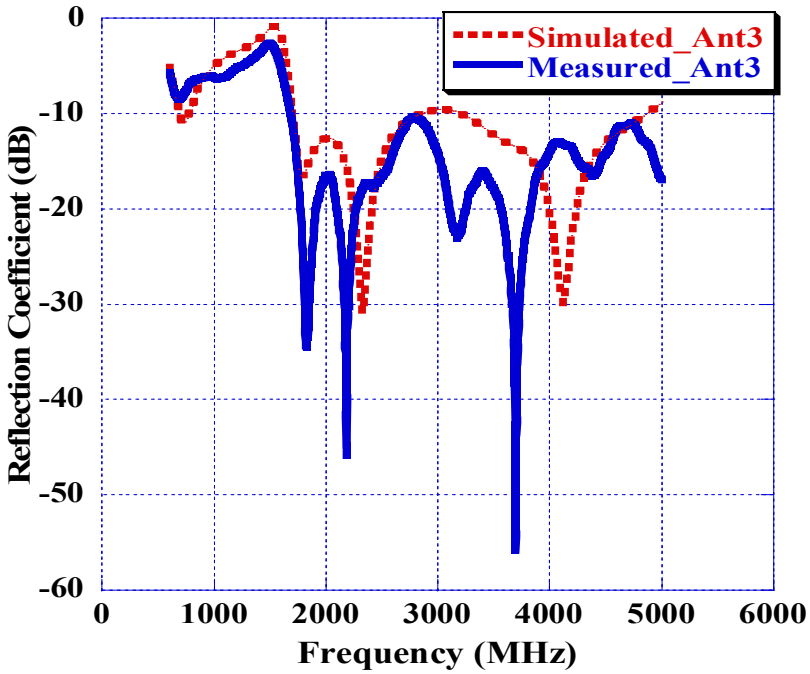

(a)

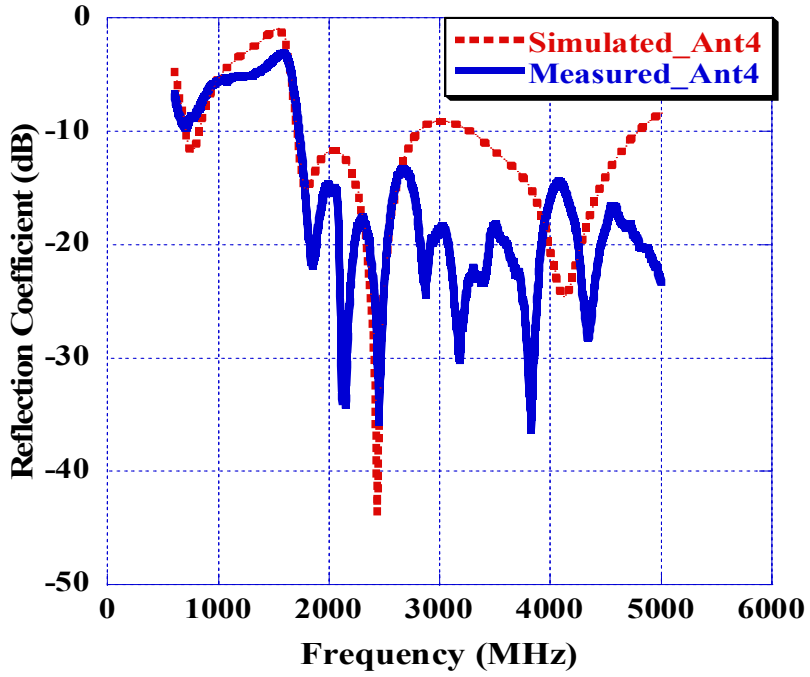

(b)

Figure 3.13. Continued.

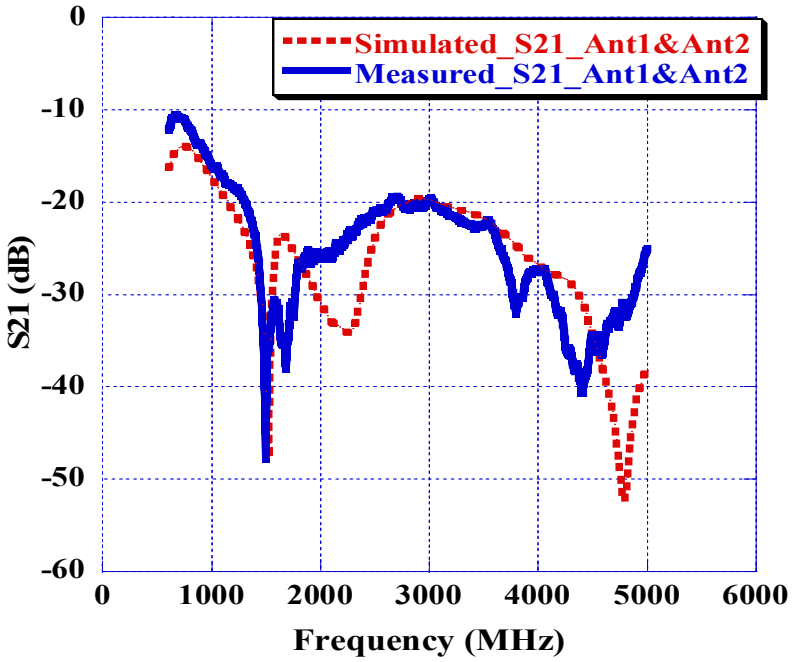

(a)

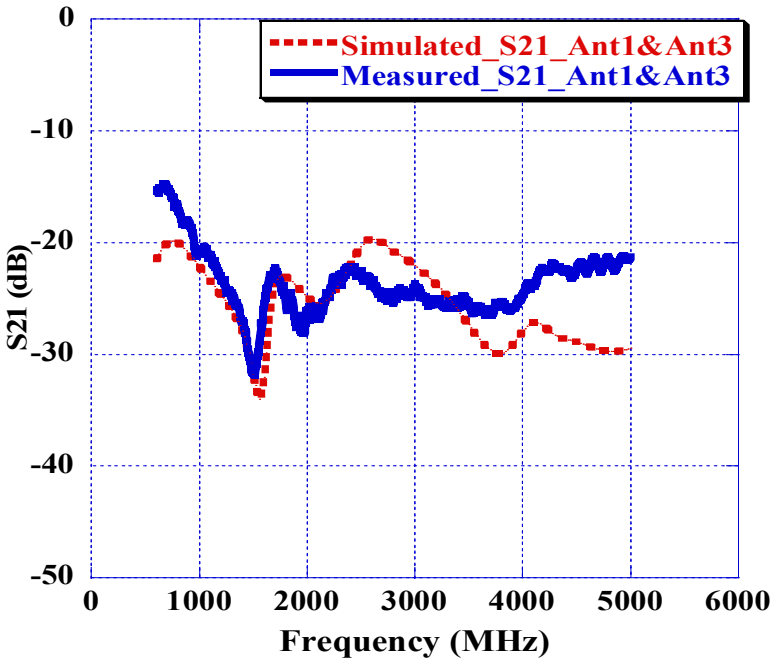

(b)

Figure 3.14. 4x4 5G MIMO system simulated and measured Isolation in dB between: (a) Ant1- Ant2, (b) Ant1- Ant3, (c) Ant1- Ant4, (d) Ant2- Ant3, (e) Ant- Ant4 and (d) Ant3- Ant4.

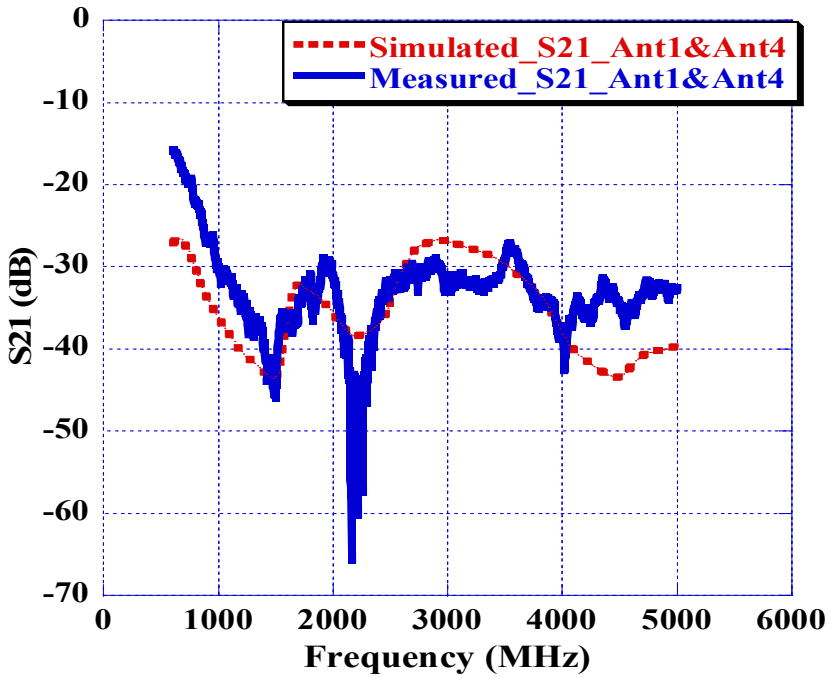

(c)

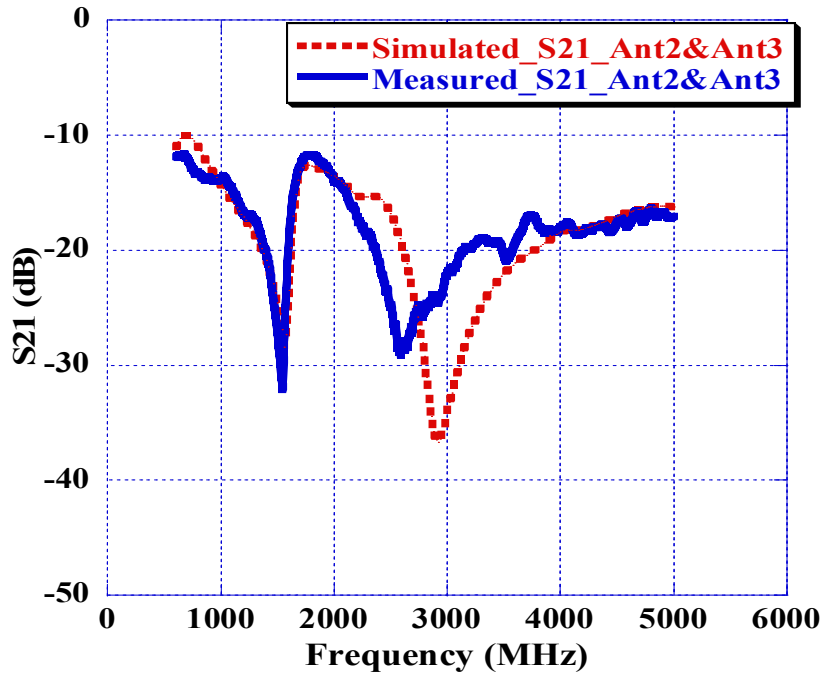

(d)

Figure 3.14. Continued.

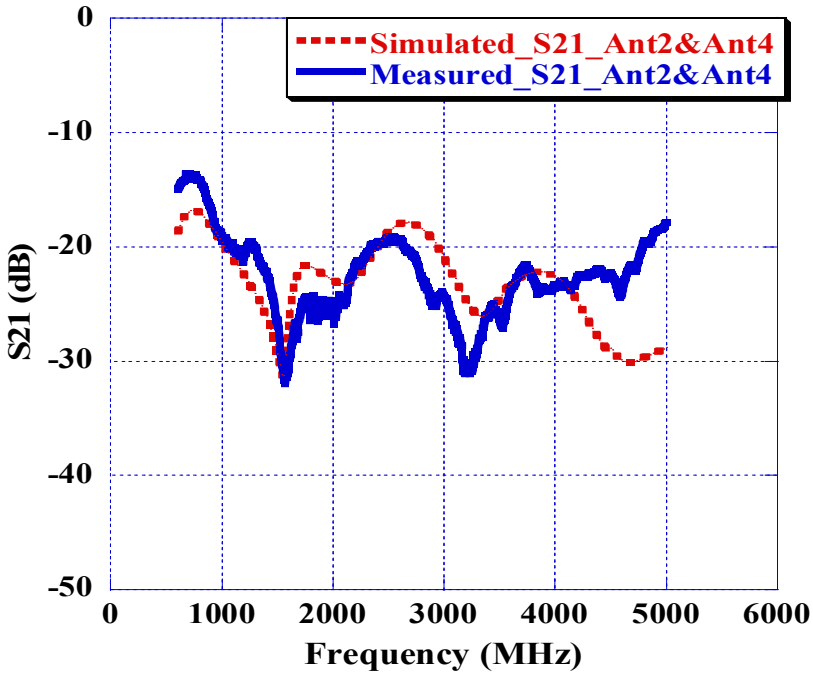

(e)

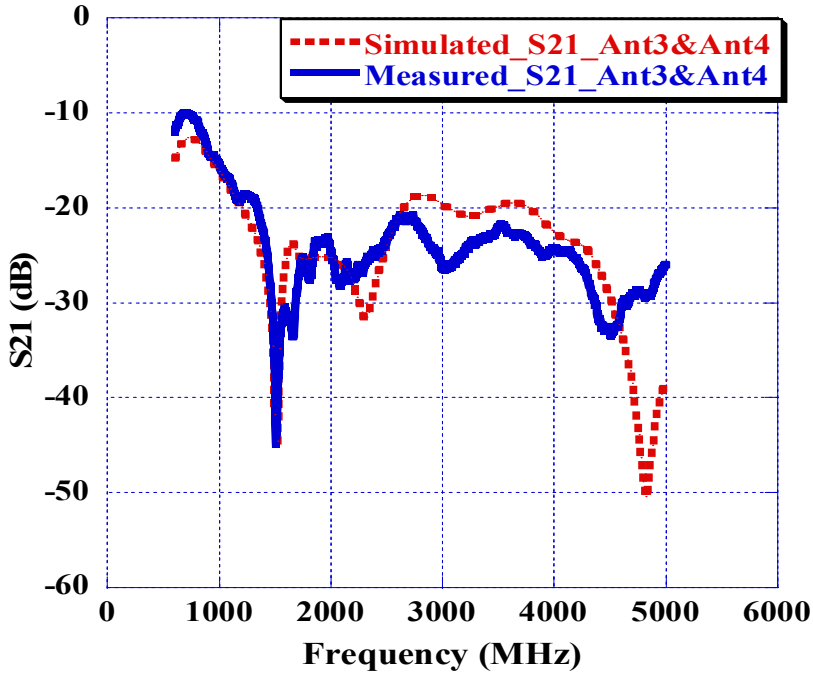

(f)

Figure 3.14. Continued.

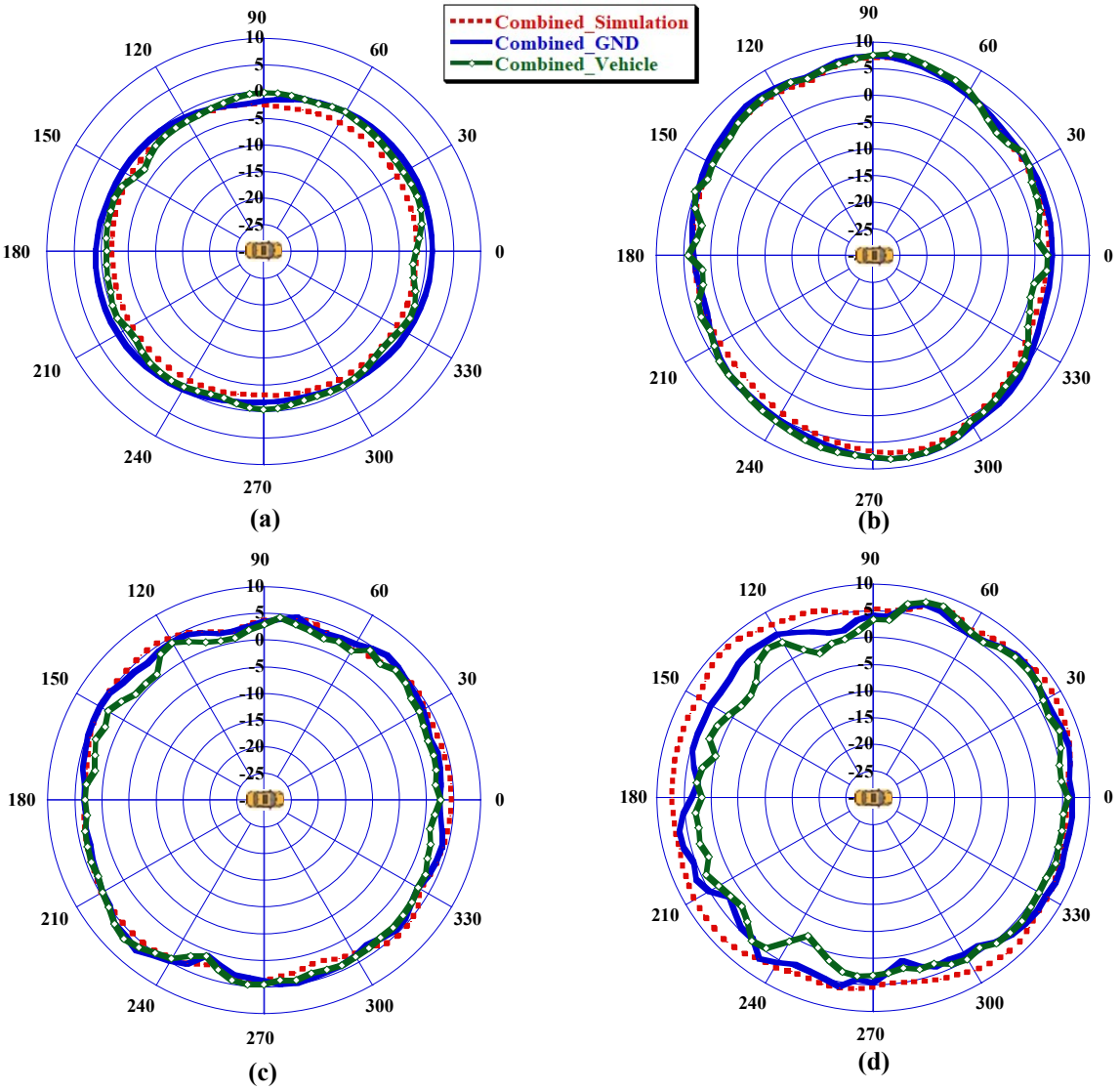

Figure 3.15. 4x4 5G MIMO system combined radiation pattern of simulation, GND measurement, and vehicle measurement in (dBi) at θ = 80 deg. for frequencies: (a) 617 MHz, (b) 1900 MHz, (c) 3900 MHz, (d) 5000 MHz.

The on GND and on car roof measured efficiencies are reported in Figure 3.16, Figure 3.17, Figure 3.18, and Figure 3.19 for the four antenna elements in this MIMO system. It can be noticed that the GND measurement has an average total efficiency higher than 72.5% for all the four elements across the whole 5G frequency bands whereas the vehicle measurement has a reduced average total efficiency of slightly higher than 65% for all elements. The ECC and DG were also calculated in this MIMO configuration with the help of equations (3.1) and (3.2) using Octave script. As Figure 3.20 suggests, the ECC is well kept below 0.5 in all the 6 correlation cases with corresponding DG values of higher than 8.9dB. The worst value of ECC (0.45) and DG exists at low frequency bands, and it is the same case where worst passive isolation occurs namely between Ant3 and Ant4.

Detailed literature review comparison of MIMO antennas systems used in automotive industry is attached in Table A.2 in the APPENDIX. The table also compares works in terms type of type of antennas, bandwidth of operations, systems volume, and method of ECC calculation in use.

Chapter 3 conclusion is discussed next, and it summarize all the work done throughout this chapter.

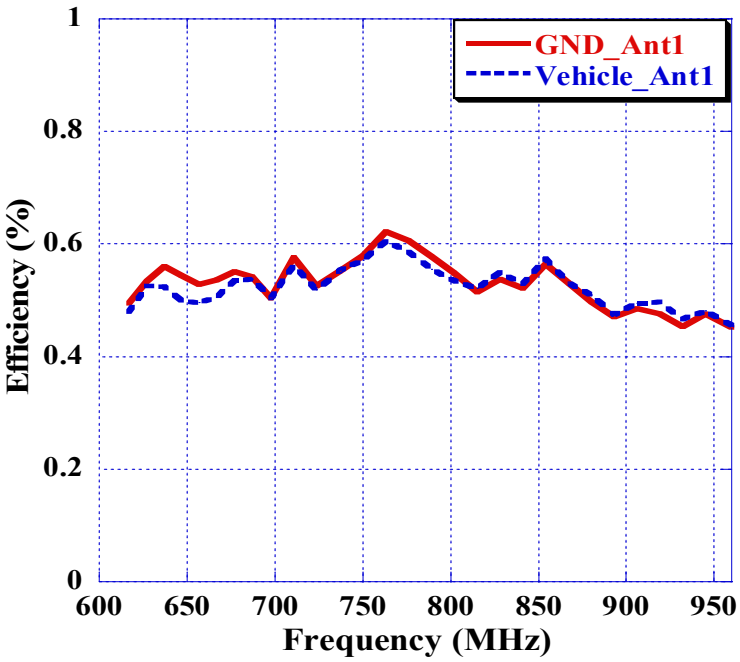

(a)

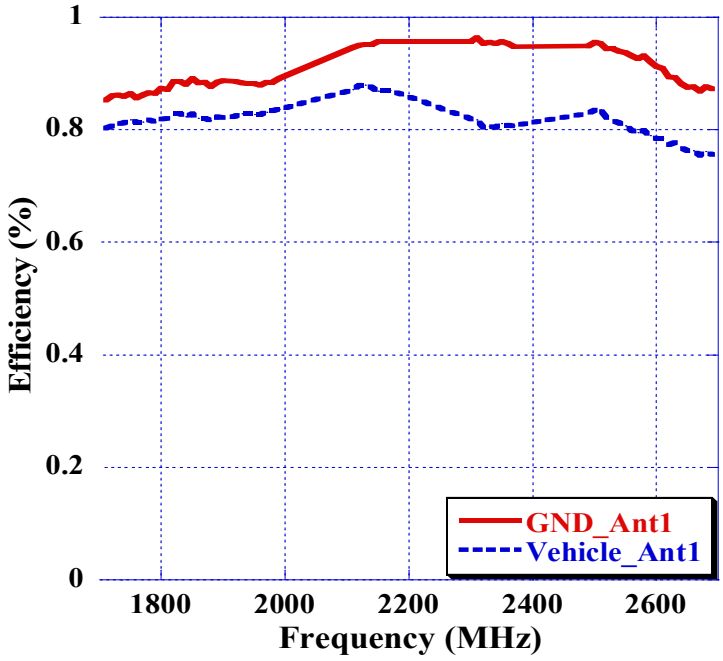

(b)

Figure 3.16. Ant1 efficiency for 4x4 5G MIMO system measured on GND and on vehicle roof for frequency ranges (a) 617MHz- 960MHz, (b) 1710MHz- 2690MHz, and (c) 3400MHz- 5000MHz.

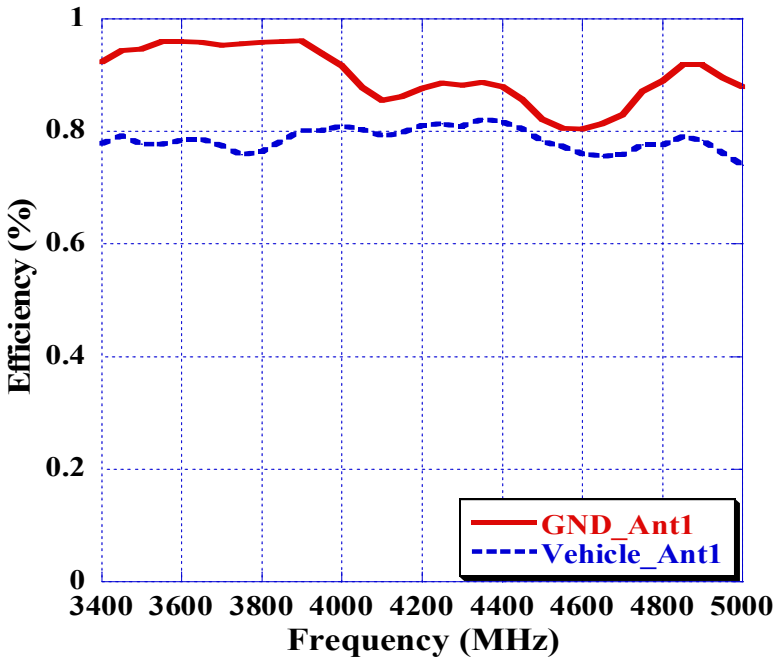

(c)

Figure 3.16. Continued.

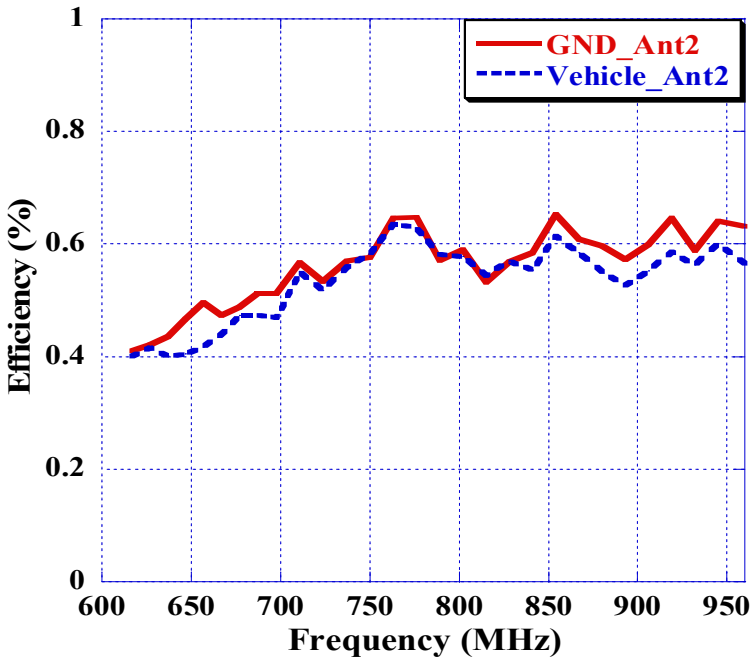

(a)

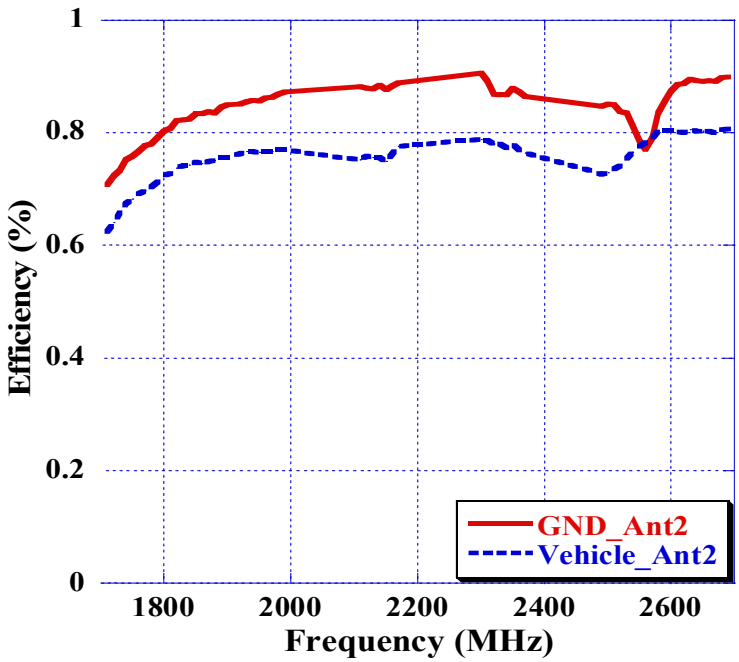

(b)

Figure 3.17. Ant2 efficiency for 4x4 5G MIMO system measured on GND and on vehicle roof for frequency ranges (a) 617MHz- 960MHz, (b) 1710MHz- 2690MHz, and (c) 3400MHz- 5000MHz.

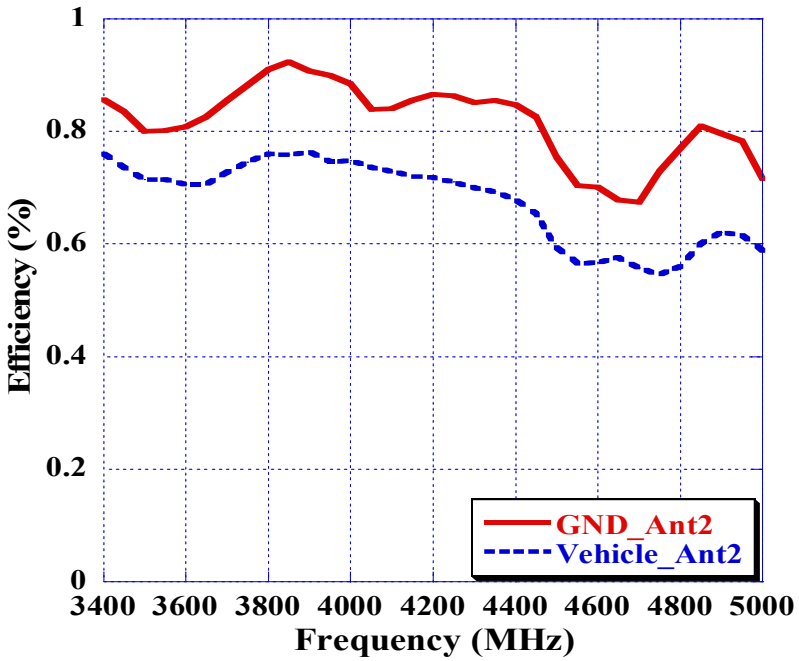

(c)

Figure 3.17. Continued.

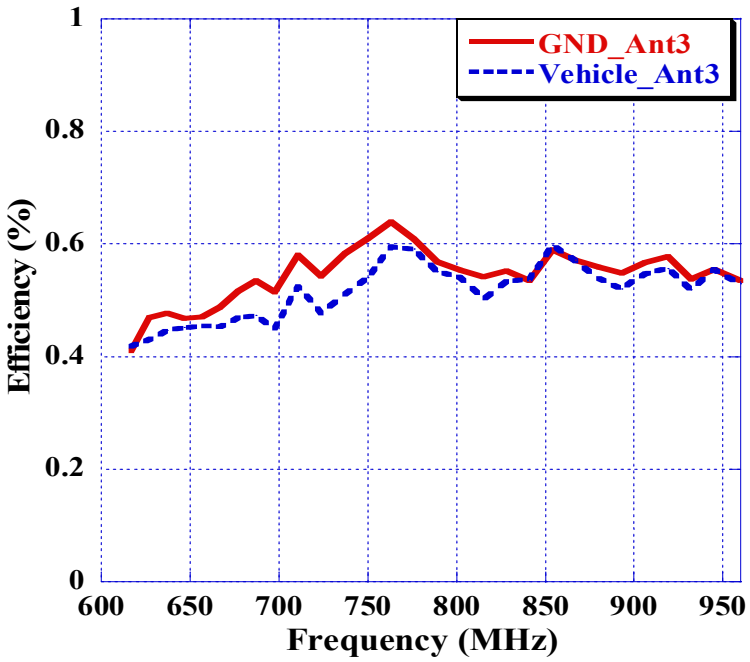

(a)

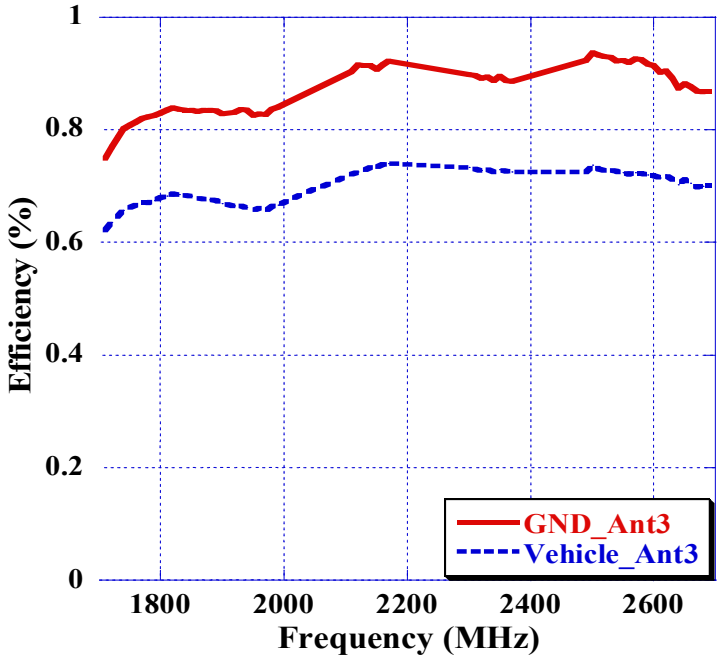

(b)

Figure 3.18. Ant3 efficiency for 4x4 5G MIMO system measured on GND and on vehicle roof for frequency ranges (a) 617MHz- 960MHz, (b) 1710MHz- 2690MHz, and (c) 3400MHz- 5000MHz.

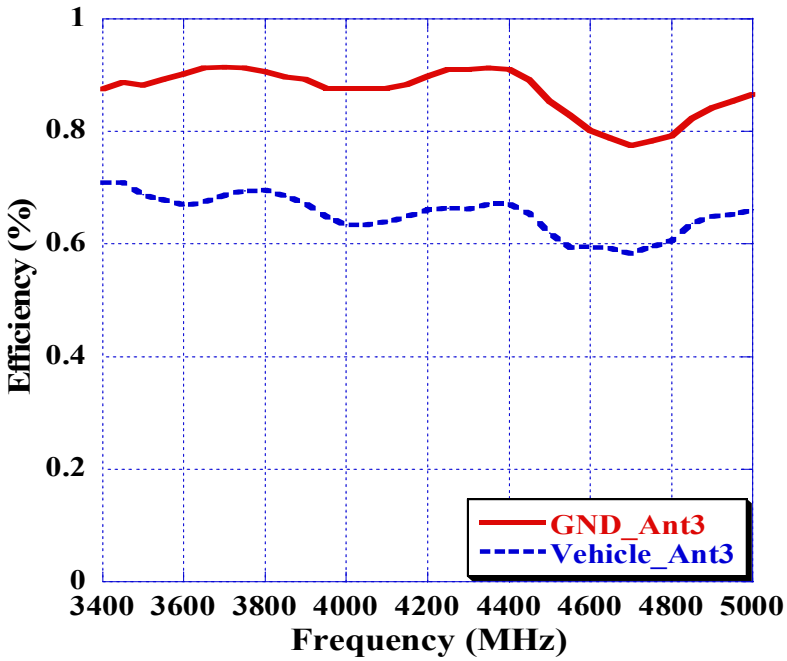

(c)

Figure 3.18. Continued.

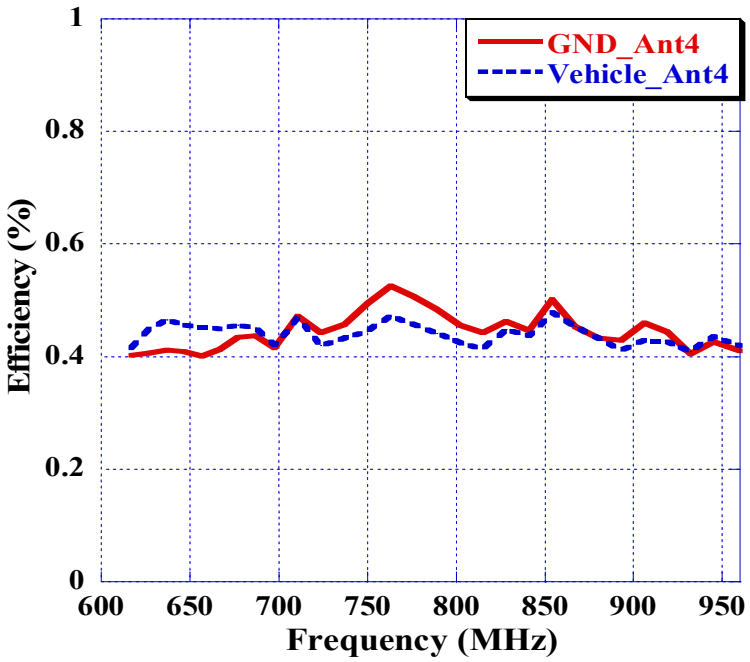

(a)

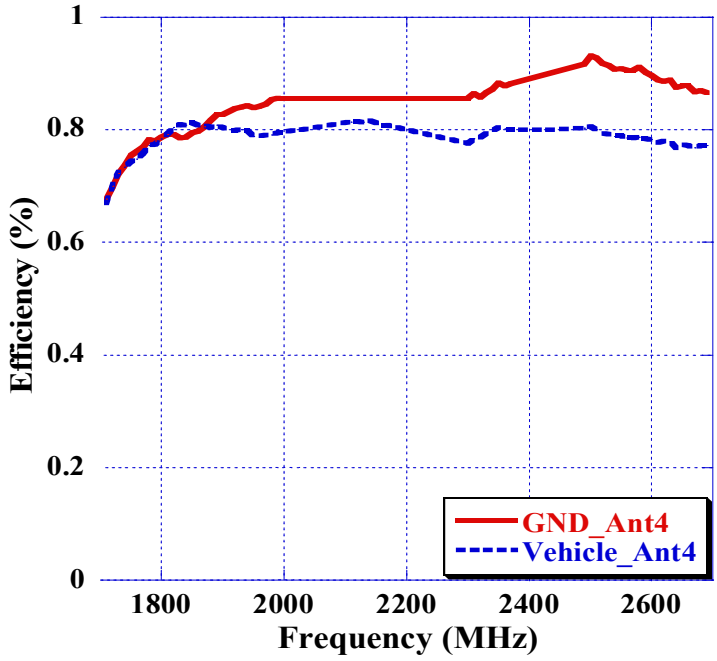

(b)

Figure 3.19. Ant4 efficiency for 4x4 5G MIMO system measured on GND and on vehicle roof for frequency ranges (a) 617MHz- 960MHz, (b) 1710MHz- 2690MHz, and (c) 3400MHz- 5000MHz.

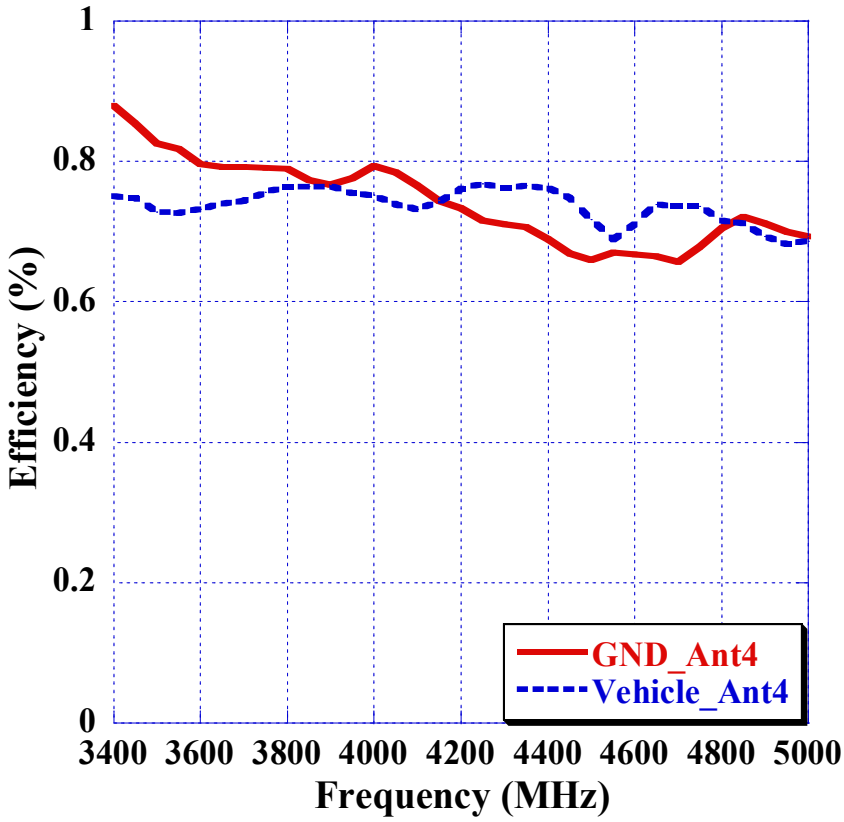

(c)

Figure 3.19. Continued.

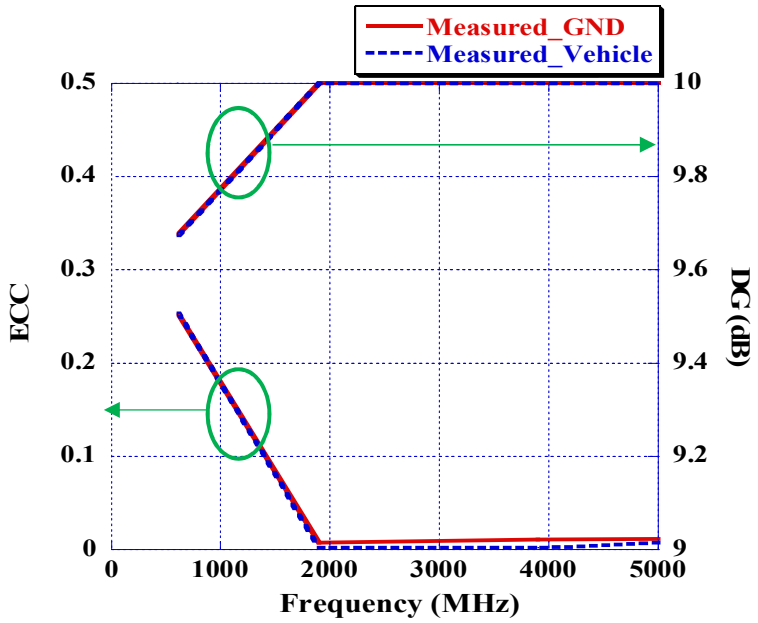

(a)

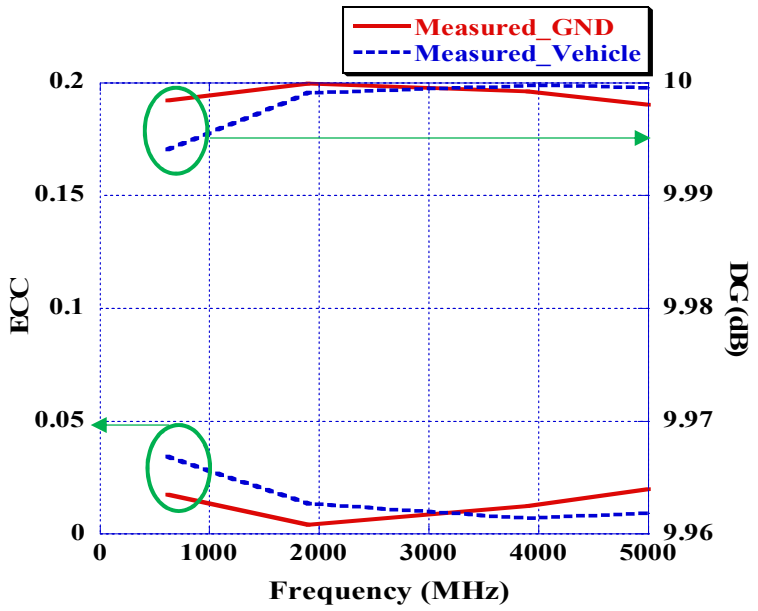

(b)

Figure 3.20. 4x4 5G MIMO system measured on GND and on vehicle ECC and DG between (a) Ant1-Ant2, (b) Ant1-Ant3, (c) Ant1-Ant4, (d) Ant2-Ant3, (e) Ant2-Ant4, and (f) Ant3-Ant4.

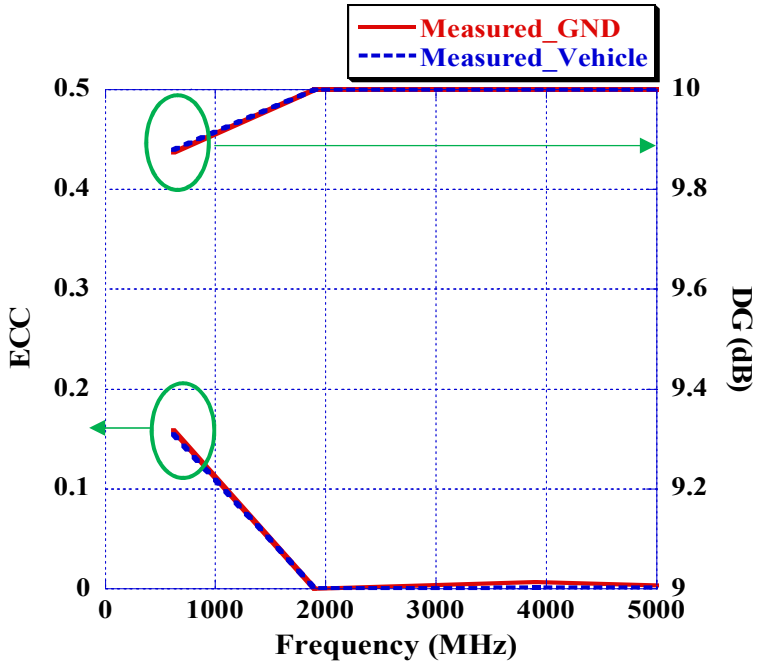

(c)

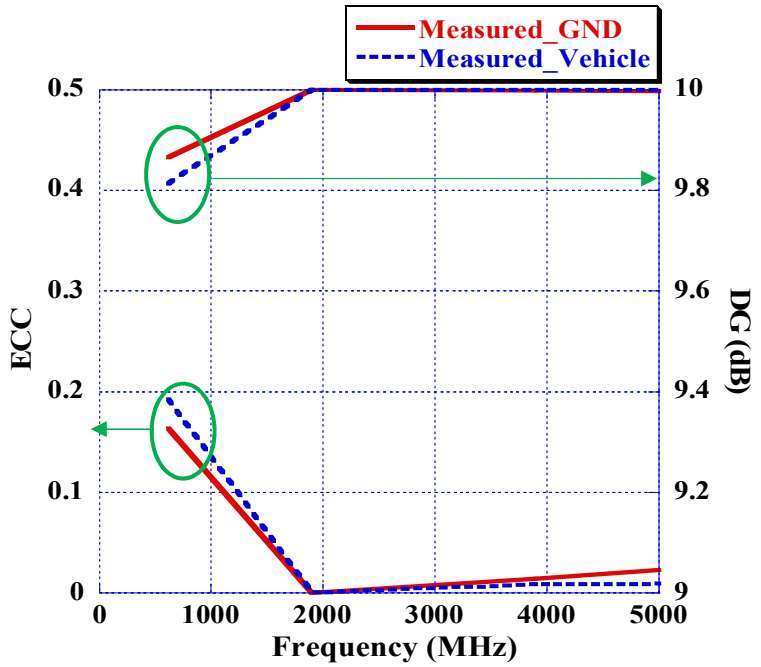

(d)

Figure 3.20. Continued.

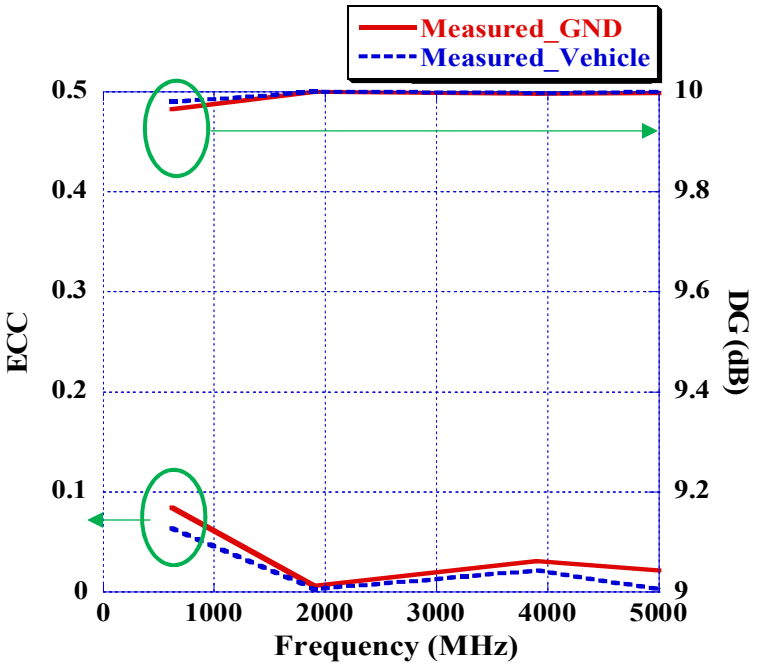

(c)

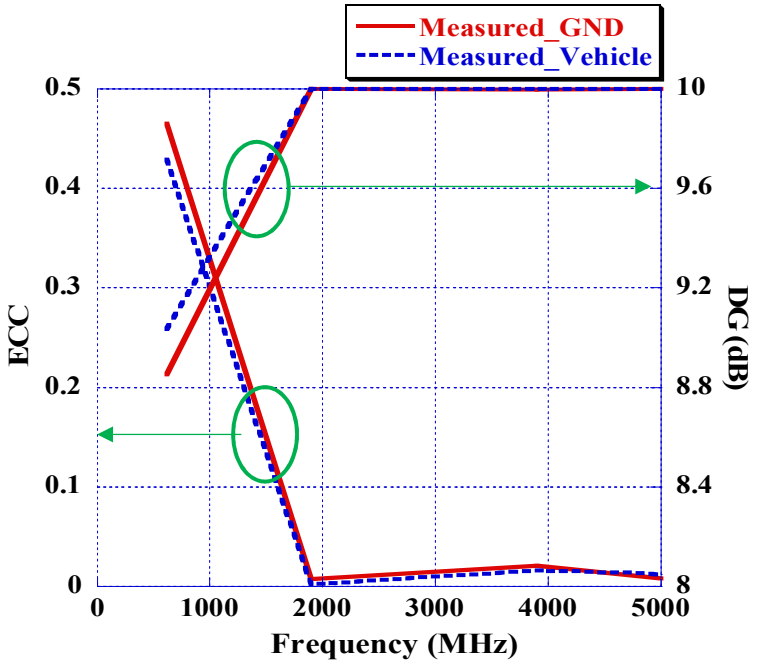

(d)

Figure 3.20. Continued.

3.4 Conclusions

Three MIMO systems based on a novel branched Monopole structure that operates in cellular 5G bands (617MHz-5GHz) and can easily be in integrated inside a Shark-fin package on a car roof have been presented in this chapter. The ECC and DG derived from the radiation patterns of each antenna element were calculated for each of the three MIMO configurations. The configuration I MIMO system in Figure 3.1 represents a 2x2 MIMO systems with antennas separated by a 135mm distance integrated on a Shark-fin module on a car roof and it allows for a passive isolation better than 12dB, total average efficiencies higher than 71% on vehicle across all bands, ECC lower than 0.13, and DG higher than 9.9dB. The configuration II MIMO system in Figure 3.7 represents a 2x2 MIMO systems with antennas separated by a 125mm distance integrated on a Shark-fin module on a car roof and it provides a passive isolation better than 15dB, total average efficiencies higher than 71.7% on vehicle across all bands, ECC lower than 0.02, and DG of 10dB. Finally, a 4x4 MIMO antenna system constructed of four monopole elements as in Figure 3.12 was designed. It achieves passive isolation better than 10dB, total average efficiencies higher than 65% on vehicle across all bands, ECC lower than 0.46, and DG higher than 8.9dB. In general, each MIMO configuration has a satisfactory performance and can be used easily in the vehicular application depending on the desired requirement and dimensions.

CHAPTER FOUR

V2X CAVITY-BACKED SLOT ANTENNA

4.1 Introduction

There are two implementable schemes for V2X: Dedicated Short-Range Communication (DSRC) and 5G network. Both schemes can operate with each other to result in a complete solution for V2X communication. The 5G cellular communication can be considered as a backup to the DSRC while supporting high data rates that can lengthen the communication path beyond the short range of the DSRC technology [53]. Vehicular V2X antennas are required to communicate with vehicles, infrastructure, network, and pedestrians that are located at various elevations with respect to the vehicle's antenna. Thus, good coverage in Theta angles range $75deg < \theta < 95deg$ is important to make sure that good reception performance is achieved for electromagnetic waves originating from antennas mounted in high locations like base station towers as well as to cover waves incident from below-horizon angles [52].

Since V2X antenna works at a relatively high frequency (5.85GHz- 5.925GHz), the size of the antenna is typically small. With such small size, the antenna is exposed to EM waves blockage from other antenna packaged within the same Shark-fin. Moreover, V2X antenna needs to cover some below horizon angles for proper operation which makes mounting the antenna on car's roof inappropriate. For the previous reasons and in addition to styling purposes, a cavity-backed slot V2X antenna was developed to be mounted on vehicle's windshield or attached to the rear-view mirror. The antenna layout, design goals, simulation, and measurements results are discussed in this chapter.

4.2 Cavity-Backed Slot V2X Antenna Design Layout

The cavity-backed slot antenna is constructed of metal sheet with volume of (40.5mm height X 38.7mm length X 16.8mm width). A coaxial cable is used to feed the antenna where its center pin used as a monopole to excite the cavity-backed slot antenna. Figure 4.1 and Figure 4.2 show the proposed antenna with geometrical dimensions highlighted. The feeding monopole is made of two parts, the lower part which is coaxial cable center pin with a length (LFL) of 1.74mm and diameter of 0.2mm whereas the top part has a length (FL) of 10.97mm and a wider diameter (FD) of 1.7mm to help in having wider overall bandwidth for the monopole.

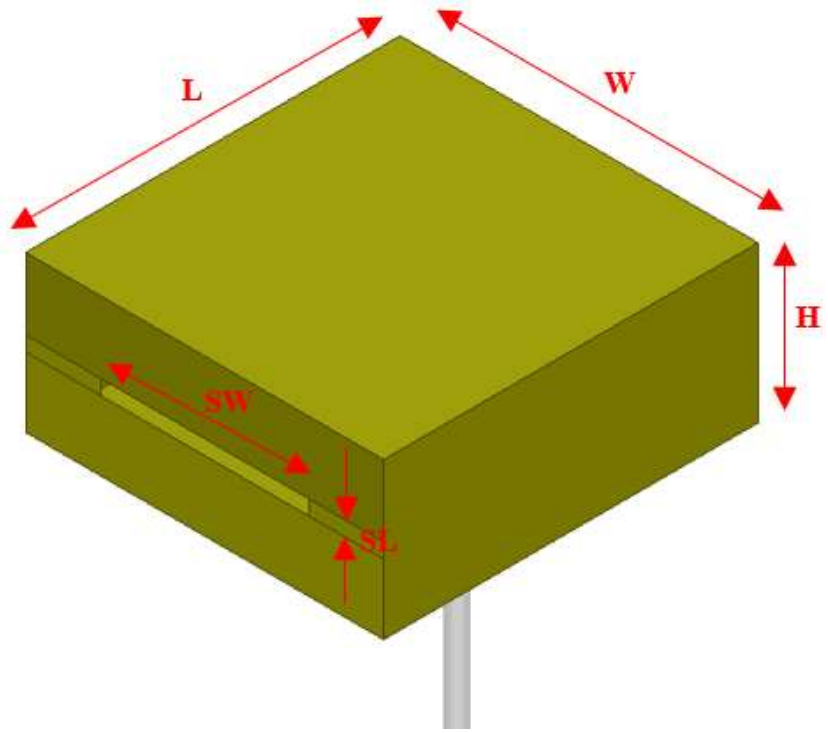

Figure 4.1. Cavity-backed slot antenna dimension.

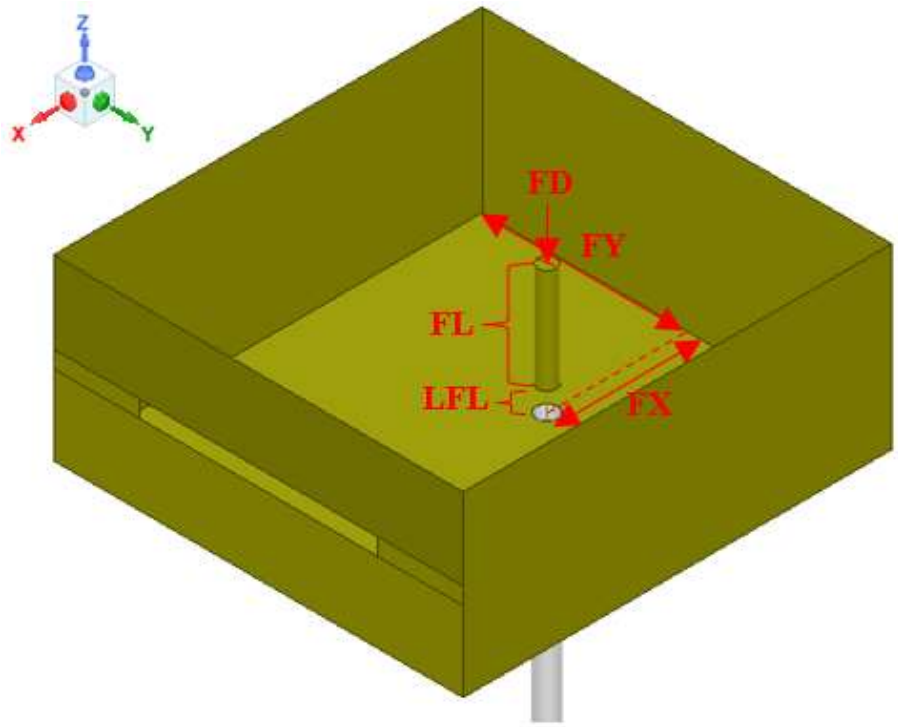

Figure 4.2. Cavity-backed slot antenna dimensions with top side removed.

The total length of the monopole is set to be 12.71mm which is a quarter-wavelength at 5.9GHz and can be calculated as in equation (4.1) below:

$$\text{Monopole length} = \frac{c}{4*f} \tag{4.1}$$

Where c is the speed of light ($c = \lambda f = 3 * 10^8\ m/s$) and f = 5.9 GHz. The feeding monopole is located at approximately $\text{FX} = \frac{\lambda_{\text{center-fre}}}{4}$ from the back side (opposite to the slot side) of the cavity to allow for an in-phase reflection of energy from the back of the cavity to the slot side. It is assumed that the cavity is filled with air and experimental trials are used to determine the geometrical dimensions of the cavity with the assumption that TE_{101} mode will be excited in the antenna.

Table 4.1 shows the values of various antenna parameters with their final values. The listed values were obtained after careful optimization of the antenna parameters. Table 4.2 lists the targeted design goals for the proposed V2X antenna in terms of polarization, reflection coefficient, efficiency, and LAG. The design goals are generated based on the anticipated coverage and performance of V2X antenna to allow for efficient operation of the V2X system. The antenna was simulated with HFSS then measured on-foam and on-vehicle's windshield inside anechoic chamber as depicted in Figure 4.3 and Figure 4.4.

Table 4.1. Values of the Cavity-Backed Slot Antenna Geometrical Parameters

Parameter	Value (mm)
H	16.8
L	40.5
W	38.7
SW	22.5
SL	1.6
FL	11
LFL	1.74
FD	1.7
FX	13.5
FY	19.35

Table 4.2. V2X Antenna Design Goals and Guidelines

Parameter	Value
Polarization	VLP
Reflection Coefficient	-10 dB (2:1 VSWR)
Avg. Total Efficiency	45%
LAG for solid angle: $-55deg < \Phi < 55deg$ $86deg < \theta < 93deg$	2dB minimum

Figure 4.3. V2X cavity-backed slot antenna measured on foam inside anechoic chamber.

Figure 4.4. V2X cavity-backed slot antenna mounted on vehicle's windshield ready for chamber measurement.

4.3 V2X Antenna Simulation and Measurements Results

4.3.1 V2X Antenna Matching and Surface Current Density

The proposed antenna's reflection coefficient is depicted in Figure 4.5. Similar matching characteristics between the simulation and measurements can be observed with mid-band return loss of 20dB and 22dB in simulation and measurements respectively. Keysight E5071C Network Analyzer was used to capture the V2X antenna reflection coefficient measured response while HFSS software was used for the simulated one. To further study the current path and behavior of the antenna, the surface current density is reported in Figure 4.6. The high values of surface current density at 5.9GHz near the cavity slot indicates that most of the energy radiated by the feeding monopole is exiting the cavity through the slot either directly or after it bounces from the back of the cavity.

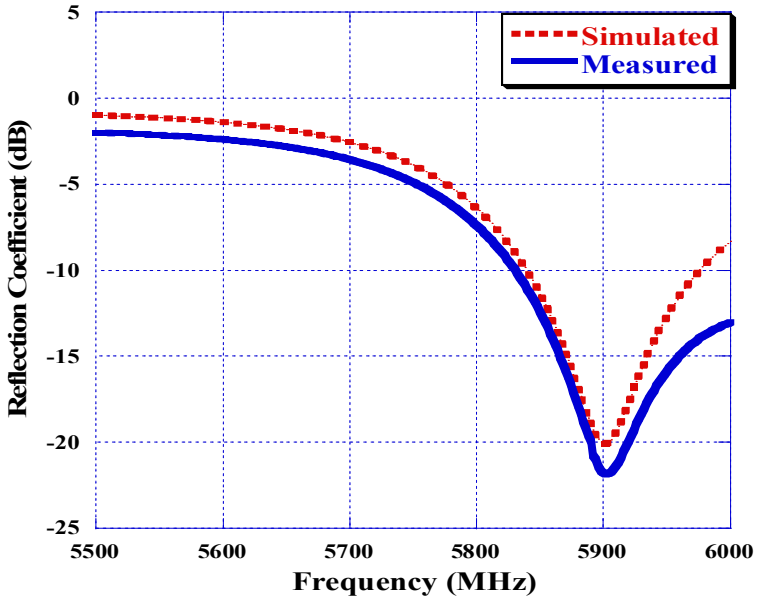

Figure 4.5. Comparison of reflection coefficient in dB between V2X antenna simulation and measurement.

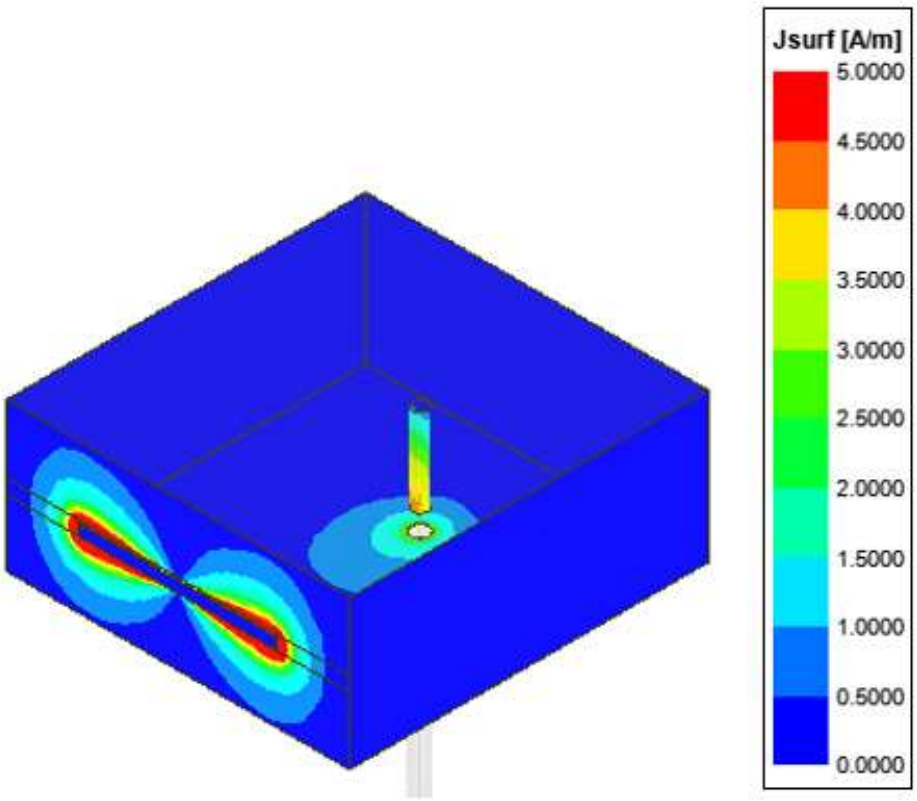

Figure 4.6. Simulated surface current density in A/m at 5.9GHz.

4.3.2 V2X Antenna Radiation Pattern, LAG, and Efficiency

To meet the V2X wide azimuth front beam (-55 < Φ < 55) and various elevation angles requirements, the cavity slot width and length must be carefully optimized. In Figure 4.7, 4.8, and 4.9, the antenna radiation patterns have been reported at different elevation angles and at sample frequencies across the V2X band. The elevation angles are selected in a way that will reflect various V2X communications scenarios. For example, vertical gain radiation pattern at Theta = 80deg will mimic electromagnetic waves incident from base station towers or traffic light signals whereas Theta =90deg and Theta =93deg will represents waves originating from other cars at or below the horizon respectively. The on-vehicle's windshield average vertical gain in azimuth angles range -55deg < Φ < 55deg at 5.9GHz was found to be 2dB, 2.8dB, and 2.2dB at Theta angles 80deg, 90deg, and 93deg respectively. Since the proposed antenna does not sit on a GND by design, the antenna demonstrates a good performance below horizon and that can be seen by looking at average vertical realized gain at Theta = 93deg which was found to be 2.4dB, 2dB, 2.3dB at 5.85GHz, 5.9GHz, and 5.925GHz respectively. It is noteworthy that, only the front beam is of interest in this since the back side can be covered by similar antenna on the rear screen of the car facing the opposite direction.

A practical way to measure automotive V2X antenna performance is by calculating the LAG across theta angles from 86 to 93 degrees as in Table 4.2. These angles simulate EM waves exchanged between vehicles. As in equation (2.2) and for easy reference, LAG measured in dB for a frequency (f) and polarization (γ) is given by:

$$LAG_{dB}(f,\gamma) = 10log_{10}\left[\frac{\sum_{i=1}^{M}\sum_{j=1}^{N} sin(\theta_i)G_{linear}(f,\theta_i,\varphi_j,\gamma)}{MN}\right] \quad (4.2)$$

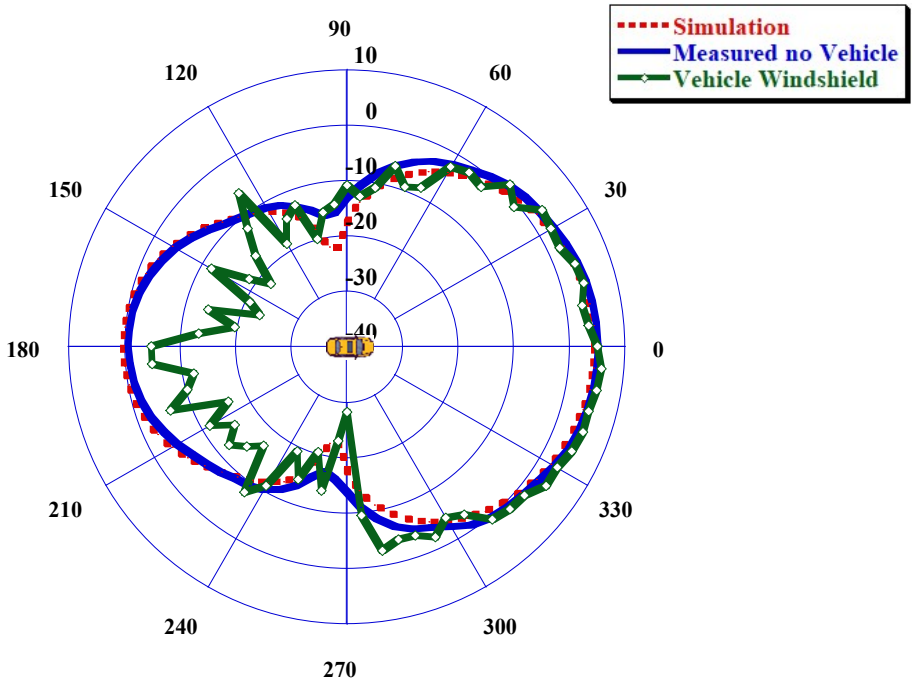

(a)

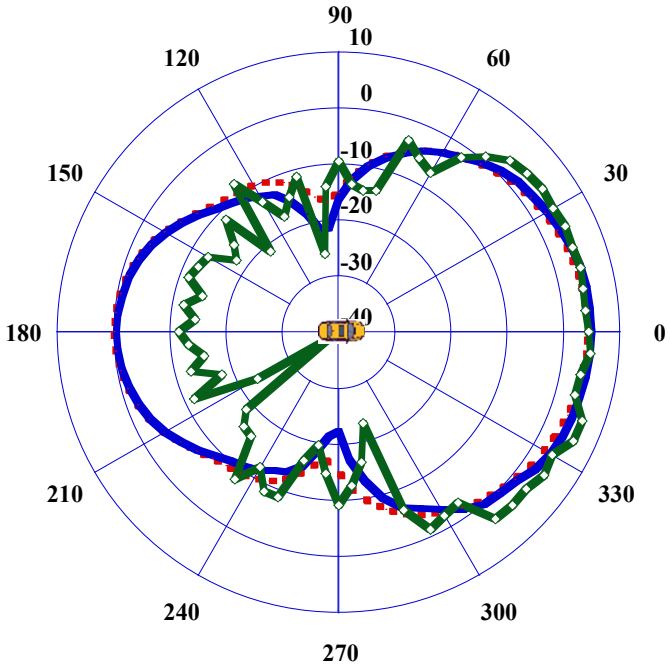

(b)

Figure 4.7. Realized vertical gain at 5.85GHz for simulated, measured on-foam, and measured on vehicle's windshield at: (a) θ = 80deg, (b) θ = 90deg, and (c) θ = 93deg.

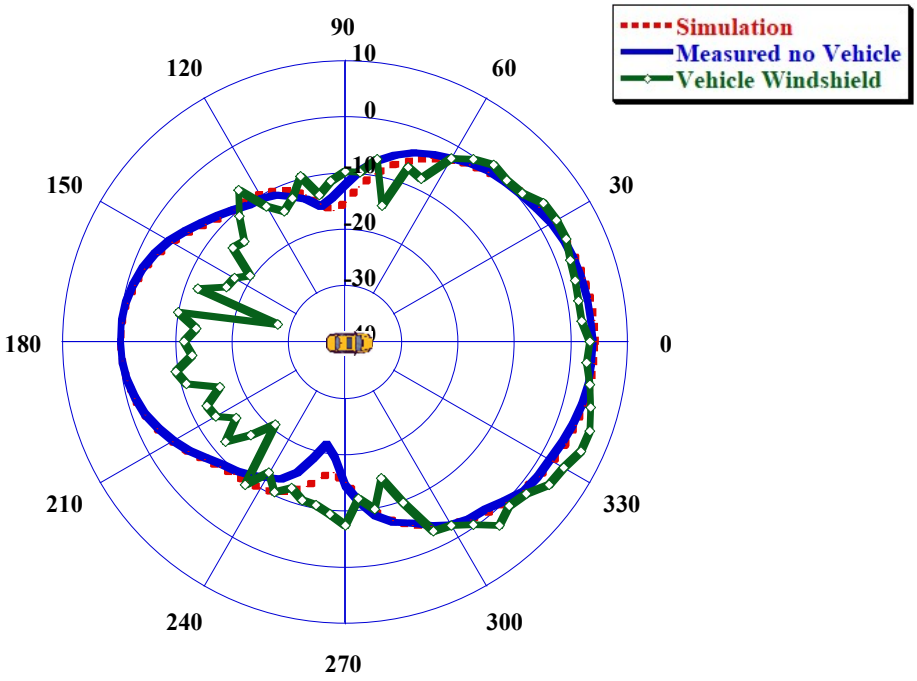

(c)

Figure 4.7. Continued.

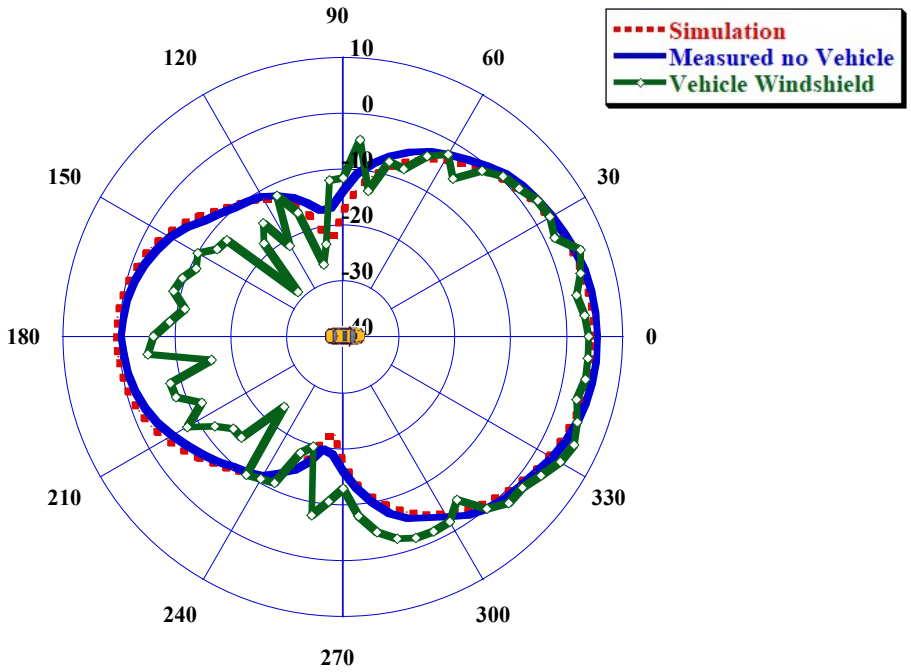

(a)

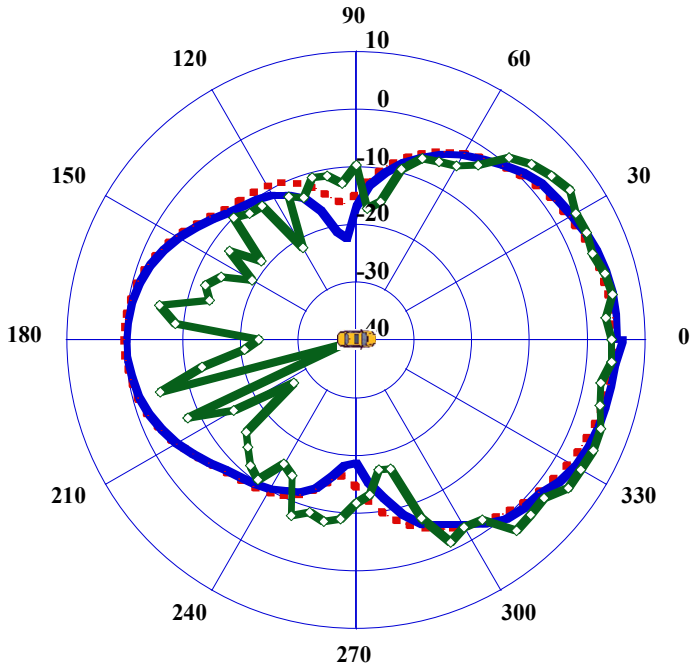

(b)

Figure 4.8. Realized vertical gain at 5.9GHz for simulated, measured on-foam, and measured on vehicle's windshield at: (a) θ = 80deg, (b) θ = 90deg, and (c) θ = 93deg.

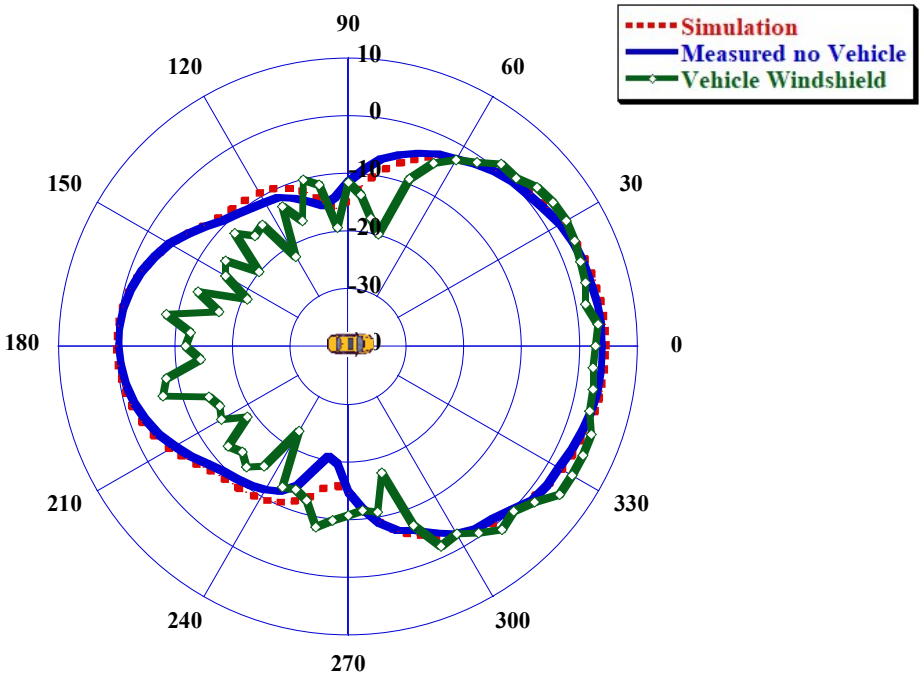

(c)

Figure 4.8. Continued.

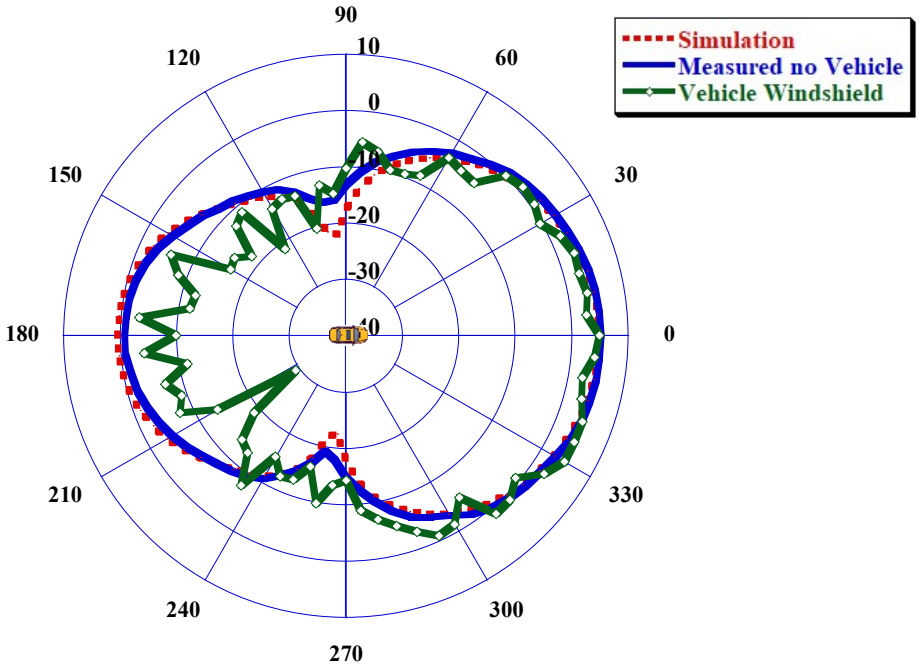

(a)

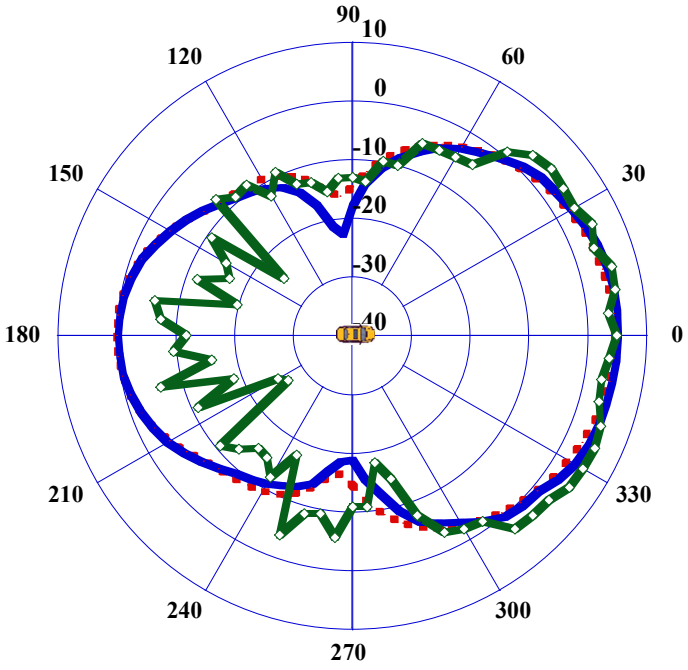

(b)

Figure 4.9. Realized vertical gain at 5.925GHz for simulated, measured on-foam, and measured on vehicle's windshield at: (a) θ = 80deg, (b) θ = 90deg, and (c) θ = 93deg.

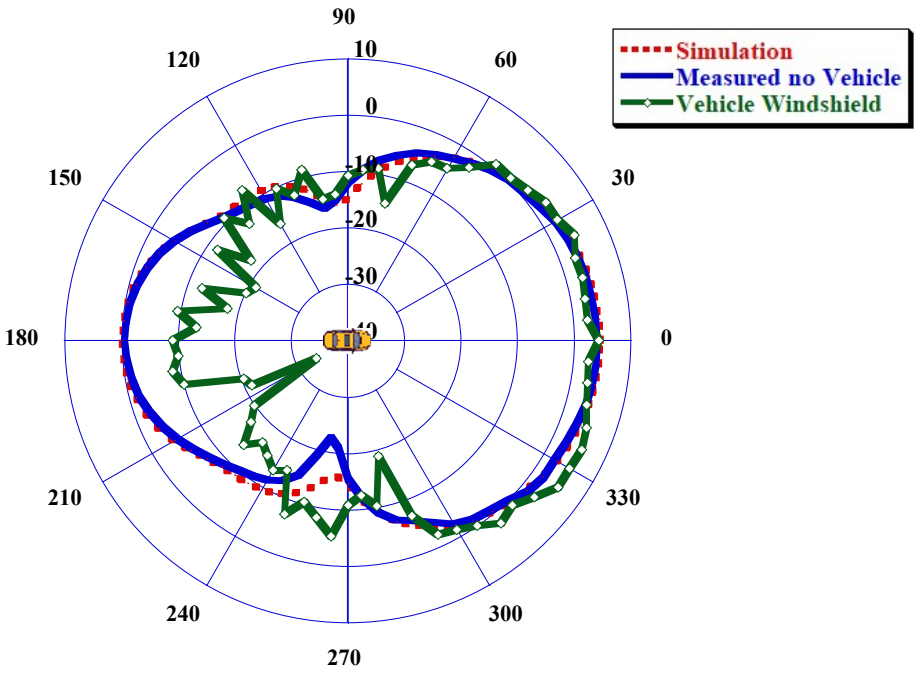

(c)

Figure 4.9. Continued.

where, θ_i is the spherical coordinate theta angle in degrees referenced by the index i; M is the total number of theta angles (8 angles for theta from 86 to 93 deg); φ_j is the spherical coordinate phi angle in degrees referenced by the index j; N is the total number of phi angles (360 angles for phi from 0 to 359 deg); and $G_{linear}(\theta_i, \varphi_j)$ in the gain in linear units for a discrete point on the spherical surface for a given frequency (f) and polarization (γ).

Figure 4.10 depicts the LAG against frequency for simulated, measured on foam, and measured on a vehicle's windshield. In all three cases the LAG has stayed above 2.5dBi across V2X frequencies satisfying the design goals listed in Table 4.2. Finally, the total efficiency of the antenna measured on-foam and on vehicle's windshield is reported across V2X frequencies in Figure 4.11. The on-foam measurements show a 56% average total efficiency whereas the on-vehicle measurements exhibit reduced average efficiency of 45.5% indicating that antenna performance is compromised at other elevation and azimuth angles apart from the targeted ones due to reflections within the vehicle.

Table A.3 in the APPENDIX compares the cavity-backed slot antenna to other V2X antennas in the literature. The proposed antenna demonstrates a good performance in terms of linear average gain and peak gain as well as below-horizon performance as it can be seen in Figures 4.7, 4.8, and 4.9. The proposed antenna with the demonstrated performance in terms of radiation pattern, reflection coefficient, LAG, and efficiency represent an ideal model for V2X antenna element that could be used to construct a complete V2X antenna solution for modern vehicle communication.

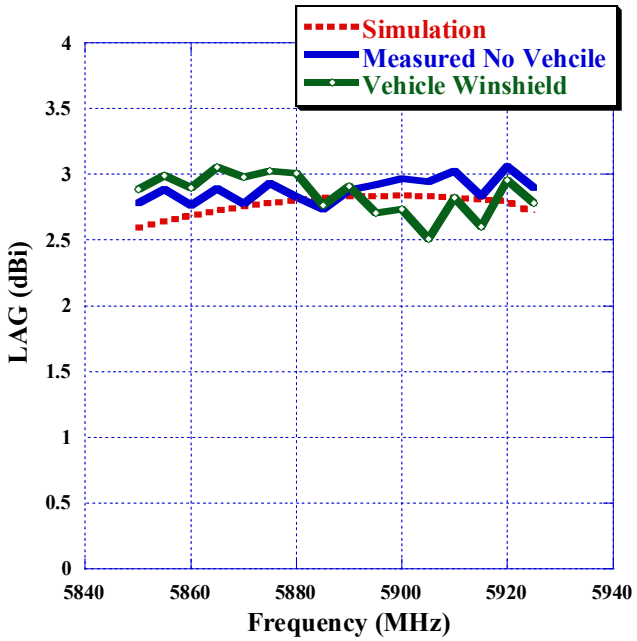

Figure 4.10. V2X antenna LAG against frequency comparison between simulation, measured on-foam, and measured on vehicle's windshield.

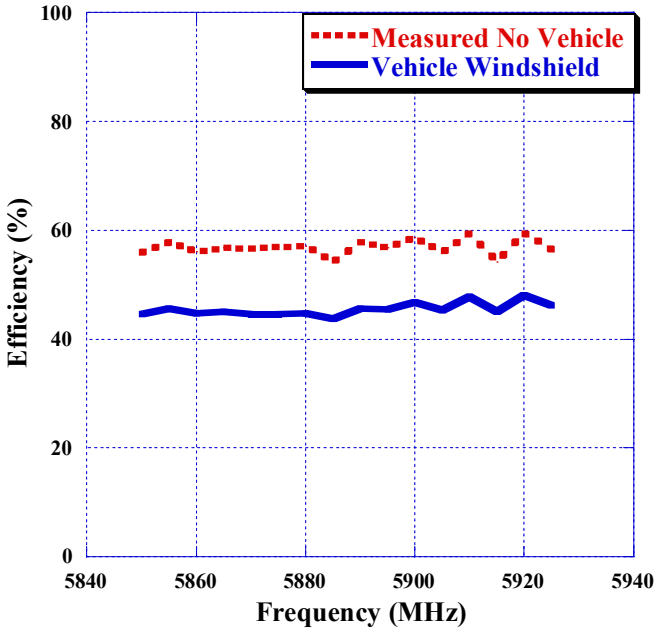

Figure 4.11. V2X antenna Efficiency against frequency comparison between measured on-foam and measured on vehicle's windshield.

4.4 Conclusions

In this chapter, a cavity-backed slot antenna was developed to work at V2X frequencies and to allow for below horizon communication by eliminating the need for GND commonly used by other automotive antennas for performance enhancement. The proposed antenna is small in size 40.5X38.7X16.8 mm^3 and can easily be integrated in a vehicle's windshield or rear-view mirror without the need for protruding parts at the vehicles' exterior. Good matching characteristics of better than 15dB return loss at V2X frequencies were observed. The realized vertical gain stayed almost above 0dBi for the azimuth beam -55deg < Φ < 55deg for all elevations between 75deg < θ < 95deg. The antenna demonstrated good performance for the solid angle -55deg < Φ < 55deg and 86deg < θ < 93deg with above than 2.5dBi LAG across the V2X band with comparable results for simulation, on-foam and on-vehicle's windshield measurements. Finally, an average total efficiency of 56% for on-foam measurements and of 45.5% for vehicle's windshield measurements were reported for the proposed antenna. In general, the proposed antenna has a satisfactory performance and can easily be used for V2X automotive applications upon the desired requirement, styling, and dimension.

CHAPTER FIVE

CONCLUSIONS AND FUTURE WORK

5.1 Conclusions

The research presented in this work addressed an area of great interest in the automotive industry. Modern automotive manufacturers started to shift to lay out the fundamentals of autonomous driving standards and requirements. In that pursuit, 5G cellular antennas, V2X antennas, high precision GNSS antennas, and 5G cellular MIMO systems play a dominant role. A novel multi-wideband branched monopole 5G cellular antenna that is easy to integrate inside an automotive Shark-fin was presented in Chapter 2. By equipping the antenna with two arms, this antenna was able to cover low cellular band (617MHz- 960MHz), mid band (1710MHz- 2690MHz), and high band (3300MHz-5000MHz) with decent rejection around GNSS bands (1160MHz- 1610MHz). This antenna element is of critical importance for OEMs because is Shark-fin compatible, leigh weighted, and cheap compared to what available in literature. In addition to that, the element has an inherited quality by design that enables it to filter out GNSS frequencies eliminating the need of extra filtering at the PCB level which reduces the cost further. The antenna has a VSWR of less than 3.2:1 (5.6dB return loss) and an average efficiency of 87% on a GND and 83% on the vehicle. The LAG performance was better than -1dBi across the entire frequency band for the elevation range from 3 degrees to 15 degrees above the horizon. The parametric study of different geometrical variables was analyzed and revealed that the antenna has a resilient design which makes it suitable for manufacturing with an acceptable tolerance of each parameter's dimension.

To increase the system capacity and throughput, three 5G cellular MIMO system configurations built from the novel 5G branched monopole antenna were presented in Chapter 3. Configuration I of a 2x2 5G cellular MIMO system was built with two branched monopole elements separated by 135mm distance and placed in such a way that will result in an omnidirectional pattern. In this system minimum total average efficiencies, lowest passive isolation, highest ECC, and lowest DG were found to be 71%, 12dB, 0.13, and 9.9dB respectively. Configuration II of a 2x2 5G cellular MIMO system was built with two branched monopole elements oriented in an opposite way to antennas in Configuration I and separated by 125mm distance and placed in such a way that will result in an omnidirectional pattern. In this system minimum total average efficiencies, lowest passive isolation, highest ECC, and lowest DG were found to be 71.7%, 15dB, 0.02, and 10dB respectively. Finally, a 4x4 5G cellular MIMO system was realized as in Figure 3.12 and in this system minimum total average efficiencies, lowest passive isolation, highest ECC, and lowest DG were found to be 65%, 10dB, 0.46, and 8.9dB respectively. In general, each MIMO configuration has a satisfactory performance and can be used easily in the vehicular application depending on the desired requirement and dimensions.

To minimize nulls in the radiation pattern and improve below-horizon gain of V2X antenna as well as to provide a modernized look of the vehicle. A cavity-backed slot antenna was developed and attached to the vehicle windshield. The antenna is GND independent, and it covers V2X frequency band with less than 2:1 VSWR. The peak realized gain was found to be 6.5dBi with almost above 0dBi for the azimuth beam -55deg < Φ < 55deg for all elevations between 75deg < θ < 95deg. A LAG of more than

2.5dB was also realized for the solid angle -55deg < Φ < 55deg and 86deg < θ < 93deg. Finally, the average efficiency for on-foam measurement and on vehicle's windshield was found to be 56% and 45.5% respectively. Based on the antenna performance, size, cost, and placement location, the antenna seems to be very attractive for automotive manufacturers and can be of great use upon the desired requirement, styling, and dimension.

The research in this work presents real life examples of futuristic antennas that prepare the automotive infrastructure for autonomous vehicles era. The work takes into account not only antenna performance but also other important factors such as: antenna size, cost, weight, ease of manufacturability, coexistence with other inevitable technologies, and mounting location in the car. It is safe to say that the developed antennas presented throughout this work have undergone high performance scrutiny since they were first accurately simulated then measured on GND and finally measured on vehicle inside a state-of-the-art anechoic chamber.

5.2 Future Work

The work presented in this dissertation can be extended in future by targeting the following areas:

- Investigate the 5G cellular antenna element to include the V2X band in the same antenna and try to use proper filtering at the board level to separate them.
- Investigate the possibility of reducing the 5G cellular antenna height further.
- Investigate the possibility of adding dielectric to the 5G cellular antenna to further reduce the antenna size and make MIMO systems out them.

- Investigate the possibility of reducing the MIMO structure ECC figures specially in the 4x4 MIMO system.
- Investigate the possibility of making a complete MIMO system using the cavity-backed slot V2X antenna to provide an omnidirectional coverage.

APPENDIX

TABULATED SUMMARY OF LITERATURE REVIEW

Table A.1. Comparison between 5G Cellular Antenna and Literature

Ref	Type	Bandwidth	Dimensions (LxWxH) (mm3)	Gain/ Efficiency
Proposed Antenna	Compact monopole	617MHz-5GHz	38.5x15x60	Average gain on vehicle -0.2 dBi @617MHz, 2 dBi @1.9GHz, 0.1dBi@3.9GHz and 2.8dBi @5GHz. Average efficiency 87% on GND, 83% on Vehicle.
14	Flat Nefer Antenna	698MHz-6GHz	80x60x30	-3dB (High band gain is in driving direction) (70% 0.7-3.7GHz, 63% 3.7-6GHz on GND)
15	Vivaldi Monopole	698MHz-6GHz	69.1x0.86x73	Simulated max gain is close to 6dB
16	Printed Yagi-Uda	2.9GHz-4.1GHz	60x1.6x55	Peak gain more than 7dB
17	3D nefer antenna	698MHz-960MHz 1.47GHz-2.7GHz	50x(2-40)x53	Average gain on GND -1 dBi @850MHz, 2 dBi @1700MHz, And 3dBi @2.4GHz (Average efficiency 74% between 698-960 MHz, 85% between 1.47-2.7GHz)
18	Printed monopole	698MHz-2690MHz	25x1.53x76	Measured gains are higher than 2 dB
19	Novel compact 3D antenna	790MHz-2.69GHz	50x50x30	Simulated Max. gain 1-2.5dB at low band, 6-8.5dB at higher bands.

Ref	Type	Bandwidth	Dimensions (LxWxH) (mm3)	Gain/ Efficiency
20	3D printed on plastic	791MHz-2.69GHz	Not reported	-2dB @0.8GHz, -3dB @ 1.8GHz, -6dB @2.6GHz.
21	T-Shape monopole	698MHz-960MHz 1.427GHz-2.7GHz	33x10x55	Max gain 2.8dBi @ 900MHz 5.2dBi @ 2.6 GHz. Average efficiency 70%.
22	Printed two-branch monopole on FR4	720MHz-960MHz 1.6GHz-4GHz	30x1.6x70	Max gain 3.54dBi @900MHz/ 5.89dBi @2.4GHz/ 3.52dBi @3.5GHz
23	Top-loaded monopole	700MHz-3GHz	80x80x28	Average gain on GND -2 dBi @752MHz, -1.5 dBi @892MHz, -2dBi @1.755GHz and -1.5dBi @1.93GHz. (73.3% @752MHz, 76.4% @892MHz, 85% @ 1.755GHz, 95.3% @1.93GHz)
24	5G and V2X PIFA	617MHz-6GHz	55x50x28	Average gain on Car -2.1 dBi @617MHz, -1 dBi @1900MHz, 0 dBi @3.6GHz, 0.9 dBi 5GHz Average efficiency 83% on GND, 72% on Vehicle.

Table A.2 Automotive MIMO Systems Literature Review Summary

Ref.	Type	BW	Antenna Dimension (LxWxH) (mm3)	ECC Method/ value
25	2x2 monopole	700MHz-900MHz	Not reported	S-param only / lower than 0.02
26	2x2 PIFA	775MHz-925MHz	59.5x12.4x21	S-param only / lower than 0.5
27	2x2 PIFA	790MHz-2.69GHz	50x50x28	E field components / lower than 0.3
28	2x2 printed monopole	790MHz-3GHz	30x0.8x80	S-param only / lower than 0.05
29	2x2 printed planar monopoles	698MHz-2700MHz	52x1.6x65	S-param only/ lower than 0.5
30	2x2 PIFA	690MHz-2700MHz	PIFA length is 75.9mm /height 25.5mm	S-param only /lower than 0.5
31	2x2 monopole	698MHz-2.69GHz	Monopole heights are 55 and 45mm	S-param only / lower than 0.5
32	2x2 printed monopoles	698MHz-2690MHz	25x2x55	Not reported / lower than 0.3
33	2x2 printed monopole PIFA	698MHz-3GHz	PIFA 65x62x20 / Monopole height is 53.	Not reported
35	2x2 Nefer Antenna	700MHz-6GHz	70x70x29	S-param only / lower than 0.16

Ref.	Type	BW	Antenna Dimension (LxWxH) (mm3)	ECC Method/ value
36	4x4 sleeve monopoles	790MHz-5GHz	Not reported	Not reported / lower than 0.12
21	2x2 printed Yagi	2GHz-4.5GHz	60x1.6x55	Not reported/ lower than 0.5
41	2x2 loaded monopoles	2.4GHz-11GHz	24x2.2x29	E-field components / lower than 0.02

Table A.3 Comparison between Cavity-Backed Slot Antenna and Literature

Ref.	Type	Antenna Dimension (LxWxH) (mm3)	Avg./Peak Gain (dBi)	Below Horizon Performance
Proposed	Cavity-Backed Slot	40.5X38.7X16.8	2.75/6.5	Yes
52	Disc Shape	$\pi X 80^2 X 20$	NA/8	NA
42	Printed Monopoles	14X0.8X28 14X1.6X50	-2.3/NA -2.9/NA	NA
43	Tri-Polarized	76X76X17	2.4/2.88	NA
45	V-Shaped Slot	$\pi X 32^2 X 3$	NA	NA
46	stacked microstrip monopolar Patch	$\pi X 85^2 X 4$	<0/7.5	NA
47	Patch Antenna	$\pi X 42^2 X 1.6$	NA/0.97	NA
48	Printed Flexible	120X70X0.1	0.043/4.6	NA
49	3-port Multiband antenna	60X87X1.6	NA/-0.5	NA
50	Combined LTE and V2X antenna	290X40X7.6	NA/2	NA
51	Vivaldi Antenna	190X187.5X187.3	-4/NA	NA

REFERENCES

[1] H. Ullah, N. Gopalakrishnan Nair, A. Moore, C. Nugent, P. Muschamp and M. Cuevas, "5G Communication: An Overview of Vehicle-to-Everything, Drones, and Healthcare Use-Cases," in IEEE Access, vol. 7, pp. 37251-37268, 2019.

[2] C. Wang, J. Bian, J. Sun, W. Zhang and M. Zhang, "A Survey of 5G Channel Measurements and Models," in IEEE Communications Surveys & Tutorials, vol. 20, no. 4, pp. 3142-3168, Fourth quarter 2018.

[3] G. Artner, W. Kotterman, G. Del Galdo and M. A. Hein, "Automotive Antenna Roof for Cooperative Connected Driving," in IEEE Access, vol. 7, pp. 20083-20090, 2019.

[4] K. Fujimoto and J. James, Mobile Antenna Systems Handbook. Boston: Artech House, 1994.

[5] S. Egashira, T. Tanaka, and A. Sakitani, “Design of AM/FM mobile telephone triband antenna,” IEEE Trans. Antennas Propag., vol. 42, pp. 538–540, 1994.

[6] S. R. Best, “A discussion on the properties of electrically small self-resonant wire antennas,” IEEE Trans. Antennas Propag., vol. 46, pp.9–22, 2004.

[7] P. Haapala, P. Vainikainen, and P.Eratuuli, “Dual frequency helical antennas for handsets,” in Proc. IEEE 46th Vehicular Technology Conf., Apr. 1996, vol. 1, pp. 336–338.

[8] G. Zhou, “A non-uniform pitch dual-band helix antenna,” in Proc. IEEE Antennas and Propagation Int. Symp., Jul. 2000, vol. 1, pp.274–277.

[9] H. Chen, “Compact CPW-fed dual frequency monopole antenna,” Electron. Lett., vol. 38, pp. 1622–1624, 2002.

[10] W. Chung and C. Huang, “CPW-fed L-shaped slot planar monopole antenna for triple band operations,” Microw. Opt. Technol. Lett., vol. 44, pp. 510–512, 2005.

[11] R. Leelaratne and R. Langley, “Multiband PIFA vehicle telematics antennas,” IEEE Trans. Ve. Technol., vol. 54, pp. 477–485, 2005.

[12] S. Yeh, K. Wong, T. Chiou, and S. Fang, “Dual-band planar inverted F antenna for GSM/DCS mobile phones,” IEEE Trans. Antennas Propagation, vol. 51, pp. 1124–1126, 2003.

[13] A. G. Domel, G. Domel, J. C. Weaver, M. Saadat, K. Bertoldi, and G. V. Lauder, “Hydrodynamic properties of biomimetic shark skin: effect of denticle size and swimming speed,” Bioinspiration & Biomimetics, vol. 13, 2018.

[14] S. Hastürkoğlu and S. Lindenmeier, “A wideband automotive antenna for actual and future mobile communication 5G/LTE/WLAN with low profile,” 11th European Conference on Antennas and Propagation (EUCAP), Paris, pp. 602-605, March 2017

[15] A. Michel, P. Nepa, M. Gallo, I. Moro, A. Filisan, and D. Zamberlan, “Printed Wideband Antenna for LTE-Band Automotive Applications,” IEEE Antennas and Wireless Propagation Letters, vol. 16, pp. 1245-1248, November 2016.

[16] D. Navarro, F. Carrera, M. Ferrando, M. Baquero and E.Antonino, M.Gallo, S. Bruni, M. Pannozzo, D. Zamberlan, "Compact wideband Vivaldi monopole for LTE mobile communications," 2013 IEEE Antennas and Propagation Society International Symposium (APSURSI), Orlando, FL, , pp. 1098-1099, 2013.

[17] V. Franchina, A. Michel, P. Nepa, R. Parolari, I. Moro, A. Polo Filisan, D. Zamberlan, “A 3D LTE antenna for vehicular applications,” IEEE International Symposium on Antennas and Propagation & USNC/URSI National Radio Science Meeting, San Diego, CA, pp. 637-638, July 2017.

[18] A. Friedrich, B. Geck, O. Klemp, H. Kellermann, “On the Design of a 3D LTE Antenna for Automotive Applications based on MID Technology,” 2013 European Microwave Conference, Nuremberg, pp. 640-643, October 2013.

[19] I. Goncharova and S. Lindenmeier, “A High Efficient Automotive Roof-Antenna Concept for LTE, DAB-L, GNSS and SDARS with Low Mutual Coupling,” 2013 9th European Conference on Antennas and Propagation (EuCAP), Lisbon, pp. 1-5, April 2015.

[20] Yong Cheng, Jing Lu, and Can Wang, “Design of a Multiple Band Vehicle-Mounted Antenna,” International Journal of Antennas and Propagation, vol. 2019, Article ID 6098014, 11 pages, December 2019.

[21] K. Sreelakshmi, P. Bora, M. Mudaliar, Y. Dhanade, and B.T.P. Madhav, “Linear array Yagi-Uda 5G antenna for vehicular application,” International Journal of Engineering & Technology, vol. 7. pp. 513-517, Dec. 2017.

[22] I. Goncharova and S. Lindenmeier, “A High–Efficient 3–D Nefer–Antenna for LTE Communication on a Car,” The 8th European Conference on Antennas and Propagation (EuCAP), The Hague, pp. 3273-3277, April 2017.

[23] E. Ghafari and D. N. Aloi, "Top-loaded UWB monopole antenna for automotive applications," Proceedings of the 2012 IEEE International Symposium on Antennas and Propagation, Chicago, IL, pp. 1-2, July 2012.

[24] A. M. Yacoub, M. O. Khalifa, and D. N. Aloi, "Wide Bandwidth Low Profile PIFA Antenna for Vehicular Sub-6 GHz 5G and V2X Wireless Systems," Progress In Electromagnetics Research C, Vol. 109, 257-273, 2021.

[25] H. J. Song, A. Bekaryan, J. H. Schaffner, T. Talty, D. Carper, E. Yasan, and A. Duzdar, "Evaluation of vehicle-level MIMO antennas: capacity, total embedded efficiency, and envelope correlation," 2014 IEEE-APS Topical Conference on Antennas and Propagation in Wireless Communications (APWC), Palm Beach, FL, pp. 89-92, Aug. 2014.

[26] O. Kwon, R. Song, and B. Kim, "A fully integrated shark-fin antenna for MIMO-LTE, GPS, WLAN, and WAVE applications," IEEE Antennas and Wireless Propagation Letters, vol. 17, no. 4, pp. 600-603, Apr. 2018.

[27] V. Franchina, A. Michel, P. Nepa, M. Gallo, R. Parolari, A. P. Filisan, and D. Zamberlan, "A compact 3D antenna for automotive LTE MIMO applications," 2017 IEEE-APS Topical Conference on Antennas and Propagation in Wireless Communications (APWC), Verona, Italy, pp. 326-329, Oct. 2017.

[28] A. Heiman, A. Badescu, and A. Saftoiu, "A new multiple input multiple output V2V automotive antenna for long term evolution band applications," 2018 International Symposium on Fundamentals of Electrical Engineering (ISFEE), Bucharest, Romania, pp. 1-5, Nov. 2018.

[29] D. Preradovic and D. N. Aloi, "Cross polarized 2x2 LTE MIMO system for automotive shark fin application," The Applied Computational Electromagnetics Society (ACES), vol. 35, no. 10, pp. 1207-1216, Oct. 2020.

[30] C. Demien and R. Sarkis, "Design of shark fin integrated antenna systems for automotive applications," 2019 PhotonIcs & Electromagnetics Research Symposium - Spring (PIERS-Spring), Rome, Italy, pp. 620-627, Jun. 2019.

[31] A. Thiel, L. Ekiz, O. Klemp, and M. Schultz, "Automotive grade MIMO antenna setup and performance evaluation for LTE-communications," 2013 International Workshop on Antenna Technology (iWAT), Karlsruhe, pp. 171-174, Mar. 2013.

[32] Y. Liu, Z. Ai, G. Liu, and Y. Jia, "An Integrated shark-fin antenna for MIMO-LTE, FM, and GPS applications," IEEE Antennas and Wireless Propagation Letters, vol. 18, no. 8, pp. 1666-1670, Aug. 2019.

[33] N. Guan, H. Tayama, M. Ueyama, Y. Yoshijima, and H. Chiba, "A roof automobile module for LTE-MIMO antennas," 2015 IEEE-APS Topical Conference on Antennas and Propagation in Wireless Communications (APWC), Turin, pp. 387-391, Sep. 2015.

[34] S. Zhekov, A. Tatomirescu, E. Foroozanfard, and G. F. Pedersen, “Experimental investigation on the effect of user’s hand proximity on a compact ultrawideband MIMO antenna array,” IET Microwaves, Antennas Propag., vol. 10, no. 13, pp. 1402–1410, Oct. 2016.

[35] S. Hastürkoğlu, M. Almarashli, and S. Lindenmeier, “A compact wideband terrestial MIMO-Antenna set for 4G, 5G, WLAN and V2X and evaluation of its LTE-Performance in an urban region,” 2019 13th European Conference on Antennas and Propagation (EuCAP), Krakow, Poland, pp. 1-5, Mar. 2019.

[36] O. Jonah, “5G Antenna for Automotive Applications,” 2020 IEEE International Symposium on Antennas and Propagation and North American Radio Science Meeting, pp. 1493-1494, Web, Jul. 2020.

[37] J. Malik, D. Nagpal, and M. V. Kartikeyan, “MIMO antenna with omnidirectional pattern diversity,” Electronics Letters, vol. 52, no. 2, pp. 102-104, Jan. 2016.

[38] L. Lanctot and O. Jonah, “Cellular antenna performance impact on MIMO in vehicle,” 2018 IEEE International Symposium on Antennas and Propagation & USNC/URSI National Radio Science Meeting, Boston, MA, pp. 353-354, Jul. 2018.

[39] A. M. Elshirkasi, A. Abdullah Al-Hadi, M. F. Mansor, R. Khan, and P. J. Soh, “Envelope correlation coefficient of a two-port MIMO terminal antenna under Uniform and Gaussian angular power spectrum with user's hand effect,” Progress In Electromagnetics Research C, Vol. 92, 123-136, Apr. 2019.

[40] S. F. Beegum and S. K. Mishra, “Compact WLAN band-notched printed ultrawideband MIMO antenna with polarization diversity,” Progress In Electromagnetics Research C, vol. 61, pp. 149-159, Jan. 2016.

[41] D. Potti, Y. Tusharika, M. G. N. Alsath, S. Kirubaveni, M. Kanagasabai, R. Sankararajan, S. Narendhiran, and P. B. Bhargav, “A novel optically transparent UWB antenna for automotive MIMO communications,” IEEE Transactions on Antennas and Propagation, vol. 69, pp. 3821-3828, Jul. 2021.

[42] B. Seungbok, K. Sangpil, K. Choulhee, K. Heeyoung, and K. Yoongi, “Design of a V2X vehicle antenna,” 2018 International Symposium on Antennas and Propagation (ISAP), Busan, South Korea, pp. 1-2, Jan. 2019.

[43] B. Feng, J. Chen, S. Yin, C. Sim, and Z. Zhao, “A Tri-Polarized antenna with diverse radiation characteristics for 5G and V2X communications,” IEEE Transactions on Vehicular Technology, vol. 69, no. 9, pp. 10115–10126, Sep. 2020.

[44] M. O. Khalifa, A. M. Yacoub, D. N. Aloi, “A Multi-wideband compact antenna design for vehicular Sub-6 GHz5G wireless systems,” IEEE Transactions on Antennas and Propagation, doi: 10.1109/TAP.2021.3083770.

[45] H. Wong, K. K. So, and X. Gao, “Bandwidth enhancement of a monopolar patch antenna with V-shaped slot for car-to-car and WLAN communications,” IEEE Transactions on Vehicular Technology, vol. 65, no. 3, pp. 1130-1136, Mar. 2016.

[46] S. Gao, L. Ge, D. Zhang, and W. Qin, “Low-Profile Dual-Band Stacked Microstrip Monopolar Patch Antenna for WLAN and Car-to-Car Communications,” IEEE Access, vol. 6, pp. 69575-69581, Oct. 2018.

[47] A. Liu, Y. Lu, and L. Huang, “Low-profile patch antennas with enhanced horizontal omnidirectional gain for DSRC applications,” IET Microwaves, Antennas and Propagation, vol. 12, no. 2, pp. 246-253, Jan. 2018.

[48] A. Chletsou, Y. He, J. F. Locke, and J. Papapolymerou, “Multi-band, Flexible, Lightweight Antenna on LCP for Automotive Applications,” 2020 IEEE International Symposium on Antennas and Propagation and North American Radio Science Meeting, Montreal, Canada, pp. 1507-1508, Feb. 2021.

[49] Y. Hua, L. Huang, and Y. Lu, “A compact 3-port multiband antenna for v2x communication,” 2017 IEEE International Symposium on Antennas and Propagation & USNC/URSI National Radio Science Meeting, San Diego, USA, pp. 639-640, Oct. 2017.

[50] E. Neira, J. Carlsson, K. Karlsson, and E. G. Strom, “Combined LTE and IEEE 802.11p antenna for vehicular applications,” 9th European Conference on Antennas and Propagation (EuCAP), Lisbon, Portugal, pp. 1-5, Aug. 2015.

[51] P. A. Dzagbletey, J. Shim and J. Chung, “Quarter-Wave Balun Fed Vivaldi Antenna Pair for V2X Communication Measurement,” IEEE Transactions on Antennas and Propagation, vol. 67, no. 3, pp. 1957-1962, Mar. 2019.

[52] J. Chen, C. Chen, J. F. Locke, “A compact 4-channel MIMO 5G Sub-6 GHz/LTE/WLAN/V2X antenna design for modern vehicles,” IEEE Transactions on Antennas and Propagation, doi: 10.1109/TAP.2021.3083765.

[53] K. Abboud, H. A. Omar, and W. Zhuang, “Internetworking of DSRC and Cellular Network Technologies for V2X communications: A Survey,” In IEEE Transactions on Vehicular Technology, vol. 65, no. 12, pp. 9457-9470, Dec.2016.